CONTROL OF MULTI-LINK ONE-LEGGED HOPPING LOCOMOTION

By

Amer Allafi

A DISSERTATION

Submitted to
Michigan State University
in partial fulfillment of the requirements
for the degree of

Mechanical Engineering – Doctor of Philosophy

2020

ABSTRACT

CONTROL OF MULTI-LINK ONE-LEGGED HOPPING LOCOMOTION

By

Amer Allafi

Controlling one-legged hopping locomotion is a challenging problem due to the hybrid dynamics of the hopper and the interaction with ground. The hybrid dynamics of the one-legged hopper consists of mainly two sub-dynamics, one when the hopper is in contact with ground, and the other when there is no contact. The ground model can effect the hopper behavior since the hopper interact with ground when the hopper in contact with ground. Here we investigate the locomotion behavior of the one-legged multi-link hopper hopes on three different ground models, namely, rigid, elastic, and viscoelastic ground. The rigid ground apply an impulsive force to the hopper when the hopper came in contact with ground resulting energy losses. A partial feedback linearization is used to control the internal dynamics of the hopper. A Poincaré map is used to construct a discrete-time system and a controller with integral action is designed to achieve the control objectives. The elastic ground, the ground modeled as massless spring, the spring in the ground store some of the energy of the hopper during the contact. A continuous backstepping controller is designed to control the energy level and internal dynamics of the hopper. A Poincaré map is used to construct a discrete-time system and a controller with integral action is designed to achieve the control objectives. The viscoelastic ground, the ground modeled as an under-damped mass-spring-damper system, the damper and the impact with ground mass resulting in energy losses and the ground spring store some of the energy of the hopper during the contact. A continuous backstepping controller is designed to control the energy level and internal dynamics of the hopper. A Poincaré map is used to construct a discrete-time system and a controller with integral action is designed to achieve the control objectives. We considered multiple versions of one-legged hoppers, namely, two-DOF two-mass, two-DOF ankle-knee-hip, and four-link hopper. Simulation results are presented to demonstrate

the efficacy of the controllers.

I dedicate this work to the memory of my mother, Hessa Almuzaini , who always believed in my and my ability to be successful in the academic arena. You are gone but your belief in me has made this journey possible. My father Lafi Allafi, who first taught me the value of education and the value of hard work. Also, I want to thank my wife, Najla Aleid, who have supported me spiritually throughout the process.

ACKNOWLEDGEMENTS

I would like to express my sincere gratitude to my advisor Dr. Ranjan Mukherjee for his patience, motivation, vast knowledge, and guidance throughout this work. I would like to thank the other members of my committee, Dr. Hassan K. Khalil, Dr. George Zhu and Dr. Brain Feeny for the assistance they provided. Finally, I would like to thanks the Saudi Ministry of Education and Qassim University for the financial support during my P.h.D program.

TABLE OF CONTENTS

LIST OF FIGURES

Chapter 1

Introduction

Legged locomotion has certain advantages over wheeled locomotion. Compared to a wheeled robot, a legged robot is better suited for climbing stairs and moving over unstructured terrain. One-legged hopping locomotion is the simplest version of legged locomotion but controlling a one-legged robot is challenging due to the hybrid nature of its dynamics. The dynamics of a one-legged hopping robot typically consists of two phases: a contact phase and a flight phase. In addition, there can be an impact phase if the ground is rigid. The nature of the ground affects the dynamic behavior of the hopping robot significantly. The ground can be modeled as rigid, elastic, or viscoelastic with inertia. A rigid ground results in energy losses when the hopping robot comes in contact, a perfectly elastic ground results in no losses, and a viscoeleastic ground with inertia results in losses due to both impact with the ground and damping. Naturally, the control problem for hopping locomotion is different for different types of ground.

Some of the early work on one-legged locomotion can be credited to Seifert [1], Matsuoka [2] and Raibert [3]. Following the work by Raibert, Alexander [4] introduced the spring loaded inverted pendulum (SLIP) model for one-legged hopping and Schwind and Koditchek used a return map of a hop to control locomotion [5]. The leg and hip model, where an actuator is mounted on the hip joint, is an extension of the SLIP model. Cherouvim and Papadopoulos controlled the forward speed and apex height of a robot with a leg and hip, hopping over unknown rough terrain [6]. Mojtaba and Buehler proposed a control strategy for stabilizing and controlling the speed of the leg and hip model [7]. Poulakakis and Grizzle [8], [9] investigated the stability and control of a SLIP model with an asymmetric mass; this model is referred to as the asymmetric spring loaded inverted pendulum (ASLIP). The

behavior of the ASLIP model was compared with that of a three-link ankle-knee-hip (AKH) hopper [10]. Saranli et al. controlled an AKH hopper by approximating its model with that of the SLIP model [11]. Zhu et al. controlled the apex height of an AKH hopper [12], Vanderborght et al. investigated the effect of elastic actuation on the apex height [13], and Vu et al. [14] investigated the relationship between energy efficiency, leg stiffness, and stride frequency.

Since the dynamics of a hopper typically consists of multiple phases and behavior of the of the hopper is affected by the ground model, researchers have commonly used the Poincaré map [4, 15–17] to investigate the stability of this hybrid dynamic system. The ground is assumed to be rigid in most investigations: both one- and two-mass models have been used. This results in an impact phase where the robot comes in contact with the ground and there is loss of energy due to the impact. To avoid the impact phase, the one-mass SLIP model assumes the leg to be massless and therefore there is no loss of energy at the time of ground contact. The dynamics of the one-mass SLIP model is qualitatively the same for both rigid and elastic grounds and therefore two-mass models have been investigated. Mikhailova [18] investigated a two-mass hopper; a spring was placed between the lower mass and the ground to prevent loss of energy from impact. Yu and Iida [19] and Mathis and Mukherjee [20, 21] also considered two-mass hoppers but a controller was designed to account for the energy loss due to impact. Saitou et al. [22] used optimal control methods to maximize the height of a two-mass robot hopping on an elastic ground. The ground was assumed to have mass but the controller was implemented in an open-loop fashion. Ishikawa et al. [23] used a port-controlled Hamiltonian method to control the maximum hopping height of a similar two-mass system; the controller is based on feedback but the ground was assumed to be massless. Hutter et al. [24] developed an apex-height controller such that a two-link hopper behaves like a SLIP model by compensating for the energy loss.

Here we design control strategies for apex height control of multi-link one-legged hoppers, hopping on rigid, elastic, and viscoelastic ground. Also, we design a control strategy for

locomotion control of a six degrees-of-freedom (DOF) four-links hopper, hopping on a rigid ground. For apex height control, the control objective is to achieve a desired value of the maximum height reached by the center-of-mass (COM) of the robot during the flight phase. For locomotion control, the control objective is to achieve a desired step size for each hop. In Chapter 2, we extend the control strategy developed by Mathis and Mukherjee [21, 25] for apex height control of a two DOFs prismatic joint robot hopping on rigid and elastic grounds to hopping on a ground that is viscoelastic and has inertia. We first use backstepping [26] to stabilize the internal dynamics of the robot in the flight and contact phases. The periodic nature of the hybrid dynamic system is then analyzed using a Poincaré map [27] and the OGY[1] method of chaos control [28] is used to adjust a parameter of the backstepping controller discretely and converge the apex height to its desired value. A integral control [26] is required to overcome the energy loss due to impact and damping for the viscoelastic ground with inertia.

In Chapter 3, we consider an Ankle-Knee-Hip (AKH) robot, hopping on a rigid ground. The AKH robot has two DOFs in the flight phase and a single DOF in the contact phase. A continuous controller is designed to stabilize the controllable states in the flight phase. In the contact phase, the continuous controller makes the robot behave like a mass-spring-damper system: positive damping is first used to arrest the motion of the COM and negative damping is then used to add energy to the system and compensate for the losses due to impact. A Poincaré map [27] is constructed to analyze the periodic nature of the hybrid dynamic system. To control the apex height, the OGY method is used to adjust one of the continuous controller parameters discretely. While this works well to stabilize the hybrid dynamics, integral control [26] is required for controlling the apex height.

In Chapter 4, we address the problem of apex height control of an AKH robot hopping on an viscoelastic ground with inertia. The apex height is defined as the maximum height reached by the COM of the robot during the flight phase. We use the same control strategy

[1] A method introduced by Ott, Grebogi and Yorke for achieving stabilization of a periodic orbit [28].

that was developed for a two-mass prismatic-joint hopping robot discussed in Chapter 2. A backstepping controller was developed to stabilize the internal dynamics of the robot in the flight and contact phases for hopping on a purely elastic ground. For hopping on a viscoelastic ground with inertia, the periodic nature of the hybrid dynamic system is analyzed using a Poincaré map [27]. The OGY method of chaos control [28] is used together with integral action [26] to adjust a parameter discretely and converge the apex height to its desired value. In Chapter 2, we investigated hopping in a prismatic-joint robot and in Chapter 4 we extend the results to a robot with a kinematic structure that is commonly found in bipeds and walking machines. The underlying objective of this transition is to investigate locomotion problems in the commonly studied platforms. The control problem for the AKH hopping robot is more challenging than the prismatic joint robot because of the constraints imposed by the kinematic structure.

In Chapter 5, we control the of apex height and hopping locomotion of a four-link anthropomorphic robot hopping on a rigid ground; the four links correspond to the foot, leg, thigh and hip. The robot has three active joints at the ankle, knee and hip; the toe is not actuated and is therefore passive. One of the active DOFs is used to control the angle of the foot to ensure point contact with the ground; the other two DOFs are used to control the position of the COM. For apex height control, we use two control strategies. The first method is similar to the control strategy that was developed in [29]; this strategy introduces negative damping in the vertical dynamics of the COM during the contact phase. However unlike [29], where the Poincaré section is chosen at the point of take-off, it is chosen at the point of touch-down - this eliminates the need for numerical search to choose the control gains. Additionally, the results are extended to the hopping locomotion problem. The second strategy relies on choosing different equilibrium heights of the vertical dynamics of the COM during the flight phase. In this regard, it should be noted that apex height control can be viewed as a special case of the hopping locomotion problem where the step size is zero. The four-link robot has six DOFs in the flight phase and four DOFs in the contact phase.

A feedback linearization controller is designed such that the COM and the foot angle have the dynamics of a mass-spring-damper system. The periodic nature of the hybrid system is analyzed using a Poincaré map [30] and the OGY method of chaos control [31] is used together with integral action [26] to adjust system parameters discretely. By adjusting the parameters, it is possible to achieve a desired apex height while hopping in one location and hop with a desired step size during locomotion.

Chapter 2

Apex Height Control of a Two-DOF Prismatic Joint Robot Hopping on a Viscoelastic Ground with Inertia

2.1 Introduction

In this chapter, we develop a strategy for controlling the apex height of a two-DOF prismatic-joint robot, hopping on a viscoelastic ground [32]. The apex height is defined as the maximum height reached by the COM of the robot during the flight phase. The problem of apex height control of the two-DOF prismatic-joint robot hopping on a rigid ground and an elastic ground has been studied earlier by Mathis and Mukherjee [21,33]. Here, we extend that work to hopping on a ground that can be modeled as viscoelastic with inertia. Hopping on a viscoelastic ground with inertia introduces an additional DOF and poses challenges due to undesired vibration of the additional DOF and dissipation due to both impact and viscous damping. A hybrid control strategy is developed to converge the apex height of the COM of the two-DOF prismatic-joint robot to a desired value. The hybrid control strategy uses backstepping in continuous time and integral control in discrete time to control the internal dynamics and the total energy. The discrete-time system is constructed using a Poincaré map at the instant of time just before the impact between the robot and the ground. This

Chapter is structured as follows. The dynamics of the robot in the flight, impact and contact phases is presented in Section 2.2. The hybrid control strategy, developed for a purely elastic ground, is presented in Section 2.3; this material is taken from [25]. The hybrid controller is extended to the more general viscoelastic ground with inertia in Section 2.4 and validated with numerical simulations. Section 2.5 contains concluding remarks.

2.2 Dynamics of Two-DOF Hopper

We consider a two-mass prismatic-joint robot hopping on a viscoelastic ground with mass m_3, stiffness constant K_{ext}, and damping coefficient C_{ext} - see Fig.2.1 (a). The vertical displacement of the mass of the ground is denoted by x_3. The robot is shown in its flight and contact phases in Figs.2.1 (b) and (c); it is comprised of an upper mass m_1 and a lower mass m_2, both of which are constrained to move in the vertical direction. The force applied on the two masses by the prismatic joint actuator is denoted by F_1. The absolute position of the two masses are denoted by X_1 and X_2. The position of mass m_1 relative to m_2 is denoted by y, and the position of mass m_2 relative to m_3 is denoted by x_2. The height of the COM of m_2 from its base is denoted by ℓ. The force of interaction between masses m_2 and m_3 is denoted by F_2.

2.2.1 Flight Phases

During the flight phase, the following conditions hold:

$$x_2 > \ell \qquad F_2 = 0 \tag{2.1}$$

Together, the robot and the ground have three degrees-of-freedom (DOF) but their dynamics

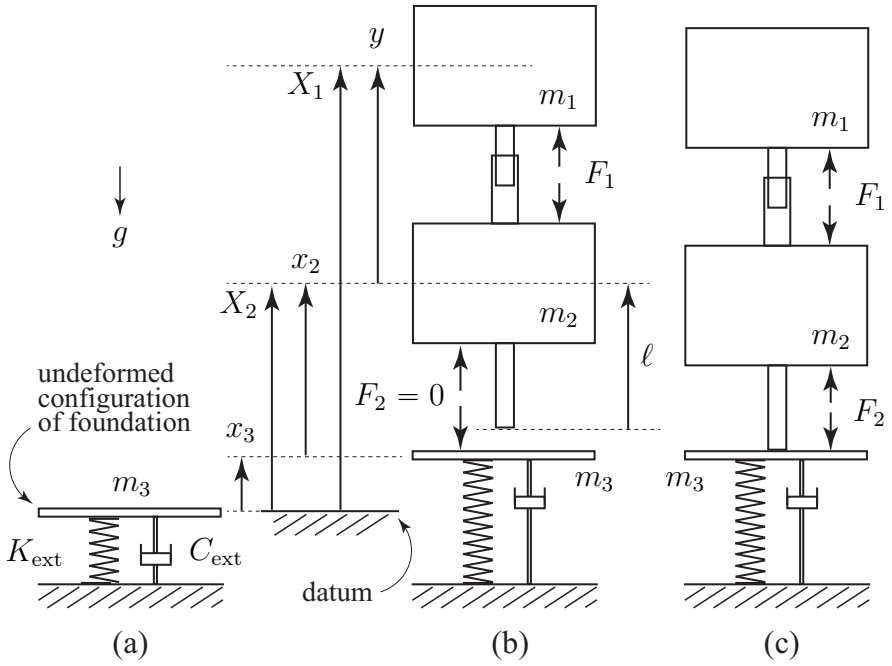

Figure 2.1: (a) Viscoelastic ground with inertia (b) flight phase and (c) contact phase of two-DOF robot hopping on the viscoelastic ground.

are decoupled. The accelerations of the two masses of the robot are as follows:

$$\begin{aligned} \ddot{X}_1 &= (\ddot{y} + \ddot{x}_2 + \ddot{x}_3) = -g + \frac{F_1}{m_1} \\ \ddot{X}_2 &= (\ddot{x}_2 + \ddot{x}_3) = -g - \frac{F_1}{m_2} \end{aligned} \tag{2.2}$$

The equation describing the motion of the ground is

$$m_3\ddot{x}_3 + C_{\text{ext}}\,\dot{x}_3 + K_{\text{ext}}\,x_3 = 0 \tag{2.3}$$

2.2.2 Impact Phase

The impact phase refers to infinitesimal intervals of time $t \in [t^-, t^+]$ during which the lower mass m_2 comes in contact with the ground mass m_3 and the condition $x_2 > \ell$ changes to $x_2 = \ell$. We make the following assumptions:

Assumption 1. *The collision between masses m_2 and m_3 is inelastic,* i.e., *m_2 and m_3 have identical velocities immediately after impact.*

Assumption 2. *The control force F_1 between masses m_1 and m_2 is not impulsive.*

The above two assumptions, along with the principle of conservation of linear momentum, give the following relations in terms of the position variables:

$$\begin{aligned} X_1(t^+) &= X_1(t^-) & y(t^+) &= y(t^-) \\ X_2(t^+) &= X_2(t^-) \quad \Rightarrow & x_2(t^+) &= x_2(t^-) \\ x_3(t^+) &= x_3(t^-) & x_3(t^+) &= x_3(t^-) \end{aligned} \tag{2.4}$$

and the following relations in terms of velocity variables:

$$\left.\begin{aligned} &\dot{X}_1(t^+) = \dot{X}_1(t^-) \\ &\dot{X}_2(t^+) = \dot{x}_3(t^+) = \frac{m_2\dot{X}_2(t^-) + m_3\dot{x}_3(t^-)}{m_2+m_3} \end{aligned}\right\} \Rightarrow \begin{aligned} \dot{y}(t^+) &= \dot{y}(t^-) + \frac{m_3}{m_2+m_3}\dot{x}_2(t^-) \\ \dot{x}_2(t^+) &= 0 \\ \dot{x}_3(t^+) &= \dot{x}_3(t^-) + \frac{m_2}{m_2+m_3}\dot{x}_2(t^-) \end{aligned} \tag{2.5}$$

2.2.3 Contact Phases

The contact phase commences immediately after the lower mass m_2 makes contact with the ground mass m_3. We make the following assumption which implies that the masses m_2 and m_3 cannot stick together:

Assumption 3. *The force F_2 acting between the masses m_2 and m_3 is non-negative,* i.e., *$F_2 \geqslant 0$.*

During contact, $x_2 = \ell$ and $\dot{x}_2 = \ddot{x}_2 = 0$. The system DOF is reduced to two and the

equations of motion are as follows:

$$\begin{aligned}\ddot{X}_1 &= (\ddot{y} + \ddot{x}_3) = -g + \frac{F_1}{m_1} \\ \ddot{x}_3 &= -g - \frac{1}{m_2 + m_3}(C_{\text{ext}}\,\dot{x}_3 + K_{\text{ext}}\,x_3 + F_1)\end{aligned} \tag{2.6}$$

The constraint force F_2 ($F_2 \geqslant 0$) associated with the constraint $x_2 = \ell$ and $\ddot{x}_2 = \dot{x}_2 = 0$is given by the expression

$$F_2 = m_1(\ddot{y} + \ddot{x}_3) + m_2\ddot{x}_3 + (m_1 + m_2)g \tag{2.7}$$

At the instant when the system switches from the contact phase to the flight phase, the reaction force F_2 equals zero.

2.2.4 Apex Height

If z denotes the height of the COM of the hopping robot in the flight phase, we have

$$\begin{aligned}z &= \frac{1}{m_1 + m_2}\left[m_1(y + x_2 + x_3) + m_2(x_2 + x_3)\right] \\ &= x_2 + x_3 + m_{\text{f}}\,y, \qquad m_{\text{f}} \triangleq \frac{m_1}{m_1 + m_2}\end{aligned} \tag{2.8}$$

where m_{f} is the mass fraction. The hopping robot will have multiple flight phases. For each flight phase, the apex height is defined as the maximum value of z, and is denoted by h.

2.3 Hybrid Control Strategy for Hopping on a Purely Elastic Ground

2.3.1 Change of Coordinates

For a purely elastic ground, we have

$$m_3 = 0, \qquad C_{ext} = 0, \qquad K_{ext} \neq 0 \tag{2.9}$$

There is no impact phase. Furthermore, substitution of (2.9) in (2.3) indicates $x_3 \equiv 0$ in the flight phase. Therefore, the system has two DOF in the flight phase. The system has two DOF in the contact phase as well since $x_2 = \ell$ and $\dot{x}_2 = 0$.

For the objective of apex height control, we define r to be the height of the COM of the robot relative to that of the lower mass m_2. Using (2.8), it can be shown

$$r \triangleq (z - x_2 - x_3) = m_{\mathrm{f}}\, y \tag{2.10}$$

Next, we define e as

$$e = (r - r_{\mathrm{d}}) \tag{2.11}$$

where $r_{\mathrm{d}} > 0$ is some desired value of r. From (2.10) and (2.11) it can be verified that $e \equiv 0 \rightarrow \dot{e} \equiv 0 \rightarrow \dot{y} \equiv 0$, which implies no relative motion between the two masses. The dynamics of the system in the flight and contact phases can be written in compact form

using (2.2), (2.6), (2.8), (2.9), (2.10) and (2.11) as follows:

$$\begin{aligned} \ddot{z} &= -g - \lambda \frac{1}{m_{\mathrm{t}}} K_{\mathrm{ext}}\, x_3, \qquad m_{\mathrm{t}} \triangleq (m_1 + m_2) \\ \ddot{e} &= \frac{1}{m_2}(F_1 - \lambda\, m_{\mathrm{f}} K_{\mathrm{ext}}\, x_3) \end{aligned} \tag{2.12}$$

where

$$\lambda = \begin{cases} 0 \quad : \quad x_2 > \ell : \text{Flight Phase} \\ 1 \quad : \quad x_2 = \ell : \text{Contact Phase} \end{cases} \tag{2.13}$$

The following choice of the control input

$$F_1 = \lambda\, m_{\mathrm{f}} K_{\mathrm{ext}} x_3 + m_2 v \tag{2.14a}$$

$$= \lambda\, m_{\mathrm{f}} F_{\mathrm{ext}} + m_2 v, \qquad F_{\mathrm{ext}} \triangleq K_{\mathrm{ext}} x_3 \tag{2.14b}$$

results in the hybrid dynamics

$$\ddot{z} = -g - \lambda \frac{1}{m_{\mathrm{t}}} K_{\mathrm{ext}}\, x_3 \tag{2.15}$$

$$\ddot{e} = v \tag{2.16}$$

where v is the new control input. Note that the control input F_1 can be chosen according to (2.14a) or (2.14b) depending on whether x_3 (displacement of the spring) or F_{ext} (force applied by the spring) is available for measurement.

2.3.2 Backstepping

The potential energy of the COM is defined relative to the datum $z = z_{\mathrm{d}}$

$$z_{\mathrm{d}} \triangleq z\,|_{(x_3=0,\, x_2=\ell,\, r=r_{\mathrm{d}})} = (r_{\mathrm{d}} + \ell) \tag{2.17}$$

In the absent of relative motion between the masses ($e = \dot{e} = 0$), the total energy can be written as

$$E = m_{\mathrm{t}} \left[\frac{1}{2} \dot{z}^2 + g(z - z_{\mathrm{d}}) \right] + \frac{1}{2} \lambda K_{\mathrm{ext}} \left(z - z_{\mathrm{d}} \right)^2 \tag{2.18}$$

For the robot to reach its desired apex height h_{d}, the total energy should be equal to

$$E \equiv E_{\mathrm{des}} = m_{\mathrm{t}}\, g(h_{\mathrm{d}} - z_{\mathrm{d}}) \tag{2.19}$$

where h_d is the desired value of apex height. In addition to $e \equiv 0$. The desired equilibrium configuration is therefore given by

$$(E - E_{\mathrm{des}}, e, \dot{e}) = (0, 0, 0) \tag{2.20}$$

With the objective of stabilizing the equilibrium in (2.20), we define the Lyapunov function candidate

$$V_1 = \frac{1}{2} k_e \left(E - E_{\mathrm{des}} \right)^2, \qquad k_e > 0 \tag{2.21}$$

It should be noted that V_1 is a function of λ (since E is a function of λ) but it is continuously differentiable in both the flight phase and contact phase. The Lyapunov function candidates introduced in this section will be used for stability analysis in the two phases separately; therefore, we treat λ as constant and do not make any distinction between the two phases in our derivation. Using (2.11), (2.16), and (2.18), $\dot{V}_1$ can be computed as

$$\begin{aligned} \dot{V}_1 &= k_e \left(E - E_{\mathrm{des}} \right) \dot{E} \\ &= k_e \left(E - E_{\mathrm{des}} \right) \dot{z} \left[m_{\mathrm{t}} (\ddot{z} + g) + \lambda K_{\mathrm{ext}} (z - z_d) \right] \\ &= k_e \left(E - E_{\mathrm{des}} \right) \lambda K_{\mathrm{ext}} \dot{z} e \end{aligned} \tag{2.22}$$

By choosing

$$e = \left\{ -\lambda k_e \left(E - E_{\mathrm{des}} \right) \dot{z} \right\} \triangleq \varphi_1 \tag{2.23}$$

we can make $\dot{V}_1$ negative semi-definite; therefore, integrator backstepping is introduced by defining the new variable

$$q_1 = e + \lambda k_e \left(E - E_{\text{des}}\right) \dot{z} = (e - \varphi_1) \tag{2.24}$$

and the composite Lyapunov function

$$V_2 = V_1 + \frac{1}{2} q_1^2 = \frac{1}{2} k_e \left(E - E_{\text{des}}\right)^2 + \frac{1}{2} q_1^2 \tag{2.25}$$

Differentiating V_2 and substituting (2.22) and (2.24), we get

$$\begin{aligned} \dot{V}_2 &= k_e \left(E - E_{\text{des}}\right) \lambda K_{\text{ext}} \dot{z} e + q_1 \dot{q}_1 \\ &= k_e \left(E - E_{\text{des}}\right) \lambda K_{\text{ext}} \dot{z} \left[q_1 - \lambda k_e \left(E - E_{\text{des}}\right) \dot{z}\right] + q_1 \dot{q}_1 \\ &= -\lambda^2 k_e^2 K_{\text{ext}} \left(E - E_{\text{des}}\right)^2 \dot{z}^2 \\ &\qquad + q_1 \left[\dot{q}_1 + k_e \left(E - E_{\text{des}}\right) \lambda K_{\text{ext}} \dot{z}\right] \end{aligned} \tag{2.26}$$

By choosing

$$\dot{q}_1 = \left\{-\lambda k_e K_{\text{ext}} \left(E - E_{\text{des}}\right) \dot{z} - k_1 q_1\right\} \triangleq \varphi_2 \tag{2.27}$$

where $k_1 > 0$. We can make $\dot{V}_2$ negative semi-definite. We introduce integrator backstepping again by defining the new variable

$$q_2 = (\dot{q}_1 - \varphi_2) \tag{2.28}$$

and the composite Lyapunov function

$$\begin{aligned} V_3 &= V_2 + \frac{1}{2} q_2^2 \\ &= \frac{1}{2} k_e \left(E - E_{\text{des}}\right)^2 + \frac{1}{2} q_1^2 + \frac{1}{2} q_2^2 \end{aligned} \tag{2.29}$$

Differentiating V_3 and substituting (2.26) and (2.28), we get

$$\begin{aligned}
\dot{V}_3 &= -\lambda^2 k_e^2 K_{\text{ext}} \left(E - E_{\text{des}}\right)^2 \dot{z}^2 \\
&\quad + q_1 \left[\dot{q}_1 + \lambda k_e K_{\text{ext}} \left(E - E_{\text{des}}\right) \dot{z}\right] + q_2 \dot{q}_2 \\
&= -\lambda^2 k_e^2 K_{\text{ext}} \left(E - E_{\text{des}}\right)^2 \dot{z}_2^2 \\
&\quad + q_1 \left[\dot{q}_1 - \varphi_2 - k_1 q_1\right] + (\dot{q}_1 - \varphi_2)(\ddot{q}_1 - \dot{\varphi}_2) \\
&= -\lambda^2 k_e^2 K_{\text{ext}} \left(E - E_{\text{des}}\right)^2 \dot{z}^2 - k_1 q_1^2 \\
&\quad + q_2 \left[\ddot{q}_1 - \dot{\varphi}_2 + q_1\right]
\end{aligned} \tag{2.30}$$

Our choice of

$$\ddot{q}_1 = \dot{\phi}_2 - q_1 - k_2 q_2, \qquad k_2 > 0 \tag{2.31}$$

results in a negative semi-definite $\dot{V}_3$ and yields the controller

$$v = \ddot{\phi}_1 + \dot{\phi}_2 - q_1 - k_2 q_2 \tag{2.32}$$

The above equation was obtained from (2.31) by substituting the value of $\ddot{e}$ in (2.16) and (2.24) into (2.31). From the definition of φ_1, it is clear that $\ddot{\varphi}_1$ will involve the third derivative of z. This is not a problem since the second derivative of z can be computed easily from (2.15) as

$$\dddot{z} = -\lambda \frac{1}{m_{\text{t}}} K_{\text{ext}} (\dot{z} - \dot{e}) \tag{2.33}$$

2.3.3 Stability Analysis

Using (2.10), (2.11), (2.15), (2.18), (2.24) and (2.28) it can be shown that

$$(E - E_{\text{des}}, e, \dot{e}) = (0, 0, 0) \;\Leftrightarrow\; (E - E_{\text{des}}, q_1, q_2) = (0, 0, 0)$$

Therefore, V_3 in (2.29) is a candidate Lyapunov function for investigating the stability of the equilibrium in (2.20). In both flight and contact phases ($\lambda = 0$ and $\lambda = 1$), the control law in (2.32), results in (2.30)

$$\dot{V}_3 \leqslant 0 \tag{2.34}$$

Therefore, $(E - E_{\text{des}}, q_1, q_2) = (0, 0, 0)$ is stable.

Remark 1. *The stability of* $(E - E_{\text{des}}, q_1, q_2) = (0, 0, 0)$ *in the flight and contact phases do not guarantee stability for the hybrid dynamics. The stability of the hybrid system is analyzed next .*

2.4 Hopping on a Viscoelastic Ground with Inertia

2.4.1 Discrete Controller for Stabilization and Control Apex Height

To investigate the stability of the hybrid dynamic system, we use a Poincaré map with the Poincaré section defined at the point of touch-down, *i.e.* the time instant prior to impact. To restrict the Poincaré section to a one-dimensional configuration space, we make the following assumption:

Assumption 4. *The parameters of the viscoelastic ground (m_3, C_{ext}, K_{ext}) are such that the settling time of the system is less than the hopping period of the robot.*

Remark 2. *The above assumption allows us to infer that $x_3, \dot{x}_3 \approx 0$ at the time of touch-down. It will be shown later that the assumption is not overly restrictive.*

Assuming that $x_3, \dot{x}_3, e, \dot{e} \approx 0$ at the time of touch-down, the modified Poincaré section is chosen as

$$\mathcal{Z} := \{X \in \mathbb{R} |\ z = z_d, e = 0, \dot{e} = 0,\ \dot{z} < 0\} \tag{2.35}$$

where X is defined as

$$X = \dot{z} \tag{2.36}$$

To use the same set of variables used in the backstepping controller in section 2.3 (designed for the purely elastic ground), namely, $(E - E_{\text{des}})$, we defined the Poincaré section using the coordinates Ψ, where Ψ is defined by the coordinate transformation $H(\cdot) : \mathbb{R} \Rightarrow \mathbb{R}$, as follows

$$\Psi = (E - E_{\text{des}}) = H(X) \tag{2.37}$$

The Poincaré map $Q(\Psi)$ and the sequence of points $\Psi_k \in H(\bar{\mathcal{Z}})$ now satisfy

$$\Psi_{k+1} = Q(\Psi_k), \quad Q(\Psi) : H(\bar{\mathcal{Z}}) \mapsto H(\bar{\mathcal{Z}}) \tag{2.38}$$

with periodic point Ψ^* defined as

$$\Psi^* = Q(\Psi^*) \tag{2.39}$$

For the elastic ground, the periodic point which achieves the desired apex height is given by

$$\Psi^* = (\bar{E} - E_{\text{des}}) \tag{2.40}$$

where $\bar{E}$ is the energy of the system in steady state when the backstepping controller is invoked with $E_{\rm d} = E_{\rm des}$. The value of $\bar{E}$ is initially unknown but can be determined after the robot has hopped a few times - see section 2.4.2. We define the error state η_k as

$$\eta_k = (\Psi_k - \Psi^*) = (E_k - \bar{E})$$

By linearizing the Poincaré map about Ψ^*, we have the approximate discrete dynamics given by

$$\eta_{k+1} = A_0\, \eta_k \qquad A_0 \stackrel{\Delta}{=} \left.\frac{dQ(\Psi)}{d\Psi}\right|_{\Psi=\Psi*} \tag{2.41}$$

The periodic point will be asymptotically stable if and only if

$$\rho(A_0) < 1 \tag{2.42}$$

where $\rho(A_o)$ is the spectral radius of A_o. To design the discrete controller, we describe Ψ as follows

$$\begin{aligned} &\Psi = \Phi + u \\ &\Phi \stackrel{\Delta}{=} (E - E_{\rm d}), \quad u \stackrel{\Delta}{=} (E_{\rm d} - E_{\rm des}) \end{aligned} \tag{2.43}$$

where $E_{\rm d}$ is desired level of energy for a given hop. The new Poincaré map $\bar{Q}(\Phi, u)$ and the sequence of points $\Phi_k \in H(\bar{\mathcal{Z}})$ satisfy

$$\Phi_{k+1} = \bar{Q}(\Phi_k, u_k), \quad \bar{Q}(\Phi, u) : H(\bar{\mathcal{Z}}) \times R \mapsto H(\bar{\mathcal{Z}}) \tag{2.44}$$

with periodic point Φ^* defined as

$$\Phi^* = \bar{Q}(\Phi^*, u^*) \tag{2.45}$$

For the viscoelastic ground with inertia, there exists the following equilibrium point

$$\Phi^* = (\bar{E} - E_{\rm d}), \qquad u^* = 0 \tag{2.46}$$

If we define the error state

$$\mu_k \stackrel{\Delta}{=} (\Phi_k - \Phi^*) = (E_k - \bar{E}) \tag{2.47}$$

the Poincaré map $\bar{Q}(\Phi_k, u_k)$ can be linearized about (Φ^*, u^*) to yield the following linear discrete-time system

$$\begin{aligned} &\mu_{k+1} = \bar{A}\,\mu_k + \bar{B}u_k, \quad y_k = \mu_k \\ &\bar{A} \stackrel{\Delta}{=} \left.\frac{d\bar{Q}(\Phi,u)}{d\Phi}\right|_{\substack{\Phi=\Phi^* \\ u=u^*}}, \quad \bar{B} \stackrel{\Delta}{=} \left.\frac{d\bar{Q}(\Phi,u)}{du}\right|_{\substack{\Phi=\Phi^* \\ u=u^*}} \end{aligned} \tag{2.48}$$

To converge the system energy from its level at the equilibrium configuration $\bar{E}$ to the desired value $E_{\rm des}$, we propose to use integral control with the integrator defined as

$$\theta_{k+1} = \theta_k + (E_0 - y_k), \quad E_0 \stackrel{\Delta}{=} (E_{\rm des} - \bar{E}) \tag{2.49}$$

where E_0 is the desired value of the output variable y. The integrator-augmented discrete system has the form

$$\begin{aligned} &\lambda_{k+1} = \mathbb{A}\lambda_k + \mathbb{B}u_k + E_0, \quad \lambda_k = \begin{bmatrix} \mu_k^T & \theta_k \end{bmatrix}^T \\ &\mathbb{A} \stackrel{\Delta}{=} \begin{bmatrix} \bar{A} & 0 \\ -1 & 1 \end{bmatrix}, \quad \mathbb{B} \stackrel{\Delta}{=} \begin{bmatrix} \bar{B} \\ 0 \end{bmatrix} \end{aligned} \tag{2.50}$$

If $\{\mathbb{A}, \mathbb{B}\}$ is controllable, the input can be chosen as

$$u_k = \mathbb{K}\lambda_k \tag{2.51}$$

where $\mathbb{K}$ satisfies

$$\rho(\mathbb{A} + \mathbb{B}\mathbb{K}) < 1$$

2.4.2 Simulation Results: Apex Height Control

We investigate the behavior of the two-DOF robot hopping on the viscoelastic ground with inertia; the discrete integral controller is used along with the continuous backstepping controller. The mass, stiffness, and damping properties were assumed to be

$$\begin{aligned} m_1 = 2.6 \text{ kg}, \qquad m_2 = 0.8 \text{ kg}, \qquad m_3 = 0.04\,\text{kg} \\ \ell = 0.06 \text{ m}, \quad K_{\text{ext}} = 2800 \text{ N/m}, \quad C_{\text{ext}} = 22\,\text{Ns/m} \end{aligned} \tag{2.52}$$

The mass of the ground was assumed to be 5% of the lower mass m_2 and the damping coefficient C_{ext} was chosen such that the ground is slightly overdamped. The desired apex height was chosen to be

$$h_{\text{d}} = 0.25 \text{ m}$$

and, similar to the last simulation, $r_{\text{d}} = 0.0994$ m was used. The continuous controller parameters were chosen as

$$k_e = 0.001, \qquad k_1 = 200, \qquad k_2 = 100$$

The matrix $\mathbb{A}$, defined in (2.50), was found to have eigenvalues: 1, and 0.004. Since $\{\mathbb{A}, \mathbb{B}\}$ is controllable, the controller gains were chosen as

$$\mathbb{K} = \begin{bmatrix} -0.35 & 0.7 \end{bmatrix}$$

This places the eigenvalues of the closed loop system at 0.9, and 0.3. The initial conditions were assumed to be

$$\begin{aligned} x_2(0) &= 0.06\,\text{m}, & x_3(0) &= -0.012\,\text{m}, & y(0) &= 0.075\,\text{m} \\ \dot{x}_2(0) &= 0.0\,\text{m/s}, & \dot{x}_3(0) &= 0.0\,\text{m/s}, & \dot{y}(0) &= 0.0\,\text{m/s} \end{aligned} \tag{2.53}$$

and the initial value of the integrator state was set to zero.

The simulation results are shown in Figs.2.2, 2.3, 2.4 and 2.5. The displacements of the upper mass, lower mass, COM, and ground mass are plotted in Fig.2.2. The contact phases (not explicitly shown in Fig.2.2) are the time intervals during which $x_2 = (X_2 - x_3) = 0.06$ m. The value of $X_2(0) = 0.048$ m indicates that the spring of the viscoelastic ground is initially compressed due to the weight of the robot. The simulation is comprised of two phases. In the initial phase, $0 \leqslant t \leqslant 1.8$ s, the discrete controller was switched off and the backstepping controller was used with $E_\text{d} = E_\text{des}$. During this phase (five hops), the apex

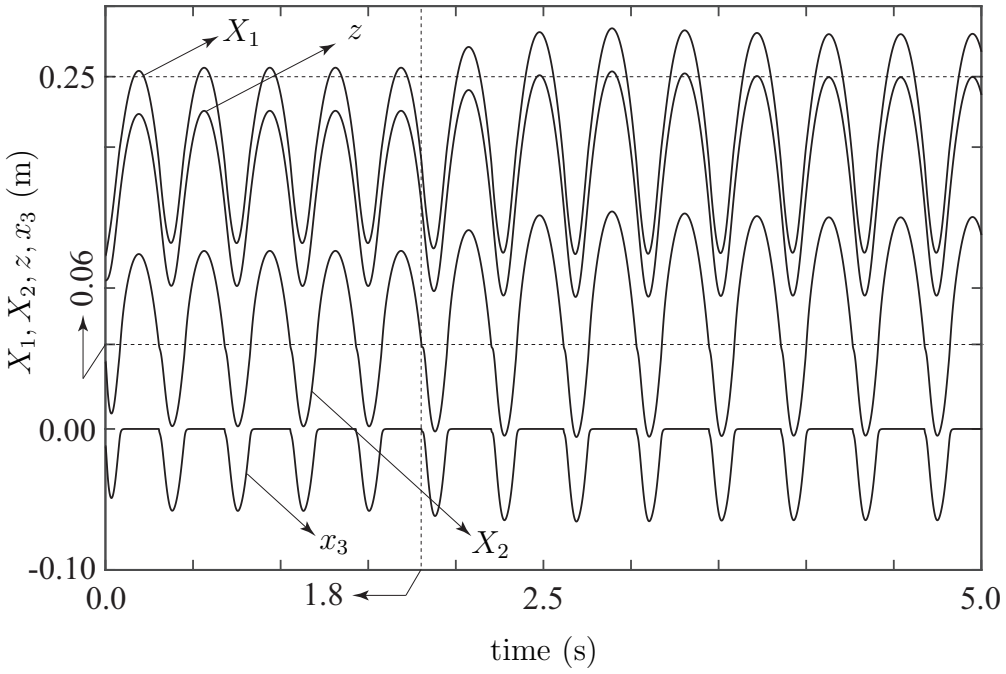

Figure 2.2: Simulation results for hopping on a viscoelastic ground with inertia. Plot of the position of the upper mass X_1, the lower mass X_2, COM z, and the ground mass x_3, as a function of time.

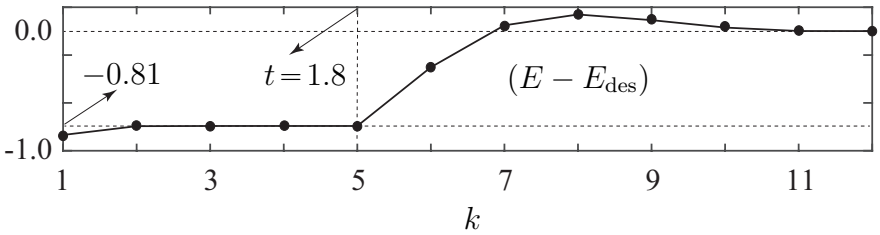

Figure 2.3: Simulation results for hopping on a viscoelastic ground with inertia: Plot of $(E - E_{\text{des}})$ at the end of the k-th hop (immediately before touch-down), $k = 1, 2, \cdots, 12$. The actual time scale in the figure is identical to the time scale in Fig.2.2

height of the robot converges to a constant value that corresponds to $E = \bar{E}$, which was defined in the context of (2.40). The value of $\bar{E}$ was found to be 2.21 J and $E_0 = 0.81$ J (the deficit) was computed using (2.49). Using the value of E_0, the discrete controller was switched on at $t = 1.8$ s. The first element of Ψ is plotted in Fig.2.3; it corresponds to the value of $(E - E_{\text{des}})$ at the end of the k-th hop, $k = 1, 2, \cdots, 12$ - see Fig.2.3. Figure 2.4 shows the control input (F_1), it can be seen that the force is zero when there is no relative displacement between the masses $(e = \dot{e} = 0)$.

The displacement of the lower mass and the ground is shown in Fig.2.5 for one hop. It can be seen that the lower mass breaks contact with the ground mass below the datum

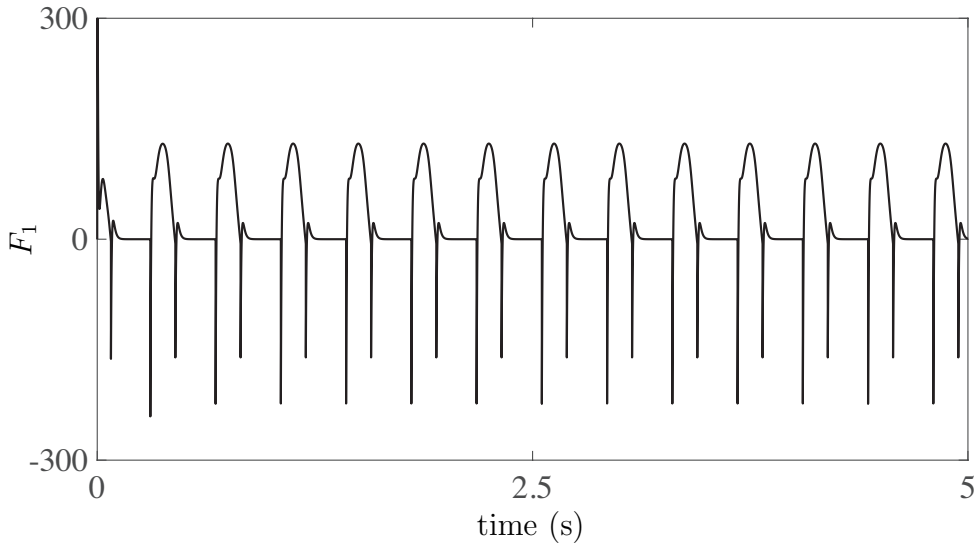

Figure 2.4: Plot of the Force F_1 applied by the prismatic joint.

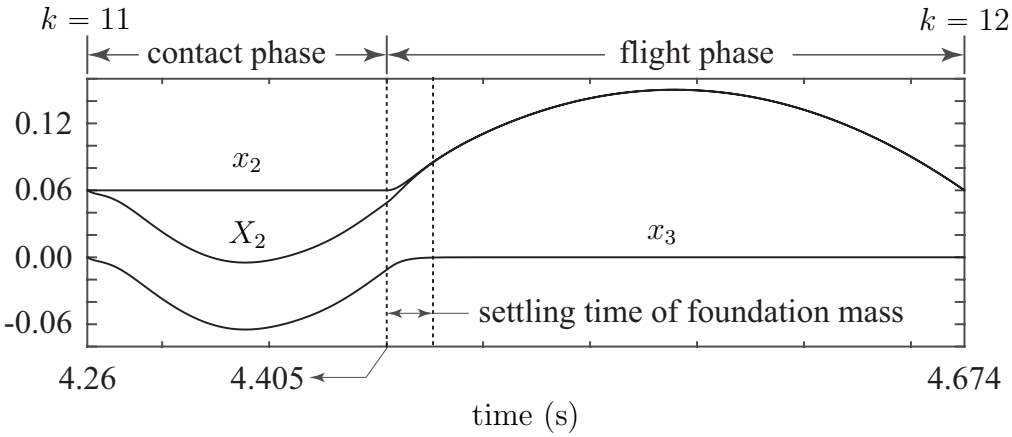

Figure 2.5: Simulation results for hopping on a viscoelastic ground with inertia: Plot of X_2, x_2, and x_3 for the hop between $k = 11$ and $k = 12$.

($x_2 > \ell$, $x_3 < 0$) at $t = 4.405$ s. While the robot is in flight, the ground mass settles to its equilibrium configuration; the response is overdamped, as expected from the choice of parameters in (2.52), and has a 2% settling time of 0.022 s. Since the settling time of the ground mass is much smaller than the flight phase, it becomes clear that *Assumption 4* is not overly restrictive.

In steady state ($k \geqslant 11$), the integral controller was found to command the backstepping controller with $E_{\mathrm{d}} = 3.93$ J. This is higher than the value of E_{des} by an amount equal to 0.91 J, which is larger than the value of $E_0 = 0.81$ J. This is not surprising since a higher value of E_{d} results in a higher deficit due to greater losses associated with hopping with a larger apex height.

A video animation of a two-DOF prismatic joint robot hopping on a viscoelastic ground with inertia has been uploaded as supplementary material. It shows the hopper reaching the desired apex height of $h_d = 0.25$ m starting from rest.

2.5 Conclusion

This chapter presents a method for controlling the apex height of a two-mass robot hop-

ping on a viscoelastic ground with inertia. This problem, which has not been investigated earlier, is more challenging than the problems of hopping on rigid and elastic grounds since the system has an extra DOF and there is energy loss due to impact and damping. A continuous-time backstepping controller was used in concert with a discrete-time integral controller to meet the control objective. The backstepping controller regulates the energy of the robot using the internal DOF and simultaneously eliminates this DOF to enable the robot reach its desired apex height. We use the same backstepping controller was developed for elastic ground results is steady-state error. The discrete-time integral controller eliminates this error by commanding the backstepping controller to regulate the energy to a commensurately higher level. Since there is loss of energy in every hop, the backstepping controller has to remain active for all hops. A video animation of apex height control is includes to provide a glimpse of the dynamic behavior.

Chapter 3

Apex Height Control of a Two-DOF Ankle-Knee-Hip Robot Hopping on a Rigid Ground

3.1 Introduction

In this chapter, we develop a strategy for controlling the apex height of a two-DOF Ankle-Knee-Hip (AKH) robot, hopping on a rigid ground [34]. Although the AKH robot has the same number of DOFs as the prismatic-joint robot, studied earlier [21,33] and in Chapter 2, its kinematic structure is more anthropomorphic and similar to biped robots. The control problem for the AKH is more challenging than the prismatic-joint robot due to the revolute nature of the joints. Hopping on a rigid ground results in energy losses due to impact of the robot with the ground. A continuous and a discrete controller with integral action are developed to drive the apex height of the AKH robot to a desired value. To compensate for the losses, the continuous controller employs negative damping while the velocity of the COM is moving upwards during the contact phase. Using a Poincaré map at the take-off point, we constructed a discrete-time system. The discrete-time controller adjusts the negative damping parameter used by the continuous controller to control the apex height. The dependence of the apex height on the controller parameters is studied to understand the

role of constraints imposed by the robot structure. Simulation results are presented to show the efficacy of the control strategy. This Chapter is structured as follows. The dynamics of the robot is presented in Section 3.2. The continuous and discrete controllers are presented in Sections 3.3 and 3.4. The effect of continuous controller parameters on hopping behavior is discussed in Section 3.5. Numerical simulation results are presented in Section 3.6. Section 3.7 contains concluding remarks.

3.2 Dynamics of AKH Robot

3.2.1 System Description and Model

Consider the AKH hopping robot shown in Fig. 3.1. It is comprised of an upper mass m_{b} and a lower mass m_{f}, both of which are constrained to move along the vertical axis. The masses are connected by two links, each of which have mass m and length ℓ. The mass moment of inertia of the two links are equal and denoted by I. The displacements of the masses m_{b} and m_{f} are denoted by y_2 and y_1, respectively. These two variables correspond to the two degrees of freedom of the robot in the flight phase. The angular displacement of the upper link, measured counter-clockwise with respect to the vertical axis, is denoted by ϕ. The robot has a single actuator that drives the angular coordinate ϕ, the torque applied by this actuator is denoted by τ. The vertical force applied on the lower mass m_{f} by the the ground during contact is denoted by F_{ext}. The dynamic model of the robot is obtained using Lagrange's equations:

$$M(q)\ddot{q} + N(q, \dot{q}) = Q \tag{3.1}$$

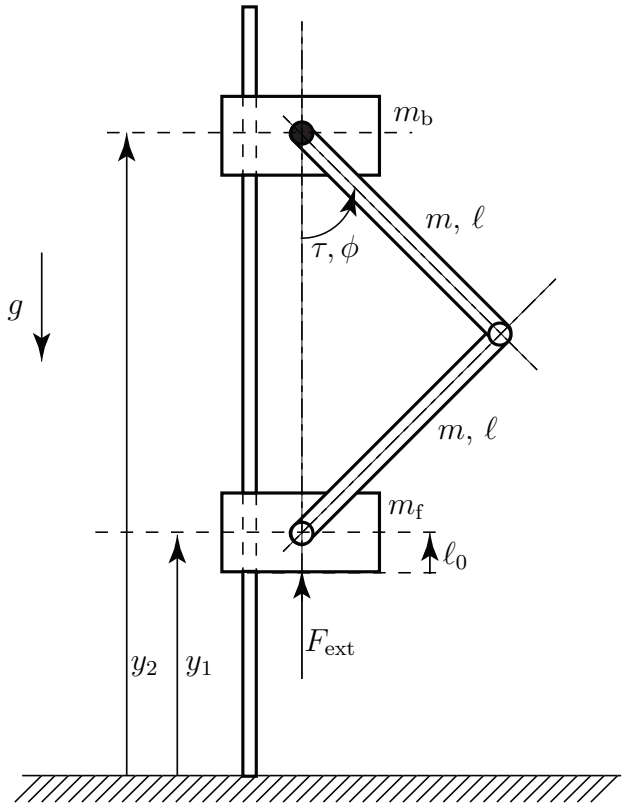

Figure 3.1: The ankle-knee-hip robot.

where $q = \begin{bmatrix} y_1 & \phi \end{bmatrix}^T$, $Q = \begin{bmatrix} F_{\rm ext} & \tau \end{bmatrix}^T$ is the vector of generalized forces, and the elements of $[M_{ij}]_{2\times 2}$ and $[N_i]_{2\times 1}$ are

$$
\begin{aligned}
M_{11} &= m_{\rm t} \triangleq (m_{\rm b} + m_{\rm f} + 2m) \\
M_{12} &= M_{21} = -2\ell(m + m_{\rm b}) \sin\phi \\
M_{22} &= \frac{1}{3}\ell^2 \left[5m + 6m_{\rm b} - 3(m + 2m_{\rm b}) \cos 2\phi\right] \\
N_1 &= g m_{\rm t} - 2\ell(m + m_{\rm b}) \cos\phi\, \dot{\phi}^2 \\
N_2 &= 2\ell \left[-g(m + m_{\rm b}) + \ell(m + m_{\rm b}) \cos\phi\right] \sin\phi
\end{aligned}
\tag{3.2}
$$

The hybrid dynamics of the hopping robot is comprised of the flight phase, the impact phase, and the contact phase.

3.2.2 Flight Phase

In the flight phase, the robot has two DOF and the following conditions hold:

$$y_1 > \ell_0 \qquad F_{\text{ext}} = 0 \tag{3.3}$$

The equation of motion is described by (3.1), where $F_{\text{ext}} = 0$.

3.2.3 Impact Phase

The impact phase refers to infinitesimal intervals of time $t \in [t^-, t^+]$ during which the lower mass m_{f} comes in contact with the ground and the condition $y_1 > \ell_0$ changes to ℓ_0 ($y_1 = \ell_0$). We make the following assumptions:

Assumption 5. *The impact between lower mass m_{f} and the ground is inelastic,* i.e., $\dot{y}_1(t^+) = 0$.

Assumption 6. *The control torque τ is not impulsive.*

The position variables satisfy:

$$y_1(t^+) = y_1(t^-) \qquad \phi(t^+) = \phi(t^-) \tag{3.4}$$

By integrating (3.1) over the interval $[t^-, t^+]$, we get

$$\dot{y}_1(t^+) = 0 \qquad \dot{\phi}(t^+) = \dot{\phi}(t^-) + \frac{M_{21}}{M_{22}}\dot{y}_1(t^-) \tag{3.5}$$

3.2.4 Contact Phase

The contact phase commences immediately after the lower mass m_{f} makes contact with the ground. We now assume:

Assumption 7. *The external force F_{ext} acting on the lower mass m_{f} is non-negative,* i.e.*, $F_{\mathrm{ext}} \geqslant 0$.*

During contact phase, $y_1 = \ell_0$ and $\dot{y}_1 = \ddot{y}_1 = 0$; the system DOF one. Using (3.1), the value of the F_{ext} can be computed as

$$F_{\mathrm{ext}} = N_1 + (M_{12}/M_{22})\,(\tau - N_2) \tag{3.6}$$

Substituting (3.5) into (3.1), we get

$$\begin{aligned} M(q)\ddot{q} + \begin{bmatrix} M_{12}/M_{22} \\ 1 \end{bmatrix} N_2 &= \begin{bmatrix} M_{12}/M_{22} \\ 1 \end{bmatrix} \tau \\ \Rightarrow \ddot{q} = M^{-1}(q) \begin{bmatrix} M_{12}/M_{22} \\ 1 \end{bmatrix} (\tau - N_2) &= \begin{bmatrix} 0 \\ 1 \end{bmatrix} \frac{(\tau - N_2)}{M_{22}} \end{aligned} \tag{3.7}$$

At the instant when the system switches from the contact phase to the flight phase, F_{ext} equals zero, which implies

$$N_1 + (M_{12}/M_{22})\,(\tau - N_2) = 0 \tag{3.8}$$

3.2.5 Apex Height

The COM in the flight phase is denoted by

$$
\begin{aligned}
z =& \frac{1}{m_{\mathrm{t}}}\left[m_{\mathrm{f}} y_1 + m(y_1 + \frac{1}{2}\ell\cos\phi) + m(y_1 + \frac{3}{2}\ell\cos\phi) + m_{\mathrm{b}}(y_1 + 2\ell\cos\phi)\right] \\
=& y_1 + 2\ell m_{\mathrm{z}}\cos\phi, \qquad m_{\mathrm{z}} \triangleq \frac{m + m_{\mathrm{b}}}{m_{\mathrm{t}}}
\end{aligned} \tag{3.9}
$$

For each flight phase, the apex height h is defined as the maximum value of z.

3.3 Continuous Control Design

3.3.1 Relative Displacement of COM

Using (3.9), we define the displacement of the COM relative to the lower mass as

$$
r \triangleq (z - y_1) = 2\ell m_{\mathrm{z}}\cos\phi \tag{3.10}
$$

$$
\Rightarrow \quad \dot{r} = -2\ell m_{\mathrm{z}}\sin\phi\,\dot{\phi} \tag{3.11}
$$

We define the desired equilibrium point of the system to be $(r, \dot{r}) = (r_{\mathrm{d}}, 0)$, where $r_{\mathrm{d}} > 0$ is the desired value of r.

3.3.2 Contact Phase Control Design

During the contact phase, the system has one DOF since $y_1 \equiv \ell_0$. To transform this dynamics described by (3.7) into the normal form [26], we use (3.10), and (3.11) to define the states

$$
\xi_1 = r - r_{\mathrm{d}}, \qquad \xi_2 = \dot{r} \tag{3.12}
$$

The dynamics of the system in normal form is

$$\dot{\xi}_1 = \xi_2, \quad \dot{\xi}_2 = -2\ell m_z \cos\phi\, \dot{\phi}^2 - 2\ell m_z \sin\phi\, \ddot{\phi} \tag{3.13}$$

Substituting the value of $\ddot{\phi}$ in (3.7) into (3.13), and defining the torque τ to be

$$\tau = N_2 + \frac{M_{22}}{2m_z\ell \sin\phi}(-v - 2m_z\ell \cos\phi\, \dot{\phi}^2) \tag{3.14}$$

we get

$$\dot{\xi}_1 = \xi_2, \qquad \dot{\xi}_2 = v \tag{3.15}$$

We choose v as

$$v = -\omega_n^2 \xi_1 - 2\zeta\omega_n \alpha \xi_2, \qquad \zeta < 1 \tag{3.16}$$

where

$$\alpha = \begin{cases} 1 & \xi_2 \leqslant 0 \\ \nu & \xi_2 > 0 \end{cases}, \qquad \nu < 0 \tag{3.17}$$

which will make the relative displacement r behave like an underdamped mass-spring-damper system when $\alpha = 1$ or $\xi_2 \leqslant 0$, and a mass-spring system with negative damping for $\xi_2 > 0$. The magnitude of ν will determine the amount of energy that will be added to the system during the contact phase to achieve the desired apex height.

3.3.3 Flight Phase Control Design

In the Flight phase, the system will have two DOF. To transform the system to the

normal form [26], we use the states defined in (3.12) together with

$$\eta_1 = z - z_{\rm d} \qquad \eta_2 = \dot{z} \tag{3.18}$$

where $z_{\rm d} = r_{\rm d} + \ell_0$. The dynamics of the system in normal form can be written as

$$\begin{aligned} \dot{\eta}_1 &= \dot{z} \qquad & \dot{\eta}_2 &= \ \ddot{y}_1 - 2m_{\rm z}\ell\cos\phi\,\dot{\phi}^2 - 2m_{\rm z}\ell\sin\phi\,\ddot{\phi} \\ \dot{\xi}_1 &= \xi_2 \qquad & \dot{\xi}_2 &= -2m_{\rm z}\ell\cos\phi\,\dot{\phi}^2 - 2m_{\rm z}\ell\sin\phi\,\ddot{\phi} \end{aligned} \tag{3.19}$$

Substituting the values of $\ddot{y}_1$ and $\ddot{\phi}$ from (3.1) into (3.19), and defining the torque τ to be

$$\tau = N_2 + (1/M_{11})\left[- M_{21}N_1 - (M_{11}M_{22} - M_{12}M_{21})\,\frac{\left(\nu + 2m_{\rm z}\ell\cos\phi\,\dot{\phi}^2\right)}{2m_{\rm z}\ell\sin\phi}\right] \tag{3.20}$$

we get

$$\begin{aligned} \dot{\eta}_1 &= \eta_2 \quad & \dot{\eta}_2 &= -g \\ \dot{\xi}_1 &= \xi_2 \quad & \dot{\xi}_2 &= \nu \end{aligned} \tag{3.21}$$

We choose v to be given by

$$v = -\omega_n^2\xi_1 - 2\zeta\omega_n\xi_2, \qquad \zeta < 1 \tag{3.22}$$

This will make the of the relative displacement r like an underdamped mass-spring-damper.

3.3.4 Closed-Loop System Dynamics

With the continuous controllers for the contact and flight phases given by (3.14), and (3.20), the hybrid dynamics of the closed-loop system is described by the following equations

in the contact phase

$$\dot{\xi}_1 = \xi_2, \qquad \dot{\xi}_2 = -\omega_n^2 \xi_1 - 2\zeta\omega_n \alpha \xi_2 \tag{3.23}$$

and the following equations in the flight phase

$$\begin{aligned} \dot{\eta}_1 &= \eta_2 \qquad \dot{\eta}_2 = -g \\ \dot{\xi}_1 &= \xi_2 \qquad \dot{\xi}_2 = -\omega_n^2 \xi_1 - 2\zeta\omega_n \xi_2 \end{aligned} \tag{3.24}$$

The contact phase ends when $F_{\text{ext}} = 0$, which is described by (3.8). By substituting (3.2), (3.9), (3.14), and (3.16) into (3.8), we get the relation

$$g - \omega_n^2 \xi_1 - 2\zeta\omega_n \nu \xi_2 = 0 \tag{3.25}$$

which will be used for analysis in section 3.5.

3.4 Discrete Control Design for the Apex Height

3.4.1 Poincaré Section

A single hop starts at the takeoff point in the flight phase and ends when the lower mass breaks contact with the ground in the contact phase, immediately prior to takeoff. Each hop can be divided into three time intervals: Δt_1 denoting the time during which the robot is in flight phase, Δt_2 denoting the time in the contact phase with $\dot{r} \leqslant 0$, and Δt_3 denoting the

time in the contact phase with $\dot{r} > 0$. The total time required for a single hop is

$$T = \Delta t_1 + \Delta t_2 + \Delta t_3 \tag{3.26}$$

For a single hop, starting at $t = 0$, it can be shown that the following conditions hold

$$\begin{aligned} &\eta_1(0) = \xi_1(0), \qquad \eta_2(0) = \xi_2(0) \\ &g - \omega_n^2 \xi_1(0) - 2\zeta\omega_n\nu\xi_2(0) = 0 \end{aligned} \tag{3.27}$$

where the last condition is obtained from (3.25). The three constraints in (3.27) imply that the takeoff point is described by one free variable, which we denote by χ. The variable χ belong to the set Ω, where

$$\Omega = \{\xi_2 \mid \eta_1 = \xi_1, \eta_2 = \xi_2, \omega_n^2\xi_1 + 2\zeta\omega_n\nu\xi_2 = g\} \tag{3.28}$$

The first return map between two hops can be described by the discrete system dynamics

$$\chi(k+1) = P(\chi(k), \Delta t_1, \Delta t_2, \Delta t_3) \tag{3.29}$$

where $P(.)$ is the Poincaré map. The time intervals Δt_1, Δt_2, and Δt_3 can be solved using the following conditions

$$\begin{aligned} &\eta_1(\Delta t_1) = \xi_1, \quad \xi_2(\Delta t_1 + \Delta t_2) = 0 \\ &g - \omega_n^2 \xi_1(T) - 2\zeta\omega_n\nu\xi_2(T) = 0 \end{aligned} \tag{3.30}$$

Therefore, the return map can be written as

$$\chi(k+1) = P(\chi(k)) \tag{3.31}$$

A fixed point χ satisfies

$$\chi^* = P(\chi^*) \tag{3.32}$$

By linearizing the dynamics described by (3.31) about χ^*, we claim asymptotic stability of χ^* if

$$\rho\left[\frac{\partial P(\chi)}{\partial \chi} \mid_{\chi=\chi^*}\right] < 1 \tag{3.33}$$

where $\rho(.)$ is the spectral radius.

3.4.2 Discrete Controller Design

For a fixed set of parameters of the continuous controller, namely, ζ, ω_n, ν and r_d, a given value of χ results in an unique apex height h. Therefore, given a desired apex height h_{d}, we first solve the inverse problem of determining continuous controller parameter values that result in $\chi = \chi_{\mathrm{d}}$. We stabilize the point $\chi = \chi_{\mathrm{d}}$ by varying one or more of the continuous controller parameters at the takeoff point. Here, we choose to vary ν only; the dynamics of the controlled system (3.31) can be described by the map

$$\chi(k+1) = P(\chi(k), \nu) \tag{3.34}$$

By linearizing the above map about the fixed point $\chi^* = \chi_{\mathrm{d}}$, $\nu^* = \nu_{\mathrm{d}}$, where ν_{d} is the parameter value that results in χ_{d}, we get

$$\begin{aligned} &\chi(k+1) = P(\chi^*, \nu^*) + A(\chi - \chi^*) + B(\nu - \nu^*) \\ &A = \left[\frac{\partial P(\chi,\nu)}{\partial \chi}\right]_{\substack{\chi=\chi^* \\ \nu=\nu^*}}, B = \left[\frac{\partial P(\chi,\nu)}{\partial \nu}\right]_{\substack{\chi=\chi^* \\ \nu=\nu^*}} \end{aligned} \tag{3.35}$$

By defining the errors

$$e(k) = \chi(k) - \chi^*, \qquad u(k) = \nu(k) - \nu^* \tag{3.36}$$

we get from (3.35)

$$e(k+1) = Ae(k) + Bu(k) \tag{3.37}$$

For purpose of integral control, we define the output as

$$y(k) = e(k) \tag{3.38}$$

To converge the apex height to the desired value, we propose to use integral control with the integrator defined as

$$\theta(k+1) = \theta(k) - y(k) \tag{3.39}$$

The integrator-augmented discrete system has the form

$$\lambda(k+1) = \mathbb{A}\lambda(k) + \mathbb{B}u(k) \quad \lambda(k) = \begin{bmatrix} e(k) & \theta(k) \end{bmatrix}^T \tag{3.40}$$

$$\mathbb{A} \triangleq \begin{bmatrix} A & 0 \\ -1 & 1 \end{bmatrix}, \quad \mathbb{B} \triangleq \begin{bmatrix} B \\ 0 \end{bmatrix}$$

where A and B is defined in (3.37). If $\{\mathbb{A}, \mathbb{B}\}$ is controllable, the input can be chosen as

$$u(k) = \mathbb{K}\lambda(k) \tag{3.41}$$

such that

$$\rho(\mathbb{A} + \mathbb{B}\mathbb{K}) < 1$$

and the closed-loop system is asymptotically stable.

3.5 Effect of Continuous Controller Parameters on Hopping Behavior

3.5.1 Effect of the Parameters on Apex Height

The apex height h depends on the total energy of the system at takeoff point, where (3.25) holds. Substituting (3.12), (3.16) and (3.17) into (3.25), we get

$$(r - r_{\mathrm{d}}) = \frac{g - 2\zeta\nu\omega_n\dot{r}}{\omega_n^2} \tag{3.42}$$

The total energy of the robot at the takeoff point is

$$E = \frac{1}{2}m_{\mathrm{t}}\dot{r}^2 + m_{\mathrm{t}}g\left[\frac{g - 2\zeta\nu\omega_n\dot{r}}{\omega_n^2} + r_{\mathrm{d}}\right] \tag{3.43}$$

Assuming that the relative motion between the upper and lower masses quickly settles to zero and no significant work is done by the actuator during this time, the apex height h is computed as

$$h = \frac{E}{m_{\mathrm{t}}g} = \frac{1}{2g}\dot{r}^2 + \frac{g - 2\zeta\nu\omega_n\dot{r}}{\omega_n^2} + r_{\mathrm{d}} \tag{3.44}$$

To examine the effect of the control parameters (ω_n, ν, ζ) and r_{d} on the apex height, we

compute the partial derivatives of h in (3.44) with respect to the parameters; they are

$$\frac{\partial h}{\partial \omega_n} = -\frac{2\left(g - \zeta\nu\omega_n\dot{r}\right)}{\omega_n^3} < 0, \quad \frac{\partial h}{\partial \nu} = -\frac{2\zeta\dot{r}}{\omega_n} < 0 \tag{3.45}$$

$$\frac{\partial h}{\partial \zeta} = -\frac{2\nu\dot{r}}{\omega_n} > 0, \qquad \frac{\partial h}{\partial r_{\mathrm{d}}} = 1 > 0 \tag{3.46}$$

Clearly, the apex height is higher for smaller values of ω_n and ν and higher values of ζ, and r_{d}. The choice of the parameters are however subject to the constraint $\phi \neq 0$, or $r < r_{\max}$ where

$$r_{\max} = \max_{\phi} 2\ell m_z \cos\phi = 2\ell m_z$$

The procedure for choosing parameters that satisfy this constraint is discussed next.

3.5.2 Limitation on Choice of Parameter Values

Contact Phase Constraint

For the contact phase, the solution of the closed-loop system dynamics described by (3.15) and (3.16) is given by

$$\begin{aligned}
\xi_1 =& e^{-\zeta\nu\omega_n t}\left[\frac{\zeta\nu\xi_{10}}{\sqrt{1-\zeta^2\nu^2}}\sin(\omega_\nu t) + \xi_{10}\cos(\omega_\nu t)\right] \\
\xi_2 =& -\zeta\nu\omega_n e^{-\zeta\nu\omega_n t}\xi_{10}\left[\frac{\zeta\nu}{\sqrt{1-\zeta^2\nu^2}}\sin(\omega_\nu t) + \cos(\omega_\nu t)\right] \\
&+ \omega_n e^{-\zeta\nu\omega_n t}\xi_{10}\left[\zeta\nu\cos(\omega_\nu t) - \sqrt{1-\zeta^2\nu^2}\sin(\omega_\nu t)\right] \\
\omega_\nu \triangleq& \omega_n\sqrt{1-\zeta^2\nu^2}
\end{aligned} \tag{3.47}$$

where ξ_{10} is the value of ξ_1 when $\xi_2 = 0$, *i.e.* when ξ_2 switches from a negative value

to a positive value and α switches from 1 to ν. To avoid oscillation during the contact phase, the system must satisfy $(\omega_n\sqrt{1-\zeta^2\nu^2}t) < \pi$ at the takeoff point. By substituting $(\omega_n\sqrt{1-\zeta^2\nu^2}t) < \pi$ in (3.47) and then substituting the expressions for ξ_1 and ξ_2 in (3.25), we can get the following condition:

$$-\omega_n^2 e^{\frac{-\pi\zeta\nu}{\sqrt{1-\zeta^2\nu^2}}}\xi_{10} > g \tag{3.48}$$

Flight Phase Constraint

For the flight phase, the initial conditions must satisfy the takeoff condition in (3.25). The solution of the controllable states in (3.21) is

$$\begin{aligned}
\xi_1 &= e^{-\zeta\omega_n t}\left[C_2\sin(\omega_d t) + C_1\cos(\omega_d t)\right] \\
\xi_2 &= -\zeta\omega_n e^{-\zeta\omega_n t}\left[C_2\sin(\omega_d t) \ + C_1\cos(\omega_d t)\right] + \omega_d e^{-\zeta\omega_n t}\left[C_2\cos(\omega_d t) - C_1\sin(\omega_d t)\right] \\
\omega_d &\triangleq \omega_n\sqrt{1-\zeta^2} \\
C_1 &\triangleq \frac{g - 2\zeta\nu\omega_n\xi_{20}}{\omega_n^2}, \quad C_2 \triangleq \frac{\xi_{20} + \zeta\omega_n C_1}{\omega_d}
\end{aligned} \tag{3.49}$$

and ξ_{20} is the initial value of ξ_2 at the takeoff point. Since the controllable states depict an underdamped mass-spring-damper system, ξ_1 will reach its maximum value during the first half of the first cycle of oscillation when $\xi_2 = 0$. By setting $\xi_2 = 0$ in (3.49), we get

$$t = \frac{1}{\omega_d}\tan^{-1}\left[\frac{\xi_{20}\omega_d}{g - \zeta\omega_n\xi_{20}}\right] \tag{3.50}$$

The value of ξ_1 at t in (3.50) must be less than $\xi_{1,max}$ where $\xi_{1,\max} = (r_{\max} - r_{\mathrm{d}}) = 2\ell m_{\mathrm{z}} - r_{\mathrm{d}}$. Therefore, the following condition must satisfied at the takeoff point

$$e^{-\zeta\omega_n t}\left[C_2\sin(\omega_d t) + C_1\cos(\omega_d t)\right] < (2lm_{\mathrm{z}} - r_{\mathrm{d}}) \tag{3.51}$$

3.6 Simulation

We present simulation results showing the AKH robot hopping to a desired apex height starting from rest. The robot parameters were assumed to be

$$m_{\rm b} = 0.7\,{\rm kg}, \qquad m_{\rm f} = 0.15\,{\rm kg}, \quad m = 0.4\,{\rm kg}, \qquad \ell = 0.2\,{\rm m}, \qquad \ell_0 = 0.05\,{\rm m} \tag{3.52}$$

The apex height was chosen as

$$h_{\rm d} = 0.35\,{\rm m} \tag{3.53}$$

and the continuous controller parameters were chosen to be

$$\zeta = 0.13, \quad r_{\rm d} = 0.13\ {\rm m} \tag{3.54}$$

Note that the value of $r_{\rm d}$ was chosen to be approximately half the value of $r_{\max}$. We find the values of ν^* and χ^* that corresponds to $h_{\rm d} = 0.35$ through an exhaustive numerical search; the results are shown in Figs. 3.2 (a)-(d) for four different values of controller parameter ω_n. The figures show that for a given value of ν, there may be multiple apex heights, each of which will correspond to an unique value of χ. The specific value of h to which the apex height will depend on the initial conditions. To converge to the desired value, we use integral control. In our simulation, the remaining two controller parameters ω_n and ν were chosen as follows: ω_n was chosen to be 30 since Fig. 3.2 (c). admits a solution for ν corresponding to $h_{\rm d} = 0.35$. The values of ν, ω_n and χ are provided below:

$$\nu = -1.19, \qquad \omega_n = 30, \qquad \chi^* = 1.669{\rm m/s} \tag{3.55}$$

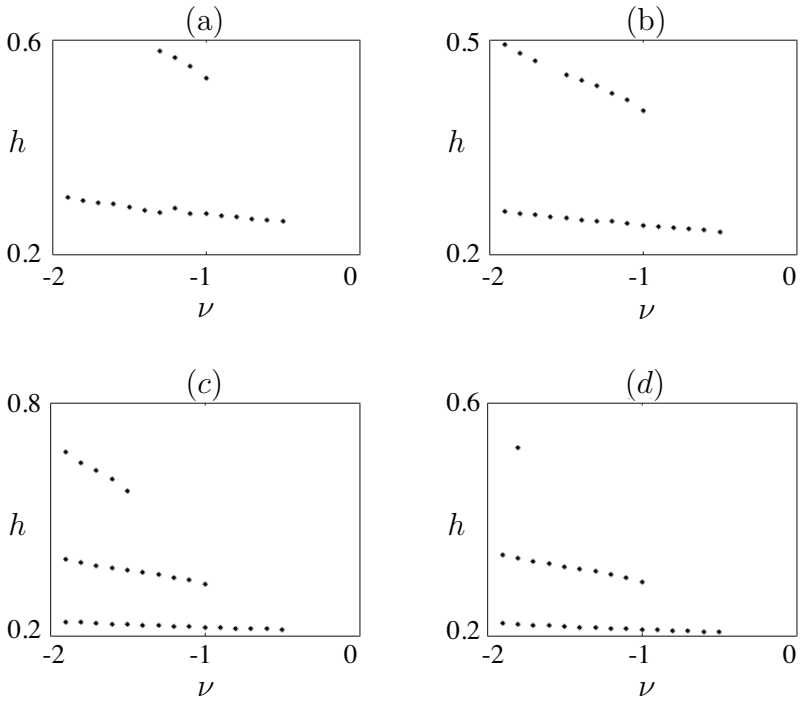

Figure 3.2: Apex height h is plotted with respect to ν for periodic orbits obtained with $r_{\mathrm{d}} = 0.13$ m, $\zeta = 0.13$ and (a) $\omega_n = 20$, (b) $\omega_n = 25$, (c) $\omega_n = 30$, and (d) $\omega_n = 35$.

The gains of the discrete controller were chosen to place the eigenvalues inside the unit circle. The choice

$$\mathbb{K} = \begin{bmatrix} 0.2 & 0.5 \end{bmatrix} \tag{3.56}$$

placed the eigenvalues at 0.814 and -0.87. Initially, the robot was assumed to be at rest on the ground; the initial conditions are

$$\begin{aligned} y_1(0) &= 0.05\,\mathrm{m} \qquad \dot{y}_1 = 0\,\mathrm{m/s} \\ \phi(0) &= 0.75\,\mathrm{rad} \qquad \dot{\phi} = 0\,\mathrm{rad/s} \end{aligned} \tag{3.57}$$

The simulation results are shown in Figs. 3.3, 3.4 and 3.5. The height of the upper and lower masses and the COM are plotted in Fig. 3.3; it can be seen that the apex height

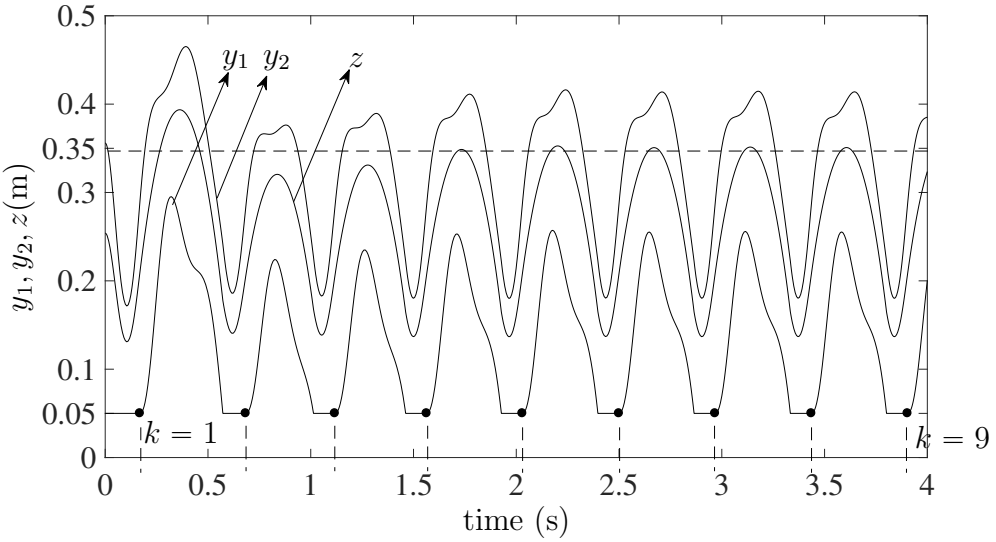

Figure 3.3: Plots of the heights of the upper and lower masses and the COM.

converges to its desired value in seven hops. The contact phase is the period when the value of y_1 remains constant at 0.05 and $y_1 > 0.05$ denotes the flight phase. The state of the discrete-time system is shown in Fig. 3.4; once again it can be seen that it converges to its desired value in seven hops. There is some overshoot but this can be eliminated by properly choosing the controller gains. The control input (hip torque) is shown in Fig.3.5. In this context, it should be pointed out that the control torque can be reduced by 50% if the actuator is moved from the hip to the knee as the angular displacement of the knee is twice that of the hip.

A video animation of a two-DOF AKH robot hopping on a rigid ground has been uploaded

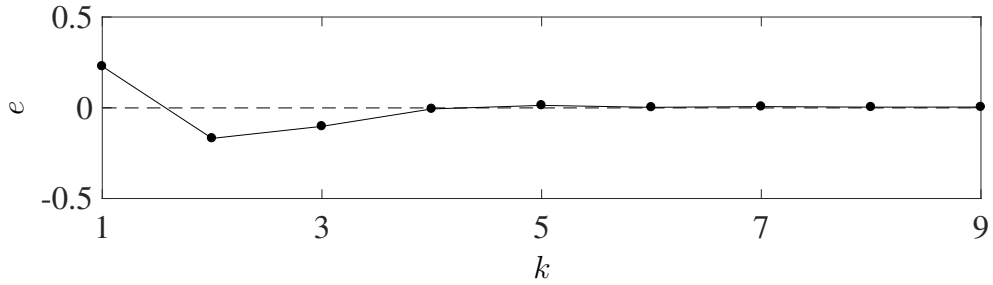

Figure 3.4: Plot of the state of the discrete-time system at the beginning of the first nine hops.

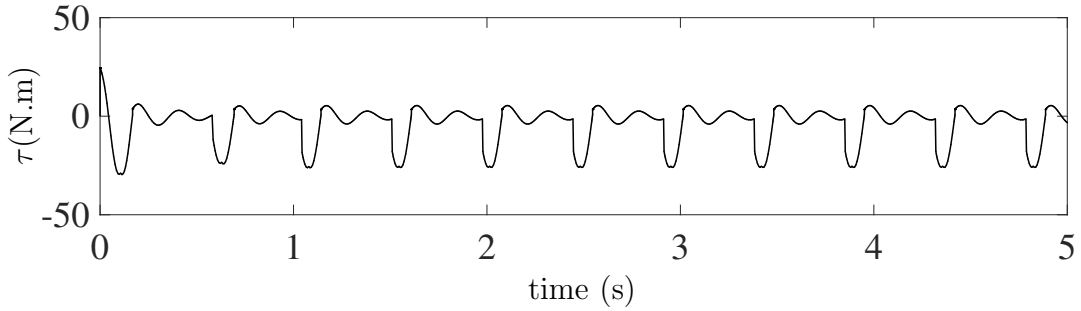

Figure 3.5: Plot of the torque applied by the hip actuator.

as supplementary material. It shows the hopper reaching the desired apex height of $h_d = 0.35$ m starting from rest.

3.7 Conclusion

This chapter presented a method for controlling the apex height of a two-DOF AKH robot, hopping on a rigid ground. The dynamics of the robot is modeled in flight, impact, and contact phases separately. A continuous-time controller is designed to make the robot behave like a mass-spring-damper system. In the contact phase, the continuous controller employs positive damping to arrest the motion of the COM when it is moving downwards, and negative damping when the COM is moving upwards. The negative damping is introduced to compensate for the energy loss due to impact. A Poincaré map of the hopping behavior is constructed and asymptotic stability of the hybrid system to the desired apex height is guaranteed by designing a discrete controller with integral action. The constraint imposed by the robot structure and the effect of continuous controller parameters on hopping behavior is discussed. A simulation of the AKH robot, hopping to a desired apex height from rest, is presented. A video animation of apex height control is includes to provide a glimpse of the dynamic behavior.

Chapter 4

Apex Height Control of a Two-DOF Ankle-Knee-Hip Robot Hopping on an Elastic Ground and a Viscoelastic Ground with Inertia

4.1 Introduction

In this chapter, we develop a strategy for controlling the apex height of the Ankle-Knee-Hip (AKH) robot introduced in Chapter 3 for hopping on an elastic ground and a viscoelastic ground with inertia. The ground is modeled as massless spring for the elastic ground case and a mass-spring-damper system for the viscoelastic ground with inertia. Since the elastic ground is massless, there is no loss of energy when the robot makes contact with the ground. A continuous backstepping controller is designed to control the mechanical energy of the robot to a desired values and stabilize the internal dynamics to reach the desired apex height. For the viscoelastic ground, there will be energy losses due to impact between the robot and the ground and from dissipation in the ground due to damping. These losses are unknown but have to be compensated; this makes the apex height control problem challenging. The continuous backstepping controller developed for the elastic ground is used to converge the energy of the robot to a desired value and stabilize the internal dynamics

of the robot. This results in steady-state error, which is eliminated using a discrete-time controller with integral action. The discrete-time controller is constructed using Poincaré map at the point just before impact. Simulation results are presented to demonstrate the efficacy of the controller. This chapter is structured as follows. The dynamics of the robot and the ground is presented in Section 4.2. The continuous and discrete controllers are presented in Sections 4.3 and 4.4. Numerical simulation results are presented in Section 4.5. Section 4.6 contains concluding remarks.

4.2 Dynamics of AKH Robot

4.2.1 System Description and Model

Consider the AKH hopping robot shown in Fig. 4.1. The robot hops on a viscoelastic ground of mass m_{g}, stiffness constant K_{ext}, and damping coefficient C_{ext}. The displacements of the ground mass m_{g} is denoted by x_1. The robot is comprised of an upper mass m_{b} and a lower mass m_{f}; these masses are connected by two links, each of which have mass m and length ℓ. The mass moment of inertia of the two links about of their COM are equal and denoted by I. The masses m_{b} and m_{f} are constrained to move along the vertical axis; their displacement are denoted by y_3 and y_2, respectively. The relative displacement between the lower mass m_{f} and the ground mass m_{g} is denoted by x_2. The angular displacement of the upper link, measured counter-clockwise with respect to the vertical axis, is denoted by ϕ. The robot has a single actuator that drives the angular coordinate ϕ, the torque applied by this actuator is denoted by τ. The dynamic model of the robot is obtained using Lagrange's

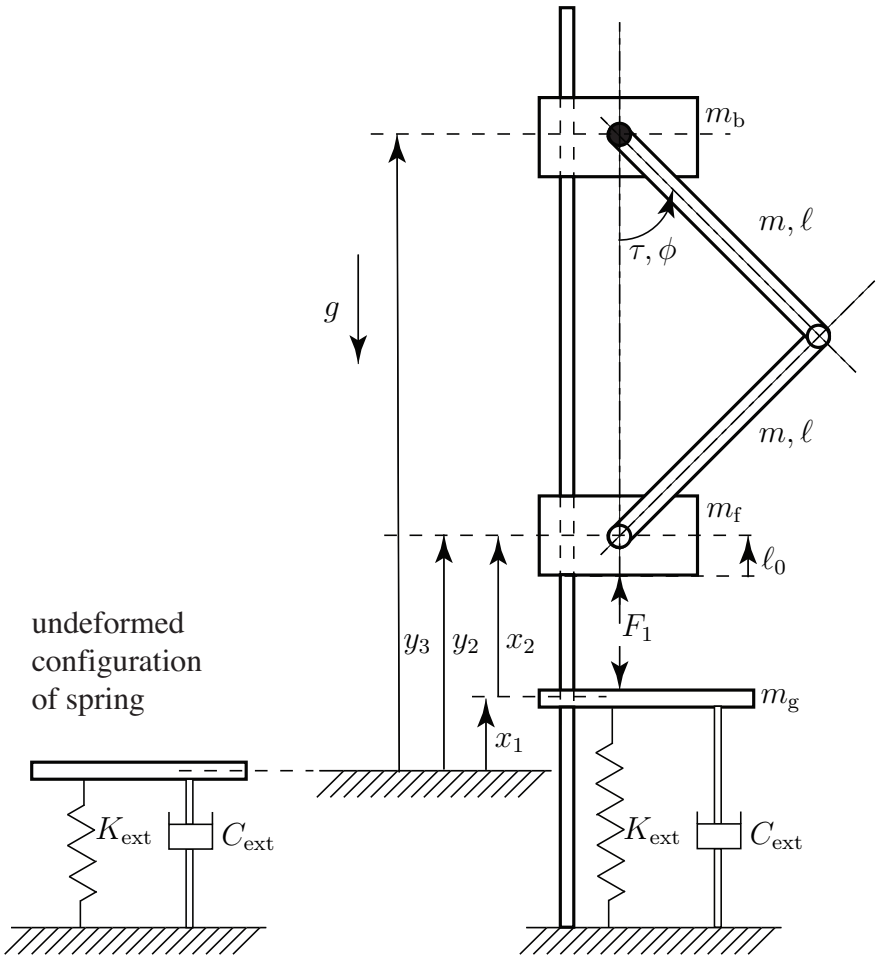

Figure 4.1: The ankle-knee-hip robot.

equations:

$$M(q)\ddot{q} + N(q, \dot{q}) = Q \tag{4.1}$$

where $q = \begin{bmatrix} x_1 & x_2 & \phi \end{bmatrix}^T$ and $Q = \begin{bmatrix} F_{\mathrm{ext}} & F_1 & \tau \end{bmatrix}^T$ are the vectors of generalized dis-

placement and forces, and the elements of $[M_{ij}]_{3\times3}$ and $[N_i]_{3\times1}$ are

$$
\begin{aligned}
M_{11} &= m_{\mathrm{t}} + m_{\mathrm{g}} \\
M_{12} &= M_{21} = M_{22} = m_{\mathrm{t}} \\
M_{13} &= M_{23} = M_{31} = M_{32} = -2\ell(m + m_{\mathrm{b}})\sin\phi \\
M_{33} &= \frac{1}{3}\ell^2\Big(5m + 6m_{\mathrm{b}} - 3(m + 2m_{\mathrm{b}})\cos(2\phi)\Big) \\
N_1 &= N_2 = g(m_{\mathrm{f}} + m_{\mathrm{b}} + 2m) - 2\ell(m + m_{\mathrm{b}})\cos\phi\dot{\phi}^2 \\
N_3 &= \frac{1}{2}\ell\Big(4\ell(m + 2m_{\mathrm{b}})\cos\phi\dot{\phi}^2 - g(m_{\mathrm{f}} + m_{\mathrm{b}} + 2m)\Big)\sin\phi
\end{aligned}
$$

$$
\begin{aligned}
F_{\mathrm{ext}} &= -C_{\mathrm{ext}}\dot{x}_1 - K_{\mathrm{ext}}x_1 \\
m_{\mathrm{t}} &\triangleq (m_{\mathrm{f}} + m_{\mathrm{b}} + 2m)
\end{aligned}
\tag{4.2}
$$

The hybrid dynamics of the hopping robot is comprised of the flight phase, the impact phase, and the contact phase.

4.2.2 Flight Phase

In the flight phase, the robot has three DOF and the following conditions hold:

$$x_2 > \ell_0 \qquad F_1 = 0 \tag{4.3}$$

The equation of motion is described by (4.1), where $F_1 = 0$.

4.2.3 Impact Phase

The impact phase refers to infinitesimal intervals of time $t \in [t^-, t^+]$ during which m_f comes in contact with m_g and $x_2 = \ell_0$. We make the following assumptions:

Assumption 8. *The impact between mass m_f and m_g is inelastic,* i.e., *m_f and m_g have identical velocities immediately after impact.*

Assumption 9. *The control torque τ is not impulsive.*

The position variables satisfy:

$$x_1(t^+) = x_1(t^-) \qquad x_2(t^+) = x_2(t^-), \qquad \phi(t^+) = \phi(t^-) \tag{4.4}$$

By integrating (4.1) over the interval $[t^-, t^+]$, we compute the velocity variables

$$\begin{aligned} \dot{x}_1(t^+) &= \dot{x}_1(t^-) + \frac{m_\mathrm{g}}{m_\mathrm{f} + m_\mathrm{g}} \dot{x}_2(t^-), \qquad \dot{x}_2(t^+) = 0 \\ \dot{\phi}(t^+) &= \dot{\phi}(t^-) + \frac{M_{13}}{M_{33}} (\dot{x}_2(t^-) - \dot{x}_1(t^+)) \end{aligned} \tag{4.5}$$

4.2.4 Contact Phase

The contact phase commences immediately after impact and continues for the time duration in which m_f remains in contact with m_g. We assume:

Assumption 10. *The force F_1 acting on both m_f and m_g is non-negative,* i.e. *$F_1 \geqslant 0$.*

During the contact phase, $x_2 = \ell_0$ and $\dot{x}_2 = \ddot{x}_2 = 0$; the system has two DOF. Using

(4.1), the value of the F_1 can be computed as

$$F_1 = N_2 + \frac{\big((M_{21}M_{33} - M_{23}M_{31})(F_{\text{ext}} - N_1) + (M_{11}M_{23} - M_{13}M_{21})(\tau - N_3)\big)}{(M_{11}M_{33} - M_{13}M_{31})} \tag{4.6}$$

At the instant when the system switches from the contact phase to the flight phase, F_1 equals zero.

4.2.5 Apex Height

The COM of the robot is denoted by

$$\begin{aligned} z =& \frac{1}{m_{\text{t}}}\big[m_{\text{f}}(x_1 + x_2) + m(x_1 + x_2 + \frac{1}{2}\ell\cos\phi) \\ &+ m(x_1 + x_2 + \frac{3}{2}\ell\cos\phi) + m_{\text{b}}(x_1 + x_2 + 2\ell\cos\phi)\big] \\ =& x_1 + x_2 + 2\ell m_{\text{z}}\cos\phi, \qquad m_{\text{z}} \triangleq \frac{m + m_{\text{b}}}{m_{\text{t}}} \end{aligned} \tag{4.7}$$

For each flight phase, the apex height is defined as the maximum value of z, and denoted by h.

4.3 Hybrid Control Strategy for Hopping on a Purely Elastic Ground

4.3.1 New Coordinates

For a purely elastic ground, we have

$$m_{\mathrm{g}} = 0, \qquad C_{ext} = 0, \qquad K_{ext} \neq 0 \tag{4.8}$$

There is no impact phase. Furthermore, substitution of (4.8) in (4.1) indicates $x_1 \equiv 0$ in the flight phase. Therefore, the system has two DOF in the flight phase. The system has two DOF in the contact phase as well since $x_2 = \ell_0$ and $\dot{x}_2 = 0$. For the objective of apex height control, we define r to be the height of the COM of the robot relative to that of the lower mass m_{f}. Using (4.7), it can be shown

$$r \stackrel{\Delta}{=} (z - (x_1 + x_2)) = 2\, m_{\mathrm{z}}\, \ell \cos\phi \tag{4.9}$$

$$\Rightarrow \dot{r} = -2\, m_{\mathrm{z}}\, \ell \sin\phi \dot{\phi} \tag{4.10}$$

Next, we define the error e as

$$e = (r - r_{\mathrm{d}}) \tag{4.11}$$

where $r_{\mathrm{d}} > 0$ is some desired value of r. From (4.9) and (4.11) it can be verified that $e \equiv 0 \rightarrow \dot{e} \equiv 0 \rightarrow \dot{r} \equiv 0$, which implies no relative motion between the two masses.

4.3.2 Normal Form

For the convenience of control design, we transform the system to the normal form [26] using the following transformations

$$\eta_1 = z - z_d \qquad \eta_2 = \dot{z} \qquad \xi_1 = e \qquad \xi_2 = \dot{r} \tag{4.12}$$

$$z_{\mathrm{d}} \stackrel{\Delta}{=} z\,|_{(x1=0, x_2=\ell_0, r=r_{\mathrm{d}})} = r_{\mathrm{d}} + \ell_0$$

The transformation in (4.12) is diffeomorphic only if $\phi \neq 0$. The dynamic of the system in

normal form can be written as

$$\begin{bmatrix} \dot{\eta}_1 \\ \dot{\eta}_2 \\ \dot{\xi}_1 \\ \dot{\xi}_2 \end{bmatrix} = \begin{bmatrix} \eta_2 \\ \ddot{x}_1 + \ddot{x}_2 - 2m_z\ell\cos\phi\dot{\phi}^2 - 2m_z\ell\sin\phi\ddot{\phi} \\ \xi_2 \\ -2m_z\ell\cos\phi\dot{\phi}^2 - 2m_z\ell\sin\phi\ddot{\phi} \end{bmatrix} \tag{4.13}$$

Substituting (4.1) into (4.13), we get

$$\begin{bmatrix} \dot{\eta}_1 \\ \dot{\eta}_2 \\ \dot{\xi}_1 \\ \dot{\xi}_2 \end{bmatrix} = \begin{bmatrix} \eta_2 \\ -g - \big[\lambda k_{\text{ext}}(x_1 + x_2 - \ell_0)\big]/m_{\text{t}} \\ \xi_2 \\ -2m_z\ell\big[\cos\phi\dot{\phi}^2 + \sin\phi\,(M_{21}N_1 + M_{11}(\tau - N_2)/\delta)\,\big] \end{bmatrix} \tag{4.14}$$

where

$$\lambda = \begin{cases} 0 \;\; : \;\; x_2 > \ell_0 : \text{Flight Phase} \\ 1 \;\; : \;\; x_2 = \ell_0 : \text{Contact Phase} \end{cases} \tag{4.15}$$

and δ is the determinant of $M(q)$. Define the torque τ to be

$$\tau = N_2 + \frac{1}{M_{11}}\left[-M_{21}N_1 + \delta\frac{\left(-\nu - 2m_z\ell\cos\phi\dot{\phi}^2\right)}{2m_z\ell\sin\phi}\right] \tag{4.16}$$

where v is the new control input. Substituting (4.12), and (4.16) into (4.14) results in

$$\begin{bmatrix} \dot{\eta}_1 \\ \dot{\eta}_2 \\ \dot{\xi}_1 \\ \dot{\xi}_2 \end{bmatrix} = \begin{bmatrix} \eta_2 \\ -g - \big[\lambda k_{\text{ext}}(\eta_1 - \xi_1)\big]/m_{\text{t}} \\ \xi_2 \\ v \end{bmatrix} \tag{4.17}$$

4.3.3 Backstepping

In the absence of relative motion between the masses, the total energy can be written as

$$E = m_{\mathrm{t}} \left[\frac{1}{2}\dot{z}^2 + g(z - z_{\mathrm{d}}) \right] + \frac{1}{2}\lambda K_{\mathrm{ext}} \left(z - z_{\mathrm{d}} \right)^2 \tag{4.18}$$

The second term on the right-hand side of (4.18) represents the potential energy stored in the spring when the masses are in their nominal position relative to one another. Indeed, when $r = r_{\mathrm{d}}$, $(z - z_{\mathrm{d}}) = (x_1 + x_2 + r - r_{\mathrm{d}} - \ell_0) = (x_1 + x_2 - \ell_0)$, which is equal to the spring deformation. For the robot to reach its desired apex height h_{d}, the total energy should be equal to

$$E \equiv E_{\mathrm{des}} = m_{\mathrm{t}}\, g(h_{\mathrm{d}} - z_{\mathrm{d}}) \tag{4.19}$$

in addition to $e \equiv 0$. The desired equilibrium configuration is therefore given by

$$(E - E_{\mathrm{des}}, e, \dot{e}) = (0, 0, 0) \tag{4.20}$$

With the objective of stabilizing the equilibrium in (4.20), we define the Lyapunov function candidate

$$V_1 = \frac{1}{2} k_1 \left(E - E_{\mathrm{des}} \right)^2, \qquad k_1 > 0 \tag{4.21}$$

It should be noted that V_1 is a function of λ (since E is a function of λ) but it is continuously differentiable in both the flight phase and contact phase. The Lyapunov function candidates introduced in this section will be used for stability analysis in the two phases separately; therefore, we treat λ as constant and do not make any distinction between the two phases

in our derivation. Using (4.12), (4.18), and (4.21), $\dot{V}_1$ can be computed as

$$\begin{aligned}\dot{V}_1 &= k_1 \left(E - E_{\text{des}}\right) \dot{E} \\ &= k_1 \left(E - E_{\text{des}}\right) \eta_2 \left[m_{\text{t}}(\dot{\eta}_2 + g) + \lambda K_{\text{ext}} \eta_1\right] \\ &= k_1 \left(E - E_{\text{des}}\right) \lambda K_{\text{ext}} \eta_2 \xi_1 \end{aligned} \tag{4.22}$$

By choosing

$$\xi_1 = \left\{-\lambda k_1 \left(E - E_{\text{des}}\right) \eta_2\right\} \triangleq \varphi_1 \tag{4.23}$$

we can make $\dot{V}_1$ negative semi-definite; therefore, integrator backstepping is introduced by defining the new variable

$$q_1 = \xi_1 + \lambda k_1 \left(E - E_{\text{des}}\right) \eta_2 = \left(\xi_1 - \varphi_1\right) \tag{4.24}$$

and the composite Lyapunov function

$$V_2 = V_1 + \frac{1}{2} q_1^2 = \frac{1}{2} k_1 \left(E - E_{\text{des}}\right)^2 + \frac{1}{2} q_1^2 \tag{4.25}$$

Differentiating V_2 and substituting (4.22) and (4.24), we get

$$\begin{aligned}\dot{V}_2 &= k_1 \left(E - E_{\text{des}}\right) \lambda K_{\text{ext}} \eta_2 \xi_1 + q_1 \dot{q}_1 \\ &= k_1 \left(E - E_{\text{des}}\right) \lambda K_{\text{ext}} \eta_2 \left[q_1 - \lambda k_1 \left(E - E_{\text{des}}\right) \eta_2\right] + q_1 \dot{q}_1 \\ &= -\lambda^2 k_1^2 K_{\text{ext}} \left(E - E_{\text{des}}\right)^2 \eta_2^2 \\ &\qquad + q_1 \left[\dot{q}_1 + k_1 \left(E - E_{\text{des}}\right) \lambda K_{\text{ext}} \eta_2\right] \end{aligned} \tag{4.26}$$

By choosing

$$\dot{q}_1 = \left\{-\lambda k_1 K_{\text{ext}} \left(E - E_{\text{des}}\right) \eta_2 - k_2 q_1\right\} \triangleq \varphi_2 \tag{4.27}$$

where $k_2 > 0$. We can make $\dot{V}_2$ negative semi-definite. We introduce integrator backstepping

again by defining the new variable

$$q_2 = (\dot{q}_1 - \varphi_2) \tag{4.28}$$

and the composite Lyapunov function

$$\begin{aligned} V_3 &= V_2 + \frac{1}{2} q_2^2 \\ &= \frac{1}{2} k_1 \left(E - E_{\text{des}}\right)^2 + \frac{1}{2} q_1^2 + \frac{1}{2} q_2^2 \end{aligned} \tag{4.29}$$

Differentiating V_3 and substituting (4.26) and (4.28), we get

$$\begin{aligned} \dot{V}_3 &= -\lambda^2 k_1^2 K_{\text{ext}} \left(E - E_{\text{des}}\right)^2 \eta_2^2 \\ &\quad + q_1 \left[\dot{q}_1 + \lambda k_1 K_{\text{ext}} \left(E - E_{\text{des}}\right) \eta_2\right] + q_2 \dot{q}_2 \\ &= -\lambda^2 k_1^2 K_{\text{ext}} \left(E - E_{\text{des}}\right)^2 \eta_2^2 \\ &\quad + q_1 \left[\dot{q}_1 - \varphi_2 - k_2 q_1\right] + (\dot{q}_1 - \varphi_2)(\ddot{q}_1 - \dot{\varphi}_2) \\ &= -\lambda^2 k_1^2 K_{\text{ext}} \left(E - E_{\text{des}}\right)^2 \eta_2^2 - k_2 q_1^2 \\ &\quad + q_2 \left[\ddot{q}_1 - \dot{\varphi}_2 + q_1\right] \end{aligned} \tag{4.30}$$

Our choice of

$$\ddot{q}_1 = \dot{\varphi}_2 - q_1 - k_3 q_2, \qquad k_3 > 0 \tag{4.31}$$

results in a negative semi-definite $\dot{V}_3$ and yields the controller

$$v = \ddot{\varphi}_1 + \dot{\varphi}_2 - q_1 - k_3 q_2 \tag{4.32}$$

The above equation was obtained from (4.31) by substituting the value of $\dot{\xi}_2$ in (4.17) and (4.24) into (4.31). From the definition of φ_1, it is clear that $\ddot{\varphi}_1$ will involve the second

derivative of η_2. This is not a problem since the second derivative of η_2 can be computed easily from (4.17) as

$$\ddot{\eta}_2 = -\lambda \frac{1}{m_{\mathrm{t}}} K_{\mathrm{ext}} (\eta_2 - \xi_2) \tag{4.33}$$

4.3.4 Stability Analysis

Using (4.12), (4.17), (4.18), (4.24) and (4.28) it can be shown that

$$(E - E_{\mathrm{des}}, \xi_1, \xi_2) = (0, 0, 0) \;\Leftrightarrow\; (E - E_{\mathrm{des}}, q_1, q_2) = (0, 0, 0)$$

Therefore, V_3 in (4.29) is a candidate Lyapunov function for investigating the stability of the equilibrium in (4.20). In both flight and contact phases ($\lambda = 0$ and $\lambda = 1$), the control law in (4.32), results in (4.30)

$$\dot{V}_3 \leqslant 0 \tag{4.34}$$

Therefore, $(E - E_{\mathrm{des}}, q_1, q_2) = (0, 0, 0)$ is stable.

Remark 3. *The stability of* $(E - E_{\mathrm{des}}, q_1, q_2) = (0, 0, 0)$ *in the flight and contact phases do not guarantee stability for the hybrid dynamics. The stability of the hybrid system is analyzed next .*

4.4 Discrete Controller for Stabilizing Hybrid Dynamics and Controlling the Apex Height

4.4.1 Elastic Ground

To investigate the stability of the hybrid dynamic system, we use a Poincaré map with the Poincaré section defined at the point of touch-down, *i.e.* the time instant prior to impact. Assuming that $\eta_1, \xi_1, \xi_2 \approx 0$ at the time of touch-down, the Poincaré section is chosen as

$$\bar{\mathcal{Z}} := \{X \in \mathbb{R} | \, \eta_1 = 0, \xi_1 = 0, \xi_2 = 0, \eta_2 < 0\} \tag{4.35}$$

where X is defined as

$$X = \eta_2 \tag{4.36}$$

We define the Poincaré section using the coordinate Ψ, where Ψ is defined by the coordinate transformation $H(\cdot) : \mathbb{R} \Rightarrow \mathbb{R}$, as follows

$$\Psi = (E - E_{\text{des}}) = H(X) \tag{4.37}$$

It can be shown that the map $H(\cdot)$ is a local homeomorphism and therefore locally topologically conjugate [27]; this implies that the stability of the Poincaré maps in Ψ and X coordinates are equivalent. The Poincaré map $P(\Psi)$ and the sequence of points $\Psi_k \in H(\mathcal{Z})$ satisfy

$$\Psi_{k+1} = P(\Psi_k), \quad P(\Psi) : H(\mathcal{Z}) \mapsto H(\mathcal{Z}) \tag{4.38}$$

with periodic point Ψ^* defined as

$$\Psi^* = P(\Psi^*) \tag{4.39}$$

For the elastic ground, the periodic point which achieves the desired apex height is given by

$$\Psi^* = 0 \tag{4.40}$$

which follows from (4.19).We define the error state χ_k as

$$\chi_k = (\Psi_k - \Psi^*) = \Psi_k$$

By linearizing the Poincaré map about Ψ^*, we have the approximate discrete dynamics given by

$$\chi_{k+1} = A\,\chi_k \qquad A \triangleq \left.\frac{dP(\Psi)}{d\Psi}\right|_{\Psi=\Psi^*} \tag{4.41}$$

The periodic point will be asymptotically stable if and only if

$$\rho(A) < 1 \tag{4.42}$$

where $\rho(A)$ is the spectral radius of A. Since the condition in (4.42) may not be satisfied, we design a discrete controller to stabilize the closed-loop system; the discrete controller is discussed next.

To design the discrete controller, we redefine Ψ as follows

$$\Psi = \Phi + u, \quad \Phi \triangleq (E - E_{\mathrm{d}}), \quad u \triangleq (E_{\mathrm{d}} - E_{\mathrm{des}}) \tag{4.43}$$

where E_{d} is desired level of energy for a given hop. The new Poincaré map $\bar{P}(\Phi, u)$ and the sequence of points $\Phi_k \in H(\mathcal{Z})$ satisfy

$$\Phi_{k+1} = \bar{P}(\Phi_k, u_k), \quad \bar{P}(\Phi, u) : H(\mathcal{Z}) \times R \mapsto H(\mathcal{Z}) \tag{4.44}$$

with periodic point Φ^* defined as

$$\Phi^* = \bar{P}(\Phi^*, u^*) \tag{4.45}$$

For the elastic ground, the periodic point which achieves the desired apex height is given by

$$\Phi^* = 0, \qquad u^* = 0 \tag{4.46}$$

We define the error state $\bar{\chi}_k$ as

$$\bar{\chi}_k = (\Phi_k - \Phi^*) = \Phi_k$$

By linearizing the Poincaré map about (Φ^*, u^*), we have the approximate discrete dynamics given by

$$\begin{aligned} &\bar{\chi}_{k+1} = \bar{A}\,\bar{\chi}_k + \bar{B}u_k \\ &\bar{A} \triangleq \left.\frac{d\bar{P}(\Phi,u)}{d\Phi}\right|_{\Psi=\Psi*,u=u*}, \quad \bar{B} \triangleq \left.\frac{d\bar{P}(\Phi,u)}{du}\right|_{\Psi=\Psi*,u=u*} \end{aligned} \tag{4.47}$$

For our choice of input

$$u_k = K\bar{\chi}_k \tag{4.48}$$

The closed-loop system dynamics takes the form

$$\bar{\chi}_{k+1} = (\bar{A} + \bar{B}K)\bar{\chi}_k$$

If $\{\bar{A}, \bar{B}\}$ is controllable, we can choose K such that

$$\rho(\bar{A} + \bar{B}K) < 1 \tag{4.49}$$

and the hybrid dynamical system is asymptotically stable.

Remark 4. *If the condition in (4.42) is not satisfied and the discrete controller in (4.48) is implemented, the continuous controller will have to be modified. In particular, the fixed desired value of the energy E_{des} will have to be replaced by the desired value of energy for each hop E_{d} to account for the change in the Poincaré map from $P(\Psi)$ to $\bar{P}(\Phi, u)$.*

4.4.2 Viscoelastic Ground with Inertia

The viscoelastic ground results in energy losses due to impact between the lower mass m_{f} and the ground mass m_{g}, and the damping in the ground. We defined the Poincaré section using the coordinate $\bar{\Psi}$, where $\bar{\Psi}$ is defined by the coordinate transformation $H(\cdot) : \mathbb{R} \Rightarrow \mathbb{R}$, defined as follows

$$\bar{\Psi} = (E - E_{\mathrm{des}}) = H(X) \tag{4.50}$$

The Poincaré map $Q(\bar{\Psi})$ and the sequence of points $\bar{\Psi}_k \in H(\bar{\mathcal{Z}})$ now satisfy

$$\bar{\Psi}_{k+1} = Q(\bar{\Psi}_k), \quad Q(\bar{\Psi}) : H(\bar{\mathcal{Z}}) \mapsto H(\bar{\mathcal{Z}}) \tag{4.51}$$

with periodic point $\bar{\Psi}^*$ defined as

$$\bar{\Psi}^* = Q(\bar{\Psi}^*) \tag{4.52}$$

For the viscoelastic ground, the periodic point is

$$\bar{\Psi}^* = (\bar{E} - E_{\mathrm{des}}) \tag{4.53}$$

where $\bar{E}$ is the energy of the system in the steady state when the backstepping controller is invoked with $E_{\mathrm{d}} = E_{\mathrm{des}}$. The value of $\bar{E}$ is initially unknown but can be determined after

the robot has hopped a few times - see section 4.5.2. We define the error state γ_k as

$$\gamma_k = (\Psi_k - \bar{\Psi}^*) = (E_k - \bar{E})$$

By linearizing the Poincaré map about $\bar{\Psi}^*$, we have the approximate discrete dynamics given by

$$\gamma_{k+1} = A_0\,\gamma_k \qquad A_0 \triangleq \left.\frac{dQ(\bar{\Psi})}{d\bar{\Psi}}\right|_{\Psi=\bar{\Psi}*} \tag{4.54}$$

The periodic point will be asymptotically stable if and only if

$$\rho(A_0) < 1 \tag{4.55}$$

where $\rho(A_o)$ is the spectral radius of A_o. To design the discrete controller, we describe $\bar{\Psi}$ as follows

$$\bar{\Psi} = \bar{\Phi} + \bar{u}, \quad \bar{\Phi} \triangleq (E - E_{\mathrm{d}}), \quad \bar{u} \triangleq (E_{\mathrm{d}} - E_{\mathrm{des}})$$

where E_{d} is desired level of energy for a given hop. The new Poincaré map $\bar{Q}(\bar{\Phi}, \bar{u})$ and the sequence of points $\bar{\Phi}_k \in H(\bar{\mathcal{Z}})$ satisfy

$$\bar{\Phi}_{k+1} = \bar{Q}(\bar{\Phi}_k, \bar{u}_k), \quad \bar{Q}(\bar{\Phi}, \bar{u}) : H(\bar{\mathcal{Z}}) \times R \mapsto H(\bar{\mathcal{Z}}) \tag{4.56}$$

with periodic point $\bar{\Phi}^*$ defined as

$$\bar{\Phi}^* = \bar{Q}(\bar{\Phi}^*, \bar{u}^*) \tag{4.57}$$

For the viscoelastic ground with inertia, there exists the following equilibrium point

$$\bar{\Phi}^* = (\bar{E} - E_{\mathrm{d}}), \qquad \bar{u}^* = 0 \tag{4.58}$$

If we define the error state

$$\mu_k \triangleq (\bar{\Phi}_k - \bar{\Phi}^*) = (E_k - \bar{E}) \tag{4.59}$$

the Poincaré map $\bar{Q}(\bar{\Phi}_k, \bar{u}_k)$ can be linearized about $(\bar{\Phi}^*, \bar{u}^*)$ to yield the following linear discrete-time system

$$\begin{aligned} &\mu_{k+1} = \hat{A}\,\mu_k + \hat{B}\bar{u}_k, \quad y_k = \mu_k \\ &\hat{A} \triangleq \left.\frac{d\bar{Q}(\bar{\Phi}, u)}{d\Phi}\right|_{\substack{\bar{\Phi}=\bar{\Phi}^* \\ \bar{u}=\bar{u}^*}}, \quad \hat{B} \triangleq \left.\frac{d\bar{Q}(\bar{\Phi}, u)}{du}\right|_{\substack{\bar{\Phi}=\bar{\Phi}^* \\ \bar{u}=\bar{u}^*}} \end{aligned} \tag{4.60}$$

To converge the system energy from its level at the equilibrium configuration $\bar{E}$ to the desired value E_{des}, we propose to use integral control with the integrator defined as

$$\theta_{k+1} = \theta_k + (E_0 - y_k), \quad E_0 \triangleq (E_{\text{des}} - \bar{E}) \tag{4.61}$$

where E_0 is the desired value of the output variable y. The integrator-augmented discrete system has the form

$$\begin{aligned} &\lambda_{k+1} = \mathbb{A}\lambda_k + \mathbb{B}u_k + E_0, \quad \lambda_k = \begin{bmatrix} \mu_k & \theta_k \end{bmatrix}^T \\ &\mathbb{A} \triangleq \begin{bmatrix} \bar{A} & 0 \\ -1 & 1 \end{bmatrix}, \quad \mathbb{B} \triangleq \begin{bmatrix} \bar{B} \\ 0 \end{bmatrix} \end{aligned} \tag{4.62}$$

If $\{\mathbb{A}, \mathbb{B}\}$ is controllable, the input can be chosen as

$$\bar{u}_k = \mathbb{K}\lambda_k \tag{4.63}$$

where $\mathbb{K}$ satisfies

$$\rho(\mathbb{A} + \mathbb{B}\mathbb{K}) < 1$$

Assumption 11. *The parameters of the viscoelastic ground (m_{g}, C_{ext}, K_{ext}) are such that the settling time of the system is less than the hopping period of the robot.*

Remark 5. *The above assumption allows us to infer that $x_1, \dot{x}_1 \approx 0$ at the time of touchdown. It will be shown later that the assumption is not overly restrictive.*

4.5 Simulation

4.5.1 Elastic Ground

We investigate the behavior of AKH robot hopping on an elastic ground. The parameters of the robot and the ground were assumed to be

$$\begin{array}{lll} m_{\mathrm{f}} = 0.15 \text{ kg}, & m = 0.4 \text{ kg}, & m_{\mathrm{b}} = 0.7 \text{ kg} \\ \ell = 0.2\text{m} & \ell_0 = 0.05 \text{ m}, & K_{\mathrm{ext}} = 2800 \text{ N/m} \end{array} \tag{4.64}$$

The desired apex height h_{d} and the relative displacement r_{d} was chosen to be

$$h_{\mathrm{d}} = 0.3 \text{ m}, \qquad r_{\mathrm{d}} = 0.13 \text{ m}$$

The parameters of the continuous backstepping controller were chosen as

$$k_1 = 0.001, \qquad k_2 = 700, \qquad k_3 = 10$$

The eigenvalue $\bar{A}$ in (4.47) was found to be 0.21. The discrete controller gain were chosen as

$$K = -0.3$$

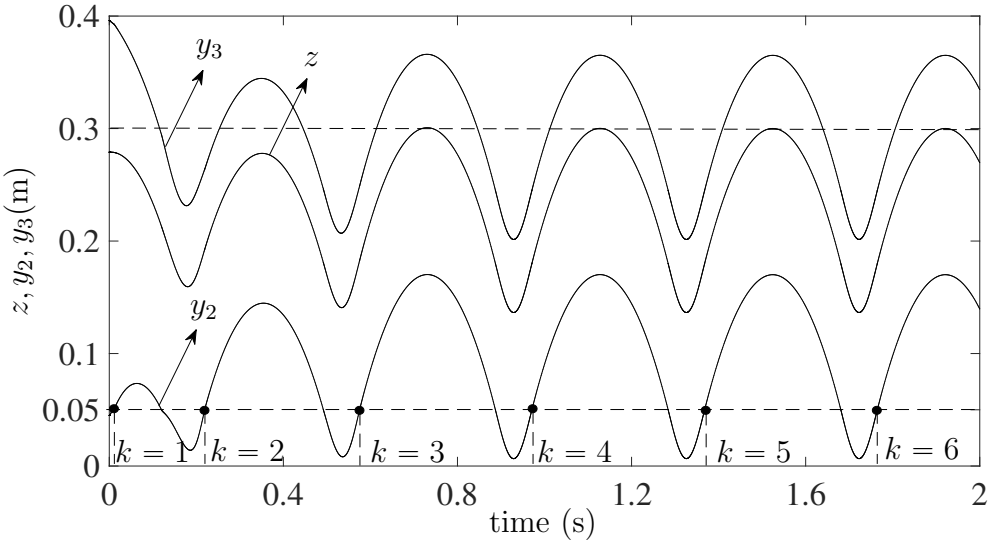

Figure 4.2: Simulation results for hopping on the elastic ground. Absolute height of the two masses y_2 and y_3, and COM height are plotted as a function of time.

This places the eigenvalue of the closed loop system at -0.053. The initial conditions were assumed to be

$$\begin{aligned} x_1 &= -0.005\,\text{m}, & x_2 &= 0.05\,\text{m}, & \phi(0) &= 0.5\,\text{rad}, \\ \dot{x}_1(0) &= 0.0\,\text{m/s}, & \dot{x}_2(0) &= 0.0\,\text{m}, & \dot{\phi}(0) &= 0.0\,\text{m/s} \end{aligned} \tag{4.65}$$

The simulation results are shown in Figs. 4.2, and 4.3. The displacements of m_b, m_f, and the COM are shown in Fig. 4.2. The initial conditions indicates that the spring of the elastic ground is initially compressed due to the weight of the robot, and the robot starts from the rest. Fig. 4.2 shows that the apex height of the COM converge to the desired value at $h = 0.3$ m after three hops. The contact phase is the period where $y_2 < \ell_0$. The period where $y_2 > \ell_0$ is the flight phase. The discrete-time system state Ψ is plotted in Fig. 4.3. The state of the discrete system converges to zero after three hops.

A video animation of a two-DOF AKH robot hopping on an elastic ground has been uploaded as supplementary material. It shows the hopper reaching the desired apex height of $h_d = 0.3$ m starting from rest.

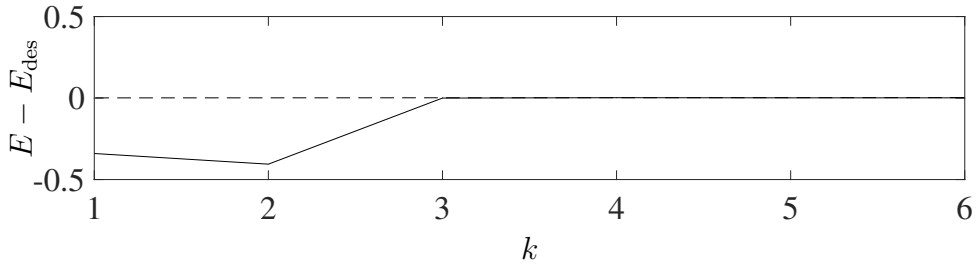

Figure 4.3: Simulation results for hopping on the elastic ground: Plots of $(E - E_{\text{des}})$ at the end of the k-th hop, $k = 1, 2 \cdots, 6$.

4.5.2 Viscoelastic Ground

The parameters AKH robot is given in (4.64). The parameters of the ground assumed to be

$$m_{\text{g}} = 0.015\text{kg}, \quad K_{\text{ext}} = 2800\text{N/m}, \quad C_{\text{ext}} = 13 \text{ Ns/m} \tag{4.66}$$

The mass of the ground was assumed to be 10% of the lower mass m_f and the damping coefficient C_{ext} was chosen such that the ground is slightly over-damped. The desired apex height h_{d} and the relative displacement r_{d} was chosen to be

$$h_{\text{d}} = 0.3 \text{ m}, \qquad r_{\text{d}} = 0.13 \text{ m}$$

The continuous controller gains were chosen as

$$k_1 = 0.001, \qquad k_1 = 600, \qquad k_2 = 50$$

The eigenvalues of $\mathbb{A}$ was found to be: 1, and 0.404. The pair $\{\mathbb{A}, \mathbb{B}\}$ is controllable, and the

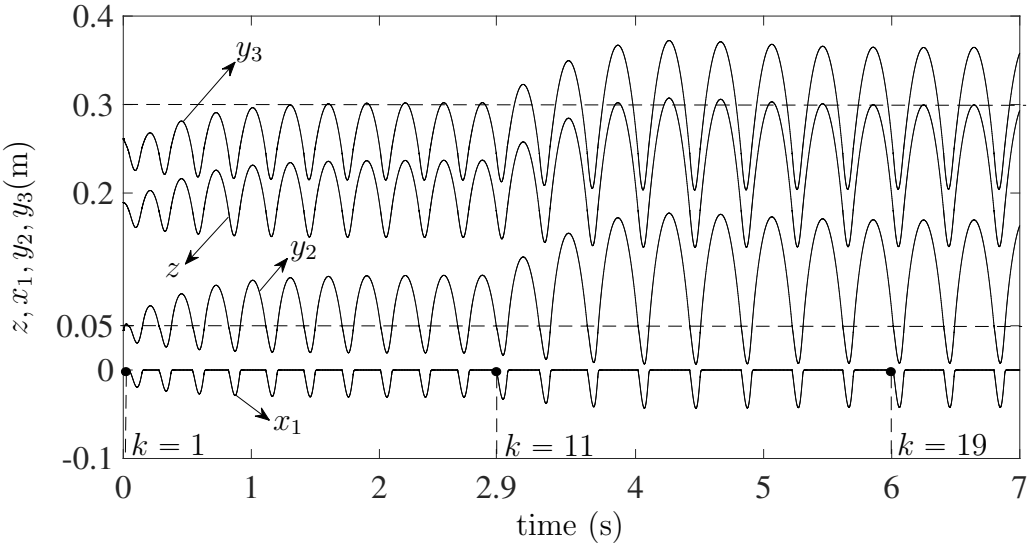

Figure 4.4: Simulation results for hopping on a viscoelastic ground with inertia. Plot of the position of the upper mass y_3, the lower mass y_2, COM z, and the ground mass x_1, as a function of time.

controller gains were chosen as

$$\mathbb{K} = \begin{bmatrix} -0.5 & 0.6 \end{bmatrix}$$

This places the eigenvalues of the closed loop system at $0.58 \pm 0.34i$. The initial conditions were described by (4.65) and the initial value of the integrator state was set to zero.

The simulation results are shown in Figs. 4.4, 4.5 and 4.6. The displacements of the

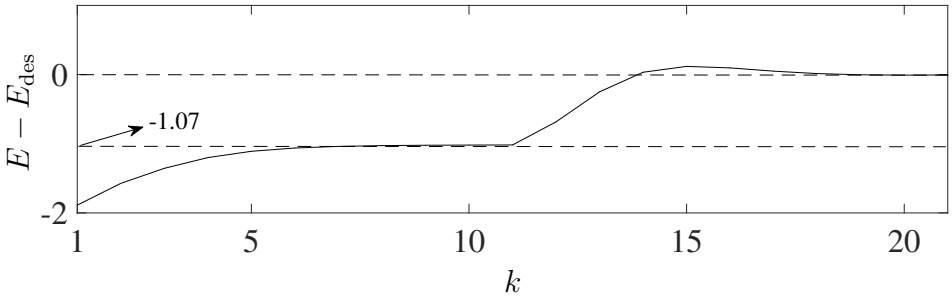

Figure 4.5: Simulation results for hopping on a viscoelastic ground with inertia: Plots of $(E - E_{\text{des}})$ at the end of the k-th hop $k = 1, 2, \cdots, 21$.

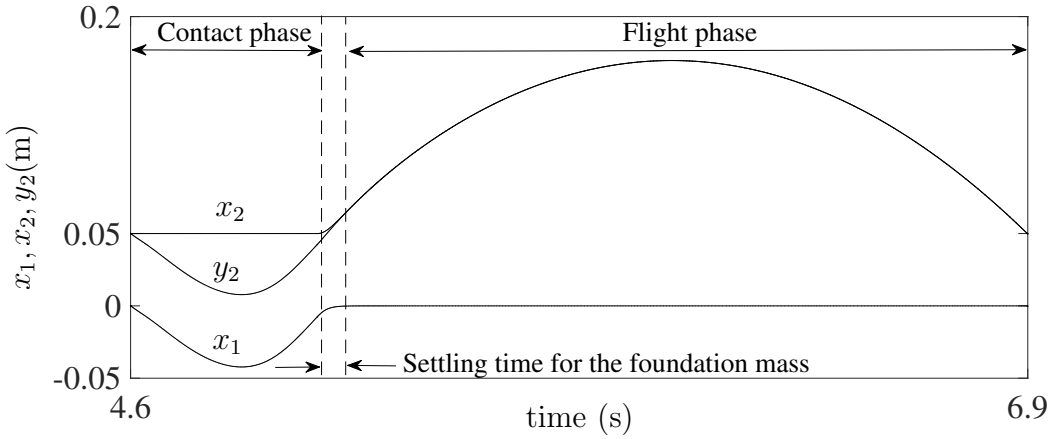

Figure 4.6: Simulation results for hopping on a viscoelastic ground with inertia: Plot of y_2, and x_1 for the hop between $k = 19$ and $k = 20$.

upper mass, lower mass, COM, and ground mass are plotted in Fig. 4.4. The contact phases (not explicitly shown in Fig. 4.4) are the time intervals during which $x_2 = (y_2 - x_1) = 0.05$ m. The initial value of $y_2(0) = 0.045$ m indicates that the spring of the viscoelastic ground is initially compressed due to the weight of the robot. The simulation is comprised of two phases. In the initial phase, $0 \leqslant t \leqslant 2.9$ s, the discrete controller was switched off and the backstepping controller was used with $E_{\rm d} = E_{\rm des}$. During this phase (ten hops), the apex height of the robot converges to a constant value that corresponds to $E = \bar{E}$, which was defined in the context of (4.53). The value of $\bar{E}$ was found to be 0.96 J and $E_0 = 1.02$ J (the deficit) was computed using (4.61). Using the value of E_0, the discrete controller was switched on at $t = 2.9$ s. The discrete time system $\bar{\Psi}$ is plotted in Fig. 4.5 at the end of the k-th hop, $k = 1, 2, \cdots, 21$. The discrete controller is active for $k > 10$ and it results in $(E - E_{\rm des})$ converging to zero in approximately nine hops, *i.e.*, $k = 19$.

The displacement of the lower mass and the ground is shown in Fig. 4.6 for one hop. It can be seen that the lower mass breaks contact with the ground mass below the datum ($x_2 > \ell_0$, $x_1 < 0$). While the robot is in flight, the ground mass settles to its equilibrium configuration; the response is overdamped, as expected from the choice of parameters in (4.66), and has a 2% settling time of 0.011 s. Since the settling time of the ground mass

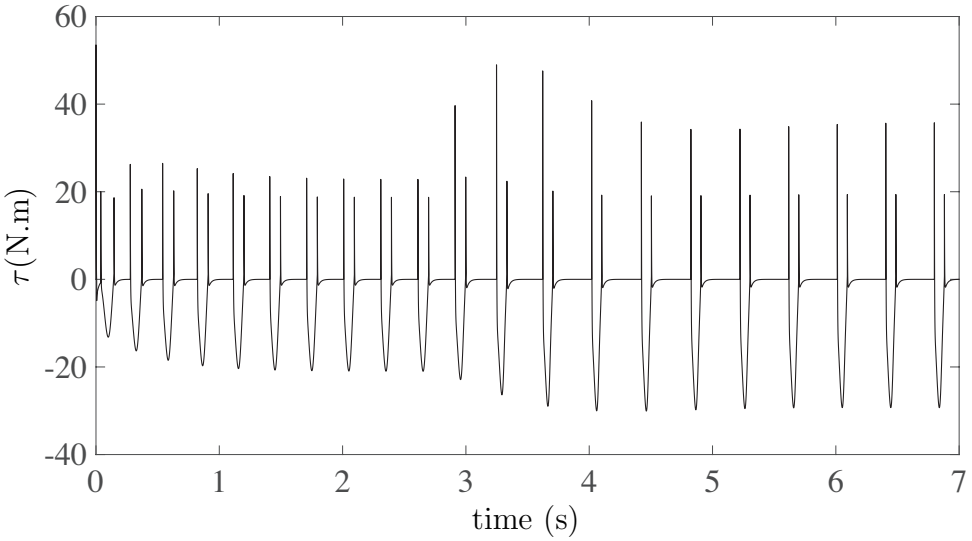

Figure 4.7: Plot of the torque applied by the hip actuator.

is much smaller than the flight phase, it becomes clear that *Assumption 4* is not overly restrictive. The control input (hip torque) is shown in Fig.4.7. In this context, it should be pointed out that the control torque can be reduced by 50% if the actuator is moved from the hip to the knee as the angular displacement of the knee is twice that of the hip.

A video animation of a Two-DOF AKH robot hopping on a viscoelastic ground with inertia has been uploaded as supplementary material. It shows the hopper reaching the desired apex height of $h_d = 0.3$ m starting from rest.

4.6 Conclusion

This chapter presents a hybrid control strategy to converge the apex height of an AKH robot hopping on an elastic ground and a viscoelastic ground with inertia. A continuous backstepping controller is used in conjunction with a discrete-time controller designed using a Poincaré map. For the elastic ground, the backstepping controller is used to control the energy level of the hopper and eliminates the relative displacement between the hopper masses. The discrete controller is used to guarantee the stability of the hybrid system and

fast convergence of the apex height to the desired value. For the viscoelastic ground, the backstepping controller results in steady state error due to losses from impact between the hopper and the ground and viscous losses in the damper. To overcome these losses, a discrete-time controller with integral action was introduced. Simulation results prove the efficacy of the control strategy for both elastic and viscoelastic grounds. A video animation of apex height control is includes to provide a glimpse of the dynamic behavior.

Chapter 5

Four-Link Planar One-Legged Hopping Locomotion

5.1 Introduction

In this chapter, we develop a strategy for controlling the apex height of a four-link robot hopping in place with a desired apex height, and moving forward or backward with a desired step size. One-legged hopping locomotion on a rigid ground is a challenging problem due to the energy loss from ground impact. After transforming the dynamic model into normal form, the controllable states are controlled to emulate the dynamics of a mass-spring-damper system with variable damping; the uncontrollable states are shown to remain bounded and well-behaved. The controllable states include the position and velocity of the center-of-mass and the foot angle. We develop two control strategies to compensate for the energy loss due to ground impact. The first strategy introduces negative damping in the dynamics of the mass-spring-damper system that describes the vertical motion of the center-of-mass (COM) in the contact phase. The second strategy alters the equilibrium height of the COM in the vertical direction for both the flight and contact phases. A Poincaré map is used to construct a discrete-time system at the point of touch-down and a controller with integral action is designed to converge the apex height to a desired value for hopping in place, and for converging the step size to the desired value in the case of locomotion. Simulation results

are presented to show the efficacy of the control designs.

This chapter is structured as follows. The dynamics of the hybrid system in flight phase, impact phase, and contact phase are presented in Section 5.2. In Section 5.3, we present the dynamical model of the hopper in normal form. A partial feedback linearizing controller is presented in Section 5.4. In Sections 5.5 and 5.6, we present the strategies for apex height control and step-size control during hopping locomotion. Simulations results are presented in Section 5.7 and concluding remarks are presented in Section 5.8.

5.2 Hybrid System Dynamics

5.2.1 System Description

Consider the four-link planar hopping robot in Fig.5.1. The hopper is comprised of four links (foot, leg, thigh and body) with link lengths $\ell_{\rm f}$, $\ell_{\rm l}$, $\ell_{\rm t}$, $\ell_{\rm b}$, masses $m_{\rm f}$, $m_{\rm l}$, $m_{\rm t}$, $m_{\rm b}$, and mass moment of inertias $I_{\rm f}$, $I_{\rm l}$, $I_{\rm t}$, $I_{\rm b}$, respectively. The tip of the foot (toe) is denoted by point O and its displacement relative to the ground is denoted by (x, y). The relative angular displacements of the links are denoted by θ_1, θ_2, θ_3, and θ_4; the torque inputs applied at the ankle, knee, and hip joints (θ_2, θ_3, and θ_4) are denoted by τ_1, τ_2, and τ_3, respectively. The ground reaction force applied at O (toe) during contact is denoted by $F_{\rm ext}$. The dynamic model of the robot is obtained using Lagrange equations:

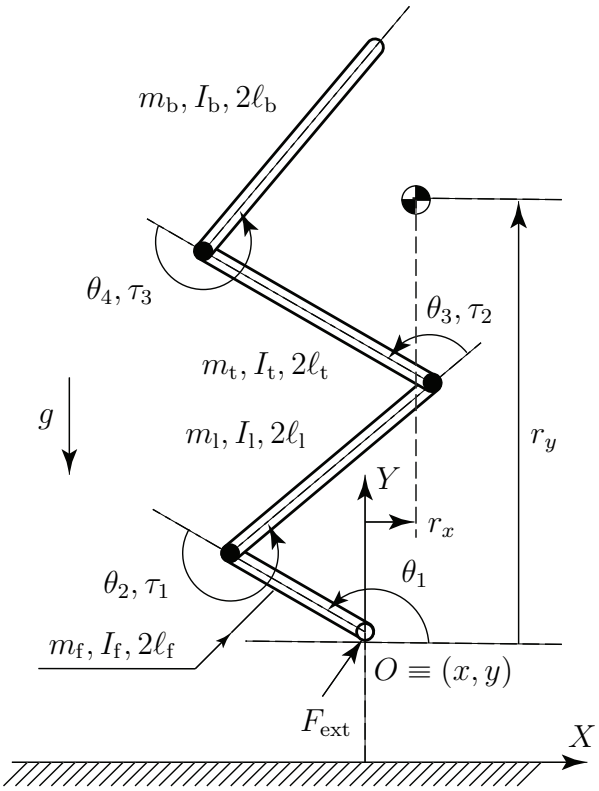

Figure 5.1: Four-link planar hopping robot in an arbitrary configuration

$$M(q)\ddot{q} + N(q,\dot{q}) = AT + F_\mathrm{ext} \tag{5.1}$$

$$A \triangleq \begin{bmatrix} 0 & 0 & 0 & 1 & 0 & 0 \\ 0 & 0 & 0 & 0 & 1 & 0 \\ 0 & 0 & 0 & 0 & 0 & 1 \end{bmatrix}^T,$$

$$T \triangleq \begin{bmatrix} \tau_1 & \tau_2 & \tau_3 \end{bmatrix}^T,$$

$$q \triangleq [\ x \quad y \ \big|\ \theta\ ]^T, \quad \theta = [\ \theta_1 \quad \theta_2 \quad \theta_3 \quad \theta_4\ ]^T$$

$$F_\mathrm{ext} \triangleq \begin{bmatrix} F_x & F_y & 0 & 0 & 0 & 0 \end{bmatrix}^T \tag{5.2}$$

where q is the vector of generalized coordinates, $M \in R^{6\times 6}$ denotes the mass matrix, N denotes the vector of centrifugal, Coriolis and forces due to gravity, and F_x, F_y are the components of the reaction force F_ext in the x and y directions. The hybrid dynamics of the

hopping robot is comprised of three phases: the flight phase, when the toe is not in contact with the ground ($y > 0$); the impact phase, the instant when the toe comes in contact with the ground; and the contact phase, during which the toe remains in contact with the ground after impact ($y = 0$).

5.2.2 Flight Phase

In the flight phase, the robot has six DOF, the following conditions hold:

$$y > 0 \qquad F_x = F_y = 0 \tag{5.3}$$

and (5.1) describes the dynamics of the robot.

5.2.3 Impact Phase

Let $t \in [t^-, t^+]$ denote the interval of impact. We make the following assumptions:

Assumption 12. *The impact between the toe and the ground is inelastic. This implies that* $\dot{x}(t^+) = \dot{y}(t^+) = 0$.

Assumption 13. *The control torques* T *are not impulsive.*

Integrating (5.1) over the infinitesimal duration $t \in [t^-, t^+]$, we get

$$\int_{t^-}^{t^+} \big[M(q)\ddot{q} + N(q,\dot{q})\big]dt = \int_{t^-}^{t^+} \big[AT + F_{\text{ext}}\big]dt \tag{5.4}$$

$$\Rightarrow \quad M(q)(\dot{q}^+ - \dot{q}^-) = I_{\text{ext}}, \quad I_{\text{ext}} \triangleq \int_{t^-}^{t^+} F_{\text{ext}}\, dt \tag{5.5}$$

We partition the inverse of the mass matrix as follows

$$M^{-1} = \left[\begin{array}{c|c} (M^{-1})_{11} & (M^{-1})_{12} \\ \hline (M^{-1})_{21} & (M^{-1})_{22} \end{array}\right] \tag{5.6}$$

From (5.5), we compute the change in the state variables:

$$\begin{aligned} q^+ &= q^- \qquad \dot{x}(t^+) = 0 \qquad \dot{y}(t^+) = 0 \\ \dot{\theta}(t^+) &= \dot{\theta}(t^-) - (M^{-1})_{21}[(M^{-1})_{11}]^{-1} \begin{bmatrix} \dot{x}^- \\ \dot{y}^- \end{bmatrix} \end{aligned} \tag{5.7}$$

5.2.4 Contact Phase

The contact phase commences immediately after the toe makes contact with the ground. For this phase, we make the following assumption:

Assumption 14. *The external forces F_y is non-negative,* i.e., $F_y \geqslant 0$.

In the contact phase, the hopper has four DOF, since

$$x = \dot{x} = \ddot{x} = 0, \quad y = \dot{y} = \ddot{y} = 0 \tag{5.8}$$

Substituting $\ddot{x} = \ddot{y} = 0$ into (5.1), the values of the F_x and F_y can be computed as

$$\begin{bmatrix} F_x \\ F_y \end{bmatrix} = \begin{bmatrix} N_1 \\ N_2 \end{bmatrix} + (M^{-1})_{11}(M^{-1})_{12} \begin{bmatrix} N_3 \\ (N_4 - \tau_1) \\ (N_5 - \tau_2) \\ (N_6 - \tau_3) \end{bmatrix} \tag{5.9}$$

where N_i's are the entries of the $N(q, \dot{q})$ vector in (5.1). The dynamical equation of the

hopper during this phase can be written as

$$DM(q)D^T D\ddot{q} + DN(q,\dot{q}) = DAT \tag{5.10}$$

where

$$D = \begin{bmatrix} 0 & 0 & 1 & 0 & 0 & 0 \\ 0 & 0 & 0 & 1 & 0 & 0 \\ 0 & 0 & 0 & 0 & 1 & 0 \\ 0 & 0 & 0 & 0 & 0 & 1 \end{bmatrix} \tag{5.11}$$

The contact phase ends when F_y in (5.9) equals zero.

5.3 Coordinate Transformation into Normal Form

5.3.1 Controlled States

To transform the system into normal form [35], we define the position of the COM relative to the position of the toe using the variable r as follows:

$$r = \begin{bmatrix} r_x \\ r_y \end{bmatrix} = \begin{bmatrix} f_x(\theta) \\ f_y(\theta) \end{bmatrix} \tag{5.12}$$

where r_x and r_y are the horizontal and vertical components of r and can be expressed as

follows

$$f_x(q) = a_1\cos(\theta_1) + a_2\cos(\theta_1+\theta_2) + a_3\cos(\theta_1+\theta_2+\theta_3) + a_4\cos(\theta_1+\theta_2+\theta_3+\theta_4) \quad (5.13)$$

$$f_y(q) = a_1\sin(\theta_1) + a_2\sin(\theta_1+\theta_2) + a_3\sin(\theta_1+\theta_2+\theta_3) + a_4\sin(\theta_1+\theta_2+\theta_3+\theta_4) \quad (5.14)$$

where

$$a_1 = \frac{\big[m_{\rm f} + 2(m_{\rm l} + m_{\rm t} + m_{\rm b})\big]\ell_{\rm f}}{\bar{m}}, \qquad a_2 = \frac{\big[m_{\rm l} + 2(m_{\rm t} + m_{\rm b})\big]\ell_{\rm l}}{\bar{m}}$$
$$a_3 = \frac{(m_{\rm t} + 2m_{\rm b})\ell_{\rm t}}{\bar{m}}, \qquad a_4 = \frac{m_{\rm b}\ell_{\rm b}}{\bar{m}}$$
$$\bar{m} = m_{\rm f} + m_{\rm l} + m_{\rm t} + m_{\rm b}$$

Differentiating with respect to time, we get

$$\dot{r} = \begin{bmatrix}\dot{r}_x \\ \dot{r}_y\end{bmatrix} = \begin{bmatrix}J_x(\theta) \\ J_y(\theta)\end{bmatrix} D\dot{q} = \begin{bmatrix}J_x(\theta) \\ J_y(\theta)\end{bmatrix}\dot{\theta} \quad (5.15)$$

where J_x and J_y are the Jacobian matrices. The output of the system described by (5.1) (flight phase) and (5.9) (contact phase) is chosen to be r_x, r_y and θ_1; it can then be shown that the system has:

$$\text{relative degree} = [2,\ 2,\ 2]^T \quad (5.16)$$

Accordingly, the six controlled states (in flight and contact phases) are chosen as

$$\zeta_1 = (r_x - x_d) \qquad \zeta_2 = (r_y - y_d) \qquad \zeta_3 = (\theta_1 - \theta_d)$$
$$\zeta_4 = \dot{r}_x \qquad \zeta_5 = \dot{r}_y \qquad \zeta_6 = \dot{\theta}_1 \quad (5.17)$$

5.3.2 Uncontrollable States - Flight Phase

In the flight phase, the dynamical system in (5.1) has six DOF or twelve states: these include the controlled states in (5.17) and the following six uncontrollable states:

$$\begin{aligned} \eta_1 &= x(t) + r_x, & \eta_2 &= \dot{x}(t) + \dot{r}_x, & \eta_3 &= y(t) + r_y, \\ \eta_4 &= \dot{y}(t) + \dot{r}_y, & \eta_5 &= H_C, & \eta_6 &= I_{\text{cm}} \end{aligned} \tag{5.18}$$

where η_1 and η_3 are the Cartesian position and η_2 and η_4 are the Cartesian velocity of the COM, $\eta_5 = H_c$ is the angular momentum of the system and $\eta_6 = I_{\text{cm}}$ is its mass-moment of inertia about its center of mass. It can be shown that the uncontrollable states satisfy [35]:

$$\frac{\partial \eta_i(q)}{\partial q}\left[(M(q))^{-1}AT\right] = 0, \quad i = 1, 2, ..., 6.$$

If T_{nf} denotes the coordinate transformation from the original states $(q^T, \dot{q}^T)^T$ to the states $(\eta_1 \cdots \eta_6, \zeta_1 \cdots \zeta_6)^T$, it can be shown that T_{nf} is a diffeomorphism. The dynamics of the

system in the normal form can now be written as:

$$\left[\begin{array}{c} \dot{\eta}_1 \\ \dot{\eta}_2 \\ \dot{\eta}_3 \\ \dot{\eta}_4 \\ \dot{\eta}_5 \\ \dot{\eta}_6 \\ \hline \dot{\zeta}_1 \\ \dot{\zeta}_2 \\ \dot{\zeta}_3 \\ \dot{\zeta}_4 \\ \dot{\zeta}_5 \\ \dot{\zeta}_6 \end{array}\right] = \left[\begin{array}{c} \eta_2 \\ 0 \\ \eta_4 \\ -g \\ 0 \\ \dot{I}_{\mathrm{cm}}(\eta,\zeta) \\ \hline \dot{r}_x \\ \dot{r}_y \\ \dot{\theta}_1 \\ J_x(q)DM^{-1}[AT - N(q,\dot{q})] + \dot{J}_x(q)\dot{\theta} \\ J_y(q)DM^{-1}[AT - N(q,\dot{q})] + \dot{J}_y(q)\dot{\theta} \\ \begin{bmatrix} 1 & 0 & 0 & 0 \end{bmatrix} DM^{-1}[AT - N(q,\dot{q})] \end{array}\right] \tag{5.19}$$

5.3.3 Uncontrollable States - Contact Phase

In the contact phase, the dynamical system in (5.9) has four DOF or eight states: these include the controlled states in (5.17) and the following two uncontrollable states:

$$\eta_1 = H_O = H_C + \bar{m}(r_x\dot{r}_y - r_y\dot{r}_x), \qquad \eta_2 = I_{cm} \tag{5.20}$$

where H_O is the angular momentum of the system about the toe - point O in Fig.5.1. Once again, it can be show that the uncontrollable states satisfy [35]

$$\frac{\partial \eta_i(q)}{\partial q}\left[(DM(q)D^T)^{-1}DAT\right] = 0, \qquad i = 1,2$$

If T_{nc} denotes the coordinate transformation from the original states $(q^T, \dot{q}^T)^T$ to $(\eta_1\, \eta_2, \zeta_1 \cdots \zeta_6)^T$, it can be shown that T_{nc} is a diffeomorphism. The dynamics of the system in the normal form can now be written as:

$$\begin{bmatrix} \dot{\eta}_1 \\ \dot{\eta}_2 \\ \hline \dot{\zeta}_1 \\ \dot{\zeta}_2 \\ \dot{\zeta}_3 \\ \dot{\zeta}_4 \\ \dot{\zeta}_5 \\ \dot{\zeta}_6 \end{bmatrix} = \begin{bmatrix} -\bar{m}\, g\, r_x \\ \dot{I}_{\text{cm}}(\eta, \zeta) \\ \hline \dot{r}_x \\ \dot{r}_y \\ \dot{\theta}_1 \\ J_x(q)(DMD^T)^{-1}D[AT - N(q, \dot{q})] + \dot{J}_x(q)\dot{\theta} \\ J_y(q)(DMD^T)^{-1}D[AT - N(q, \dot{q})] + \dot{J}_y(q)\dot{\theta} \\ \begin{bmatrix} 1 & 0 & 0 & 0 \end{bmatrix}(DMD^T)^{-1}D[AT - N(q, \dot{q})] \end{bmatrix} \tag{5.21}$$

5.4 Partial Feedback Linearization

5.4.1 Equilibrium Point

In this section, we design a continuous feedback controller to control the dynamics of the position of the COM relative to the toe (r_x, r_y) and the angle of the foot θ_1. To this end, we use feedback linearization to ensure that

$$(\zeta_1, \zeta_2, \zeta_3, \zeta_4, \zeta_5, \zeta_6) = (0, 0, 0, 0, 0, 0)$$

is an equilibrium point of the system.

5.4.2 Flight Phase

In the flight phase, the dynamics of the controlled states ζ_4, ζ_5, ζ_6 in (5.19) can be expressed as

$$\begin{bmatrix} \dot{\zeta}_4 \\ \dot{\zeta}_5 \\ \dot{\zeta}_6 \end{bmatrix} = J(q)DM^{-1}[AT - N(q,\dot{q})] + \dot{J}(q)\dot{\theta} \tag{5.22}$$

where

$$J(q) = \begin{bmatrix} J_x \\ J_y \\ C \end{bmatrix}, \quad \dot{J}(q) = \begin{bmatrix} \dot{J}_x \\ \dot{J}_y \\ 0 \end{bmatrix}, \quad C \triangleq \begin{bmatrix} 1 & 0 & 0 & 0 \end{bmatrix} \tag{5.23}$$

The control input T_f is chosen as follows

$$T_f = [JDM^{-1}A]^{-1}[v_f + JDM^{-1}N - \dot{J}\dot{\theta}] \tag{5.24}$$

where

$$v_f = \begin{bmatrix} -K_1\zeta_1 - K_4\zeta_4 \\ -K_2\zeta_2 - K_5\zeta_5 \\ -K_3\zeta_3 - K_6\zeta_6 \end{bmatrix} \tag{5.25}$$

This results in the following dynamics:

$$\begin{bmatrix} \dot{\zeta}_4 \\ \dot{\zeta}_5 \\ \dot{\zeta}_6 \end{bmatrix} = \begin{bmatrix} -K_1\zeta_1 - K_4\zeta_4 \\ -K_2\zeta_2 - K_5\zeta_5 \\ -K_3\zeta_3 - K_6\zeta_6 \end{bmatrix} \Rightarrow \begin{array}{l} \ddot{\zeta}_1 + K_4\dot{\zeta}_1 + K_1\zeta_1 = 0 \\ \ddot{\zeta}_2 + K_5\dot{\zeta}_2 + K_2\zeta_2 = 0 \\ \ddot{\zeta}_3 + K_6\dot{\zeta}_3 + K_3\zeta_3 = 0 \end{array} \tag{5.26}$$

The choice of gains K_i, $i = 1, 2, \cdots, 6$, will be discussed later.

5.4.3 Contact Phase

In the contact phase, the dynamics of the controlled states ζ_4, ζ_5, ζ_6 in (5.21) can be expressed as

$$\begin{bmatrix} \dot{\zeta}_4 \\ \dot{\zeta}_5 \\ \dot{\zeta}_6 \end{bmatrix} = J(q)(DMD^T)^{-1}D[AT - N(q, \dot{q})] + \dot{J}(q)\dot{\theta} \tag{5.27}$$

The control input T_c is chosen as follows

$$T_c = [J(DMD^T)^{-1}DA]^{-1}[J(DMD^T)^{-1}DN + v_c - \dot{J}\dot{\theta}] \tag{5.28}$$

where

$$v_c = \begin{bmatrix} -K_7\zeta_1 - K_{10}\zeta_4 \\ -K_8\zeta_2 - \alpha K_{11}\zeta_5 \\ -K_9\zeta_3 - K_{12}\zeta_6 \end{bmatrix}, \quad \alpha = \begin{cases} 1, & \text{if } \zeta_5 \leqslant 0 \\ \nu, & \text{if } \zeta_5 > 0 \end{cases} \tag{5.29}$$

This results in the following dynamics:

$$\begin{bmatrix} \dot{\zeta}_4 \\ \dot{\zeta}_5 \\ \dot{\zeta}_6 \end{bmatrix} = \begin{bmatrix} -K_7\zeta_1 - K_{10}\zeta_4 \\ -K_8\zeta_2 - \alpha K_{11}\zeta_5 \\ -K_9\zeta_3 - K_{12}\zeta_6 \end{bmatrix} \Rightarrow \begin{matrix} \ddot{\zeta}_1 + K_{10}\dot{\zeta}_1 + K_7\zeta_1 = 0 \\ \ddot{\zeta}_2 + \alpha K_{11}\dot{\zeta}_2 + K_8\zeta_2 = 0 \\ \ddot{\zeta}_3 + K_{12}\dot{\zeta}_3 + K_9\zeta_3 = 0 \end{matrix} \tag{5.30}$$

Once again, the choice of gains K_i, $i = 7, 8, \cdots, 12$, will be discussed later.

5.5 Controlling The Apex Height

5.5.1 Apex Height

The apex height h is defined as the maximum value of the vertical displacement of the COM during the flight phase. It should be mentioned that some fraction of the total energy of the system is lost during impact with the ground. To overcome this loss and reach the desired level of energy and hop to the desired value h_d, we developed two control strategies. The first strategy is based on introducing negative damping in the vertical dynamics during the contact phase by choosing the parameter ν to be less than zero. The negative damping is introduced in the vertical dynamics to overcome the energy loss due to the impact. The second strategy is based on choosing different equilibrium heights y_d of the vertical dynamics of the COM during the flight phase and contact phase. If the value of y_d in the contact phase is equal to y_{cd}, for the flight phase we choose $y_d = y_{fd} < y_{cd}$.

5.5.2 The First Strategy: Negative Damping Based Continuous-Time Controller

In this section we discuss the procedure for choosing gains and the desired values of the continuous controller. In addition, we discuss the behavior of controlled and uncontrolled states.

Flight Phase

In the flight phase, the gains of the continuous controller are chosen as:

$$\begin{aligned} K_4 =& 2\sqrt{K_1}, \qquad K_5 = 2\sqrt{K_2}, \qquad K_6 = 2\sqrt{K_3} \\ K_2 =& K_3, \qquad\qquad K_5 = K_6 \end{aligned} \tag{5.31}$$

This choice results in critically-damped dynamics of the controlled states ζ_1, ζ_2, ζ_3.

From (5.19), it can be seen that the uncontrolled states $\eta_1, \cdots, \eta_5$ are described by the relations

$$\dot{\eta}_2 = \ddot{\eta}_1 = 0, \qquad \dot{\eta}_4 = \ddot{\eta}_3 = -g, \qquad \dot{\eta}_5 = 0$$

and are therefore bounded. The uncontrolled state η_6 also remains bounded as it denotes the mass-moment of inertia about the COM and all the joints are revolute in nature.

The values of x_d, y_d, and θ_d were chosen to be constant; a particular set of choices will be shown in our simulations in section 5.7.

Contact Phase

In the contact phase, the gains of the continuous controller are chosen as:

$$\begin{aligned} K_{10} =& 2\sqrt{K_7}, \qquad K_{11} < 2\sqrt{K_8}, \qquad K_{12} < 2\sqrt{K_9} \\ K_8 =& K_9, \qquad\qquad K_{11} = K_{12} \end{aligned} \tag{5.32}$$

This choice results in critically damped controlled state ζ_1 and under-damped controlled state ζ_3; the controlled state ζ_2 is underdamped when $\dot{\zeta}_2 < 0$ and negatively damped when $\dot{\zeta}_2 > 0$. As mentioned earlier, the negative damping allows for compensation of the losses due to impact.

The uncontrolled state η_1 and its derivative can be shown to be

$$\eta_1 = H_O = H_C + \bar{m}(r_x\dot{r}_y - r_y\dot{r}_x), \quad \dot{\eta}_1 = \dot{H}_O = -\bar{m}g\, r_x \tag{5.33}$$

The values of y_d, and θ_d were chosen to be constant but x_d is chosen as

$$x_d = \gamma H_O, \qquad \gamma > 0 \tag{5.34}$$

This results in $\dot{H}_O \to -\gamma\bar{m}gH_O$, which in turn results in

$$H_O \to 0 \quad \Rightarrow \quad r_x, \dot{r}_x \to 0 \quad \Rightarrow \quad H_C \to 0$$

As in the flight phase, the uncontrolled state η_2 remains bounded as it denotes the mass-moment of inertia about the COM and all joints of the system are revolute.

5.5.3 The Second Strategy: Equilibrium Height Based Based Continuous-Time Controller

In this section we discuss the procedure for choosing gains and the desired values of the continuous controller. In addition, we discuss the behavior of controlled and uncontrolled states.

Flight Phase

In the flight phase, the gains of the continuous controller are chosen as:

$$\begin{aligned} K_4 =& 2\sqrt{K_1}, \qquad K_5 = 2\sqrt{K_2}, \qquad K_6 = 2\sqrt{K_3} \\ K_2 =& K_3, \qquad\qquad K_5 = K_6 \end{aligned} \tag{5.35}$$

This choice results in critically-damped dynamics of the controlled states ζ_1, ζ_2, ζ_3.

From (5.19), it can be seen that the uncontrolled states $\eta_1, \cdots, \eta_5$ are described by the relations

$$\dot{\eta}_2 = \ddot{\eta}_1 = 0, \qquad \dot{\eta}_4 = \ddot{\eta}_3 = -g, \qquad \dot{\eta}_5 = 0$$

and are therefore bounded. The uncontrolled state η_6 also remains bounded as it denotes the mass-moment of inertia about the COM and the joints are revolute.

The values of x_d, and θ_d were chosen to be constant; a particular set of choices will be shown in our simulations in section 5.7.

Contact Phase

In the contact phase, the gains of the continuous controller are chosen as:

$$\begin{aligned} K_{10} =& 2\sqrt{K_7}, \qquad K_{11} < 2\sqrt{K_8}, \qquad K_{12} < 2\sqrt{K_9} \\ K_8 =& K_9, \qquad\qquad K_{11} = K_{12} \end{aligned} \tag{5.36}$$

This choice results in critically damped controlled state ζ_1 and under-damped controlled state ζ_2 and ζ_3.

The uncontrolled state η_1 and its derivative can be shown to be

$$\eta_1 = H_O = H_C + \bar{m}(r_x\dot{r}_y - r_y\dot{r}_x), \quad \dot{\eta}_1 = \dot{H}_O = -\bar{m}g\, r_x \tag{5.37}$$

The values of y_d, and θ_d were chosen to be constant but x_d is chosen as

$$x_d = \gamma H_O, \qquad \gamma > 0 \tag{5.38}$$

This results in $\dot{H}_O \to -\gamma\bar{m}gH_O$, which in turn results in

$$H_O \to 0 \quad \Rightarrow \quad r_x, \dot{r}_x \to 0 \quad \Rightarrow \quad H_C \to 0$$

As in the flight phase, the uncontrolled state η_2 remains bounded.

5.5.4 Discrete-Time Controller

Poincaré Map

The hopping motion is comprised of the flight, impact and contact phases. The dynamics of the controlled states in the flight and contact phases were designed to emulate a mass-spring-damper system. For both continuous controller strategies , the controlled states remain bounded since they have linear dynamics. It was shown that the uncontrolled states are also bounded. To investigate the stability of the hybrid system, we use a Poincaré map with the Poincaré section defined at the point of touch-down, i.e. the time instant prior to impact. Assuming at the time of touch-down we have

$$\begin{aligned} &\eta_1 = x_d, \quad \eta_2 = 0, \quad \eta_3 = y_{fd}, \quad \eta_5 = 0, \quad \zeta_1 = 0, \\ &\zeta_2 = 0, \quad \zeta_3 = 0, \quad \zeta_4 = 0, \quad \zeta_5 = 0, \quad \zeta_6 = 0 \end{aligned} \tag{5.39}$$

The Poincaré section was chosen as

$$\begin{aligned} \mathcal{Z} \coloneqq \{X \in \mathbb{R}^2 |\, &\eta_1 = x_d, \eta_2 = 0, \eta_3 = y_{cd}, \eta_5 = 0, \zeta_1 = 0, \\ &\zeta_2 = 0, \zeta_3 = 0, \zeta_4 = 0, \zeta_5 = 0, \zeta_6 = 0\} \end{aligned} \tag{5.40}$$

where X is defined as

$$X = \begin{bmatrix} \eta_4 & \eta_6 \end{bmatrix}^T \tag{5.41}$$

We defined the Poincaré section using the coordinate Ψ, where Ψ is defined by the coordinate

transformation $H(X) : \mathbb{R}^2 \Rightarrow \mathbb{R}^2$, as follows

$$\Psi = H(X) = \left[\; (h - h_{\mathrm{d}}) \quad (I_{\mathrm{cm}} - I_{\mathrm{cmd}}) \; \right]^T \tag{5.42}$$

Assuming that there is no relative motion between the links at touch-down[1], the apex height h can be defined as

$$h = \frac{E_{\mathrm{total}}}{\bar{m}g} = \frac{1}{2g}\eta_4^2 + y_d \tag{5.43}$$

It can be shown that the map $H(\cdot)$ is a local homeomorphism; this implies that the stability of the Poincaré maps in Ψ and X coordinates are equivalent. The Poincaré map $P(\Psi)$ and the sequence of points $\Psi_k \in H(\mathcal{Z})$ satisfy

$$\Psi_{k+1} = P(\Psi_k) \tag{5.44}$$

with periodic point Ψ^* defined as

$$\Psi^* = P(\Psi^*) \tag{5.45}$$

We define the error state χ_k as

$$\chi_k = (\Psi_k - \Psi^*)$$

By linearizing the Poincaré map about Ψ^*, we have the approximate discrete dynamics given by

$$\chi_{k+1} = A\,\chi_k \qquad A \triangleq \left.\frac{dP(\Psi)}{d\Psi}\right|_{\Psi=\Psi^*} \tag{5.46}$$

The periodic point will be asymptotically stable iff

$$\rho(A) < 1 \tag{5.47}$$

[1]This is accomplished by choosing the gains in (5.31) for the first strategy and (5.35) for the second strategy, which results in critically damped behavior

where $\rho(A)$ is the spectral radius of A.

Closed-Loop Control Design - The First Strategy

We now develop a discrete-time controller to drive the discrete-time state to its desired value $\Psi = 0$. By varying two of the continuous controller parameters at touch-down, namely, ν and θ_d, we will be able to stabilize the desired state $\Psi = 0$. The dynamics of the discrete-time system can be described by

$$\Psi(k+1) = P(\Psi(k), \nu, \theta_d) \tag{5.48}$$

By linearizing the above map about the fixed point $\Psi^* = 0$, $\nu = \nu^*$, and $\theta_d = \theta_d^*$, we get

$$\chi(k+1) = A\chi(k) + Bu(k), \qquad y(k) = \chi(k) \tag{5.49}$$

where

$$\begin{aligned}
&\chi(k) = \Psi(k) - \Psi^*, \qquad u(k) = \left[\nu(k) - \nu^* \;\; \theta_d(k) - \theta_d^*\right]^T \\
&A = \left[\frac{\partial P(\Psi, \nu, \theta_d)}{\partial \Psi}\right]_{\Psi=\Psi^*, \nu=\nu^*, \theta_d=\theta_d^*}, \\
&B = \left[\frac{\partial P(\Psi, \nu, \theta_d)}{\partial \nu} \;\; \frac{\partial P(\Psi, \nu, \theta_d)}{\partial \theta_d}\right]_{\Psi=\Psi^*, \nu=\nu^*, \theta_d=\theta_d^*}
\end{aligned} \tag{5.50}$$

To converge the apex height to the desired value, we use integral control, with the integrator defined as

$$\beta(k+1) = \beta(k) - y(k) \tag{5.51}$$

The integrator-augmented discrete system has the form

$$\lambda(k+1) = \mathbb{A}\lambda(k) + \mathbb{B}u(k), \quad \lambda(k) = \begin{bmatrix} \chi^T(k) & \beta^T(k) \end{bmatrix}^T$$
$$\mathbb{A} \triangleq \begin{bmatrix} A & 0 \\ -I & I \end{bmatrix}, \quad \mathbb{B} \triangleq \begin{bmatrix} B \\ 0 \end{bmatrix} \tag{5.52}$$

where A and B are defined in (5.50). If $\{\mathbb{A}, \mathbb{B}\}$ is controllable, the input can be chosen as

$$u(k) = \mathbb{K}\lambda(k) \tag{5.53}$$

such that

$$\rho(\mathbb{A} + \mathbb{B}\mathbb{K}) < 1$$

Closed-Loop Control Design - The Second Strategy

We now develop a discrete-time controller to drive the discrete-time state to its desired value $\Psi = 0$. By varying two of the continuous controller parameters at touch-down, namely, y_{cd} and θ_d, we will be able to stabilize the desired state $\Psi = 0$. The dynamics of the discrete-time system can be described by

$$\Psi(k+1) = P(\Psi(k), y_{cd}, \theta_d) \tag{5.54}$$

By linearizing the above map about the fixed point $\Psi^* = 0$, $y_{cd} = y_{cd}^*$, and $\theta_d = \theta_d^*$, we get

$$\chi(k+1) = A\chi(k) + Bu(k), \qquad y(k) = \chi(k) \tag{5.55}$$

where

$$\begin{aligned}
&\chi(k) = \Psi(k) - \Psi^*, \qquad u(k) = \left[y_{cd} - y_{cd}^* \;\; \theta_d(k) - \theta_d^*\right]^T \\
&A = \left[\frac{\partial P(\Psi, y_{cd}, \theta_d)}{\partial \Psi}\right]_{\Psi=\Psi^*, y_{cd}=y_{cd}^*, \theta_d=\theta_d^*}, \\
&B = \left[\frac{\partial P(\Psi, y_{cd}, \theta_d)}{\partial y_{cd}} \;\; \frac{\partial P(\Psi, y_{cd}, \theta_d)}{\partial \theta_d}\right]_{\Psi=\Psi^*, y_{cd}=y_{cd}^*, \theta_d=\theta_d^*}
\end{aligned} \tag{5.56}$$

To converge the apex height to the desired value, we use integral control, with the integrator defined as

$$\beta(k+1) = \beta(k) - y(k) \tag{5.57}$$

The integrator-augmented discrete system has the form

$$\begin{aligned}
&\lambda(k+1) = \mathbb{A}\lambda(k) + \mathbb{B}u(k), \quad \lambda(k) = \left[\begin{array}{cc} \chi^T(k) & \beta^T(k) \end{array}\right]^T \\
&\mathbb{A} \triangleq \left[\begin{array}{cc} A & 0 \\ -I & I \end{array}\right], \quad \mathbb{B} \triangleq \left[\begin{array}{c} B \\ 0 \end{array}\right]
\end{aligned} \tag{5.58}$$

where A and B are defined in (5.56). If $\{\mathbb{A}, \mathbb{B}\}$ is controllable, the input can be chosen as

$$u(k) = \mathbb{K}\lambda(k) \tag{5.59}$$

such that

$$\rho(\mathbb{A} + \mathbb{B}\mathbb{K}) < 1$$

5.5.5 Effect of Continuous Controller Parameters on Apex Height

In this section we will study the effect of the controller parameters on the apex height for both strategies.

First Strategy: Negative Damping

The apex height h depends on the total energy of the system at takeoff point when $F_y = 0$. Substituting (5.17), (5.28) and (5.29) into (5.9), we get

$$(r_y - y_d) = \frac{g - K_{11}\nu\dot{r}_y}{K_8} \tag{5.60}$$

The total energy of the robot at the takeoff point is

$$E = \frac{1}{2}\bar{m}\dot{r}_y^2 + \bar{m}g\left[\frac{g - K_{11}\nu\dot{r}_y}{K_8} + y_d\right] \tag{5.61}$$

Assuming that the relative motion between hopper links quickly settles to zero and no significant work is done by the actuator during this time, the apex height h is computed as

$$h = \frac{E}{\bar{m}g} = \frac{1}{2g}\dot{r}_y^2 + \frac{g - K_{11}\nu\dot{r}_y}{K_8} + y_d \tag{5.62}$$

To examine the effect of the control parameters K_8, K_{11}, ν, and y_d on the apex height, we compute the partial derivatives of h in (5.62) with respect to the parameters; they are

$$\begin{aligned} \frac{\partial h}{\partial K_8} &= -\frac{(g - K_{11}\nu\dot{r}_y)}{K_8^2} < 0, \quad & \frac{\partial h}{\partial \nu} &= -\frac{K_{11}\dot{r}_y}{K_8} < 0, \\ \frac{\partial h}{\partial K_{11}} &= -\frac{\nu\dot{r}_y}{K_8} < 0, & \frac{\partial h}{\partial y_d} &= 1 > 0 \end{aligned} \tag{5.63}$$

Clearly, the apex height is higher for smaller values of K_8, and ν and higher values of K_{11}, and y_d.

Second Strategy: Equilibrium Height

The apex height h depends on the total energy of the system at takeoff point when $F_y = 0$. Substituting (5.17), (5.28) and (5.29) into (5.9), we get

$$(r_y - y_{cd}) = \frac{g - K_{11}\dot{r}_y}{K_8} \tag{5.64}$$

The total energy of the robot at the takeoff point is

$$E = \frac{1}{2}\bar{m}\dot{r}_y^2 + \bar{m}g\left[\frac{g - K_{11}\dot{r}_y}{K_8} + y_{cd}\right] \tag{5.65}$$

Assuming that the relative motion between hopper links quickly settles to zero and no significant work is done by the actuator during this time, the apex height h is computed as

$$h = \frac{E}{\bar{m}g} = \frac{1}{2g}\dot{r}_y^2 + \frac{g - K_{11}\dot{r}_y}{K_8} + y_{cd} \tag{5.66}$$

To examine the effect of the control parameters K_8, K_{11} and y_{cd} on the apex height, we compute the partial derivatives of h in (5.66) with respect to the parameters; they are

$$\frac{\partial h}{\partial K_8} = -\frac{(g - K_{11}\dot{r}_y)}{K_8^2}, \quad \frac{\partial h}{\partial K_{11}} = -\frac{\dot{r}_y}{K_8} < 0, \quad \frac{\partial h}{\partial y_{cd}} = 1 > 0 \tag{5.67}$$

Clearly, the apex height is higher for smaller values of K_{11} and higher values of y_{cd}. For K_8, the apex height is higher for smaller values of K_8 when

$$K_{11} < \frac{g}{\dot{r}_y} \tag{5.68}$$

the apex height is higher for higher values of K_8 when

$$K_{11} > \frac{g}{\dot{r}_y} \tag{5.69}$$

5.6 Control of Hopping Locomotion

5.6.1 Hopping Step Size

We define δ to be the hopping step size, *i.e.*, the horizontal displacement of the toe during the flight phase. To achieve a desired value of $\delta = \delta_d$, the dynamics of the state ζ_1 is controlled by varying the desired value x_d in both the flight and contact phases. To overcome the energy losses, we will use the negative damping strategy ($\nu < 0$).

5.6.2 Flight Phase

The controller gains for the controlled states are the same as in (5.31) but the value of x_d is chosen as

$$x_d = \begin{cases} 0, & \text{if } \zeta_5 \geqslant 0 \\ \mu_1 H_C, & \text{if } \zeta_5 < 0 \end{cases}, \qquad \mu_1 > 0 \tag{5.70}$$

Since H_C is negative at the time of take-off and remains constant during the flight phase, the above choice of x_d results in placement of the toe ahead of the COM in the horizontal direction.

5.6.3 Contact Phase

In the contact phase, x_d is chosen as:

$$x_d = \begin{cases} 0, & \text{if } \zeta_5 \leqslant 0 \\ \mu_2, & \zeta_5 > 0 \text{ and } \zeta_2 \leqslant 0 \,, \\ \mu_3, & \zeta_5 > 0 \text{ and } \zeta_2 > 0 \end{cases} \qquad \mu_3 > \mu_2 > 0 \tag{5.71}$$

Since the toe is ahead of the COM in the horizontal direction at the time of touch-down, the impact phase results is a positive angular impulse and instantaneously changes H_C from a negative value to a positive value. The above choice of x_d in the contact phase ensures that at the time of take-off, H_C has a small negative value and the COM has a positive velocity in the horizontal direction.

5.6.4 Poincaré Map

To investigate the stability of the hybrid system, we use a Poincaré map with the Poincaré section defined at the point of touch-down. At the time of touch-down, we assume the system states to satisfy:

$$\begin{aligned} &\eta_3 = y_d, \qquad \zeta_1 = 0, \qquad \zeta_2 = 0, \qquad \zeta_3 = 0, \\ &\zeta_4 = 0, \qquad \zeta_5 = 0, \qquad \zeta_6 = 0 \end{aligned} \tag{5.72}$$

Thus, the Poincaré section is chosen as

$$\bar{\mathcal{Z}} := \{\bar{\Psi} \in \mathbb{R}^5 | \, \eta_3 = y_d, \zeta_1 = 0, \zeta_2 = 0, \zeta_3 = 0, \zeta_4 = 0, \zeta_5 = 0, \zeta_6 = 0\} \tag{5.73}$$

where $\bar{\Psi}$ are the states that define the Poincaré section

$$\bar{\Psi} = [\ \delta \quad \eta_2 \quad \eta_4 \quad \eta_5 \quad \eta_6\ ]^T \tag{5.74}$$

The Poincaré map $P(\bar{\Psi})$ satisfies

$$\bar{\Psi}_{k+1} = P(\bar{\Psi}_k) \tag{5.75}$$

with periodic point $\bar{\Psi}^*$ defined as

$$\bar{\Psi}^* = P(\bar{\Psi}^*) \tag{5.76}$$

We define the error state $\bar{\chi}_k$ as

$$\bar{\chi}_k = (\bar{\Psi}_k - \bar{\Psi}^*)$$

By linearizing the Poincaré map about $\bar{\Psi}^*$, we have the approximately linear discrete dynamics given by

$$\bar{\chi}_{k+1} = \bar{A}\,\bar{\chi}_k \qquad \bar{A} \triangleq \left.\frac{dP(\bar{\Psi})}{d\bar{\Psi}}\right|_{\bar{\Psi}=\bar{\Psi}^*} \tag{5.77}$$

The periodic point $\bar{\Psi}^*$ will be asymptotically stable iff

$$\rho(\bar{A}) < 1 \tag{5.78}$$

where $\rho(\bar{A})$ is the spectral radius of $\bar{A}$.

5.6.5 Closed-loop Control Design

We now develop a discrete-time controller to drive δ to its desired value δ_d. By varying one of the continuous controller parameters immediately before touch-down, namely μ_2, we stabilize the discrete-time states $\bar{\Psi} = \bar{\Psi}^*$. The dynamics of the discrete-time system can be described by

$$\bar{\Psi}(k+1) = P(\bar{\Psi}(k), \mu_2) \tag{5.79}$$

By linearizing the above map about the fixed point $\bar{\Psi} = \bar{\Psi}^*$, $\mu_2 = \mu_2^*$, we get

$$\bar{\chi}(k+1) = \bar{A}\bar{\chi}(k) + \bar{B}u(k) \tag{5.80}$$

where

$$\begin{aligned} &\bar{\chi}(k) = \bar{\Psi}(k) - \bar{\Psi}^*, \qquad u(k) = \mu_2 - \mu_2^* \\ &\bar{A} = \left[\frac{\partial P(\bar{\Psi}, \mu_2)}{\partial \bar{\Psi}}\right]_{\substack{\bar{\Psi}=\bar{\Psi}^* \\ \mu_2=\mu_2^*}}, \bar{B} = \left[\frac{\partial P(\bar{\Psi}, \mu_2)}{\partial \mu_2}\right]_{\substack{\bar{\Psi}=\bar{\Psi}^* \\ \mu_2=\mu_2^*}} \end{aligned} \tag{5.81}$$

To converge δ to its desired value δ_d, we propose to use integral control with the integrator defined as

$$\bar{\beta}(k+1) = \bar{\beta}(k) - (\delta - \delta_d) \tag{5.82}$$

The integrator-augmented discrete system has the form

$$\begin{aligned} &\bar{\lambda}(k+1) = \bar{\mathbb{A}}\bar{\lambda}(k) + \bar{\mathbb{B}}u(k), \quad \bar{\lambda}(k) \triangleq \begin{bmatrix} \bar{\chi}(k) & \bar{\beta}(k) \end{bmatrix}^T \\ &\bar{\mathbb{A}} \triangleq \begin{bmatrix} \bar{A} & 0 \\ -1 & 1 \end{bmatrix}, \quad \bar{\mathbb{B}} \triangleq \begin{bmatrix} \bar{B} \\ 0 \end{bmatrix} \end{aligned} \tag{5.83}$$

where $\bar{A}$ and $\bar{B}$ is defined in (5.81). If $\{\bar{\mathbb{A}}, \bar{\mathbb{B}}\}$ is controllable, the input can be chosen as

$$u(k) = \bar{\mathbb{K}}\bar{\lambda}(k) \tag{5.84}$$

such that

$$\rho(\bar{\mathbb{A}} + \bar{\mathbb{B}}\bar{\mathbb{K}}) < 1$$

5.7 Simulation

5.7.1 Apex Height Control

We present simulation results for apex height control for both strategies starting from rest. The robot parameters were assumed to be

$$\begin{aligned} m_{\mathrm{f}} &= 0.15\,\mathrm{kg}, & m_{\mathrm{l}} &= 0.3\,\mathrm{kg}, & m_{\mathrm{t}} &= 0.3\,\mathrm{kg}, & m_{\mathrm{b}} &= 1\,\mathrm{kg}, \\ \ell_{\mathrm{f}} &= 0.05\,\mathrm{m}, & \ell_{\mathrm{l}} &= 0.15\,\mathrm{m}, & \ell_{\mathrm{t}} &= 0.15\,\mathrm{m}, & \ell_{\mathrm{b}} &= 0.15\,\mathrm{m} \end{aligned} \tag{5.85}$$

and the gains of the continuous controller were chosen to be

$$\begin{aligned} K_1 &= K_7 = 14400 & K_2 &= K_3 = 6400 & K_4 &= K_{10} = 240, \\ K_5 &= K_6 = 160 & K_8 &= K_9 = 225, & K_{11} &= K_{12} = 6 \end{aligned}$$

The robot was assumed to be initially at rest on the ground; the initial conditions are

$$\begin{aligned} x(0) &= 0\,\mathrm{m} & \dot{x}(0) &= 0\,\mathrm{m/s}, & y(0) &= 0\,\mathrm{m} & \dot{y}(0) &= 0\,\mathrm{m/s} \\ \theta_1(0) &= 2.76\,\mathrm{rad} & \dot{\theta}_1(0) &= 0\,\mathrm{rad/s}, & \theta_2(0) &= -1.84\,\mathrm{rad} & \dot{\theta}_2(0) &= 0\,\mathrm{rad/s} \\ \theta_3(0) &= 1.37\,\mathrm{rad} & \dot{\theta}_3(0) &= 0\,\mathrm{rad/s}, & \theta_4(0) &= -1.63\,\mathrm{rad} & \dot{\theta}_4(0) &= 0\,\mathrm{rad/s} \end{aligned} \tag{5.86}$$

The desired apex height and the moment of inertia about the COM were chosen as

$$h_{\mathrm{d}} = 0.6\,\mathrm{m}, \qquad I_{\mathrm{cmd}} = 0.086\,\mathrm{kg.m}^2 \tag{5.87}$$

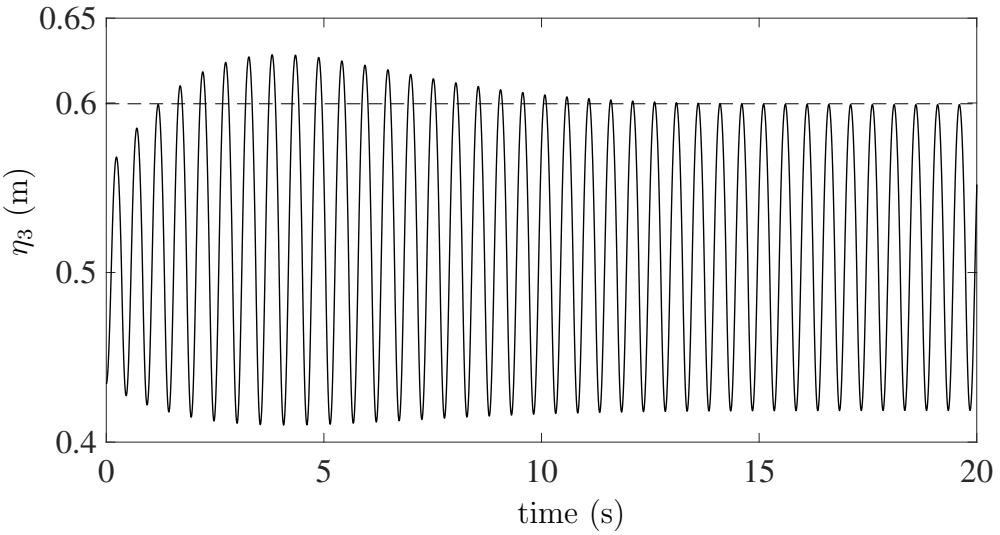

Figure 5.2: Vertical displacement of the COM during apex-height control η_3.

Negative Damping Strategy

For this strategy, we choose the parameters of the continuous controller to be

$$\nu = -0.65, \quad y_d = 0.485, \quad \theta_d = 2.2, \quad \gamma = 1$$

The initial values of the integrator state β were chosen to be zero. Since $\{\mathbb{A}, \mathbb{B}\}$ is controllable, the controller gains were chosen as

$$\mathbb{K} = \begin{bmatrix} 0.5 & 0 & -0.3 & 0 \\ 0 & -9 & 0 & 5 \end{bmatrix} \tag{5.88}$$

This places the eigenvalues of the closed loop system at $0.797 \pm 0.533i$ and $0.847 \pm 0.071i$. Figures 5.2 and 5.3 shows the results of apex height control using negative damping. Figure 5.2 plots the vertical displacement of the COM (η_3); it can be seen that the COM converges to the desired apex height. Figure 5.3 shows the states of the discrete-time system; it can be seen that both states converge to their desired values.

After the controller achieved its objective, we found the values of ν, and θ_d to be

$$\nu^* = -0.578, \qquad \theta_d^* = 2.102\,\text{rad} \tag{5.89}$$

A video animation of a four-link hopper hop in place has been uploaded as supplementary material. It shows the hopper reaching the desired apex height of $h_d = 0.6$ m starting from rest.

Equilibrium Height Control Strategy

For this strategy, we choose the parameters of the continuous controller to be

$$y_{fd} = 0.49, \quad y_{cd} = 0.53, \quad \theta_d = 2.2, \quad \gamma = 1$$

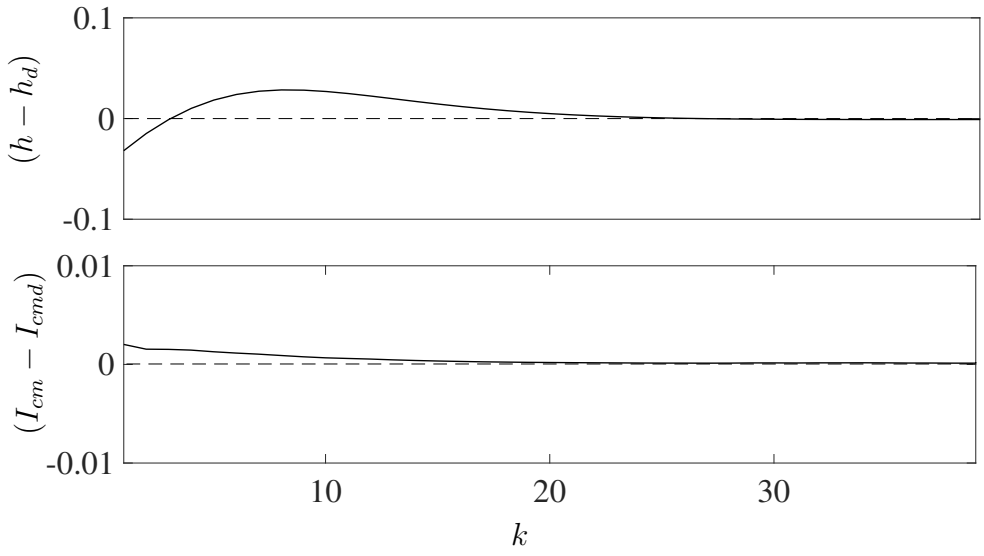

Figure 5.3: Discrete-time states $(h - h_d)$ and $(I_{cm} - I_{cmd})$ at the end of each hop fr apex-height control using negative damping.

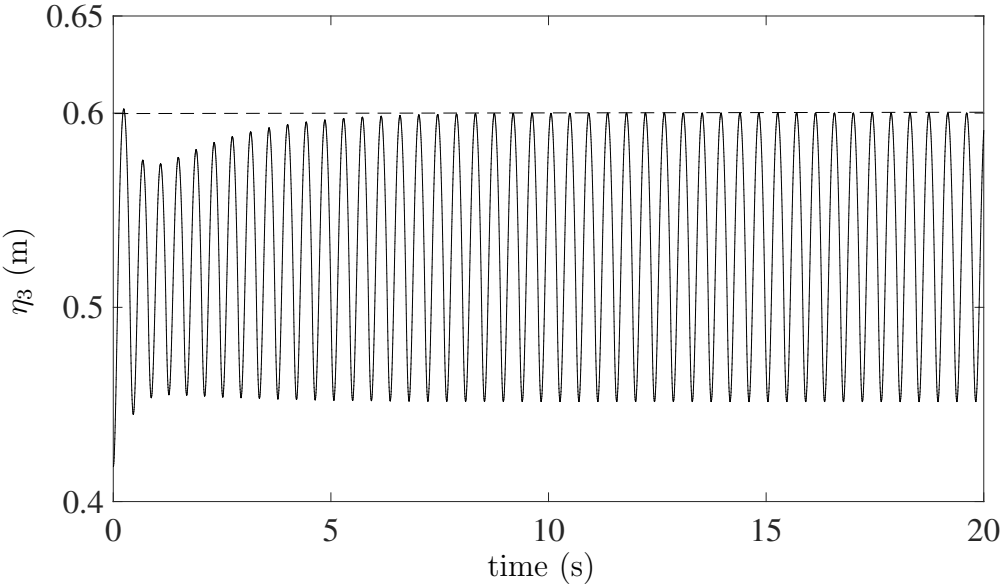

Figure 5.4: Vertical displacement of the COM during apex-height control η_3.

The initial values of the integrator state β were chosen to be zero. Since $\{\mathbb{A}, \mathbb{B}\}$ is controllable, the controller gains were chosen as

$$\mathbb{K} = \begin{bmatrix} -0.1 & 0 & 0.1 & 0 \\ 0 & -3 & 0 & 3 \end{bmatrix} \tag{5.90}$$

This places the eigenvalues of the closed loop system at -0.17, 0.3, 0.77, and 0.97.

Figures 5.4 and 5.5 shows the results of apex height control using negative damping. Figure 5.4 plots the vertical displacement of the COM (η_3); it can be seen that the COM converges to the desired apex height. Figure 5.5 shows the states of the discrete-time system; it can be seen that both states converge to their desired values.

After the controller achieved its objective, we found the values of y_{cd} and θ_d to be

$$y_{cd}^* = 0.546, \qquad \theta_d^* = 2.21\,\text{rad} \tag{5.91}$$

A video animation of a four-link hopper hop in place has been uploaded as supplementary

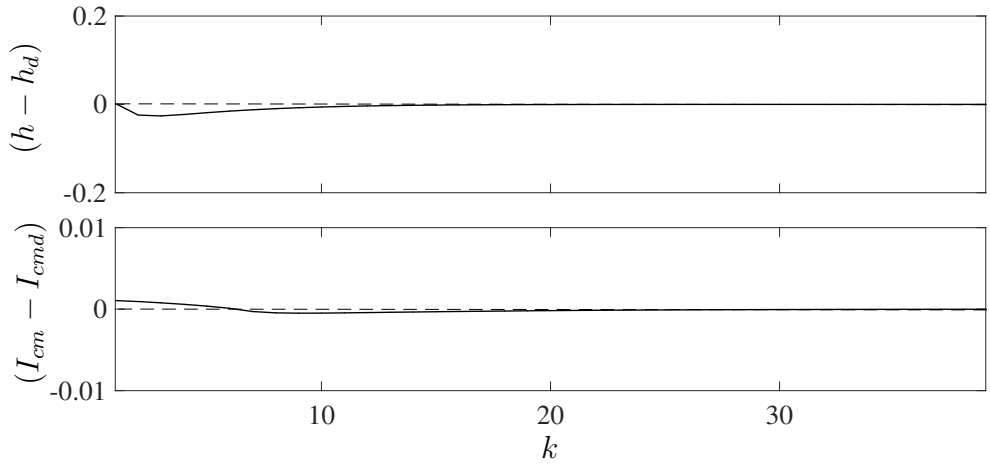

Figure 5.5: Discrete-time states $(h-h_d)$ and $(I_{cm}-I_{cmd})$ at the end of each hop fr apex-height control using negative damping.

material. It shows the hopper reaching the desired apex height of $h_d = 0.6$ m starting from rest.

5.7.2 Step Size Control in Hopping Locomotion

We present simulation results for hopping locomotion starting from rest with a desired step size. The parameters of the continuous controller is chosen to be

$$m_{\mathrm{f}} = 0.15\,\mathrm{kg}, \qquad m_{\mathrm{l}} = m_{\mathrm{t}} = 0.3\,\mathrm{kg}, \qquad m_{\mathrm{b}} = 1.0\,\mathrm{kg},$$
$$\ell_{\mathrm{f}} = 0.05\,\mathrm{m}, \qquad \ell_{\mathrm{l}} = \ell_{\mathrm{t}} = 0.15\,\mathrm{m}, \qquad \ell_{\mathrm{b}} = 0.25\,\mathrm{m}$$

and the gains of the continuous controller were chosen as

$$K_1 = K_7 = 2500, \qquad K_2 = K_3 = 400, \qquad K_4 = K_{10} = 100,$$
$$K_5 = K_6 = 6, \qquad K_8 = K_9 = 10000, \qquad K_{11} = K_{12} = 200$$

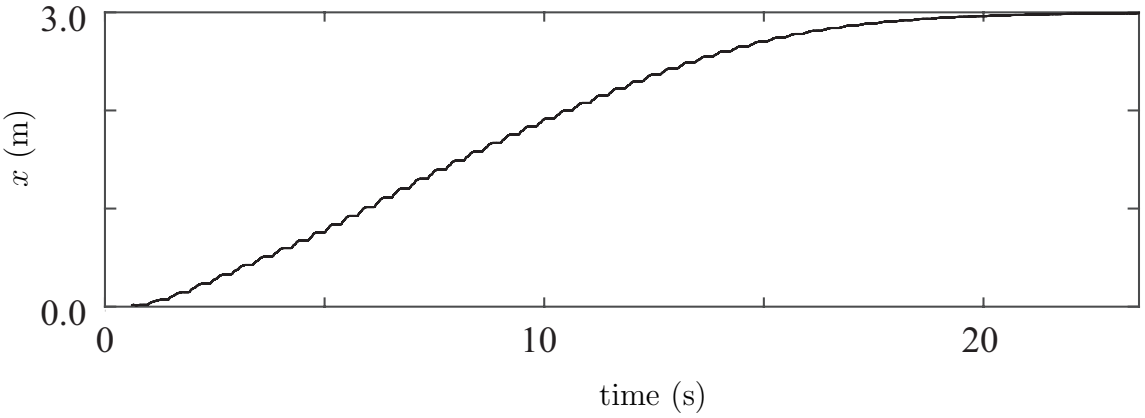

Figure 5.6: Position of the toe x during hopping locomotion.

The robot was assumed to be initially at rest and the initial states were

$$
\begin{aligned}
&x(0) = 0\,\text{m}, && \dot{x}(0) = 0\,\text{m/s}, && y(0) = 0\,\text{m},\\
&\dot{y}(0) = 0\,\text{m/s}, && \theta_1(0) = 2.276\,\text{rad}, && \dot{\theta}_1(0) = 0\,\text{rad/s},\\
&\theta_2(0) = -1.397\,\text{rad}, && \dot{\theta}_2(0) = 0\,\text{rad/s}, && \theta_3(0) = 1.7\,\text{rad},\\
&\dot{\theta}_3(0) = 0\,\text{rad/s}, && \theta_4(0) = -1.461\,\text{rad}, && \dot{\theta}_4(0) = 0\,\text{rad/s}
\end{aligned}
$$

The robot was required to hop for a distance of 3.0 m; therefore, the desired value of the uncontrolled state η_1 was set to $\eta_{1d} = 3.0$. To reach this configuration, the desired step size was selected according to the relation

$$\delta_d = \frac{0.1(\eta_{1d} - \eta_1)}{\sqrt{1 + (\eta_{1d} - \eta_1)^2}}$$

The above relation ensures that the magnitude of the step size do not exceed 0.1 m. The parameters of the continuous controller were chosen as

$$\nu = -1.1, \quad y_d = 0.54, \quad \theta_d = 1.8, \quad \mu_1 = 0.3, \quad \mu_3 = 1.3\mu_2$$

The initial values of μ_2 and the integrator state $\bar{\beta}$ were chosen to be zero. The matrix $\bar{\mathbb{A}}$,

defined in (5.83), was found to have eigenvalues: 1.0, 0.74, 0.364, 0.154, -0.034 and -0.06. Since $\{\bar{\mathbb{A}}, \bar{\mathbb{B}}\}$ is controllable, the controller gains were chosen as

$$\bar{\mathbb{K}} = \begin{bmatrix} -0.1 & 0 & 0 & 0 & 0 & 0.1 \end{bmatrix}$$

This places the eigenvalues of the closed loop system at 0.968, 0.756, -0.06, -0.034, 0.154 and 0.365.

Figures 5.6 and 5.7 show the results of hopping locomotion. Figure 5.6 shows the horizontal position of the toe x; it can be seen that the hopper moves to its desired location $\eta_1 = x = 3.0$. Figure 5.7 shows variation of the actual and desired step sizes with each hop; it can be seen that the step size tracks the desired value and both converge to zero when the robot reaches its desired location.

Figure 5.8 plots the remaining states of the discrete-time system; incidentally, these states are also the uncontrolled states of the robot in the flight phase. It can be seen that these states are well-behaved and converge to a constant value within a few hops. The hopper reached its desired position after $k = 60$ hops at $t = 26.3$ s.

A video animation of hopping locomotion has been uploaded as supplementary material. It shows the hopper reaching the desired position of $\eta_{1d} = 3.0$ m starting from rest with step size varying as shown in Fig.5.7.

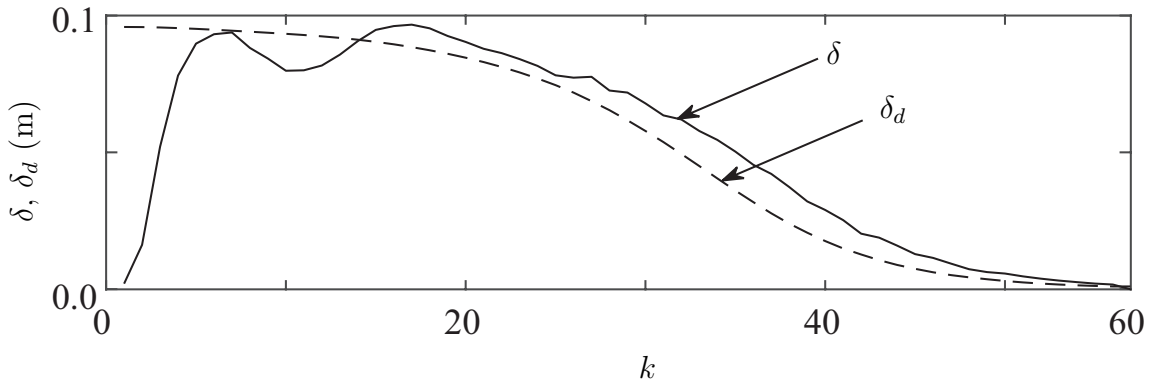

Figure 5.7: Variation of actual and desired step sizes over 60 hops.

5.8 Conclusion

This chapter presents control strategies for hopping in place with a desired apex height and hopping locomotion with a desired step size for a four-link one-legged hopper. The hybrid dynamics of the hopper is comprised of flight, impact, and contact phases and each phase is converted into normal form to identify the controllable and uncontrollable states. A partial feedback linearization controller constrains the controllable states to behave like a mass-spring-damper system. To overcome the energy losses due to the impact with ground, we used two strategies. The first strategy introduces negative damping in the dynamics of the mass-spring-damper system that corresponds to the vertical displacement of the COM during the contact phase. The second strategy varies the equilibrium height corresponding

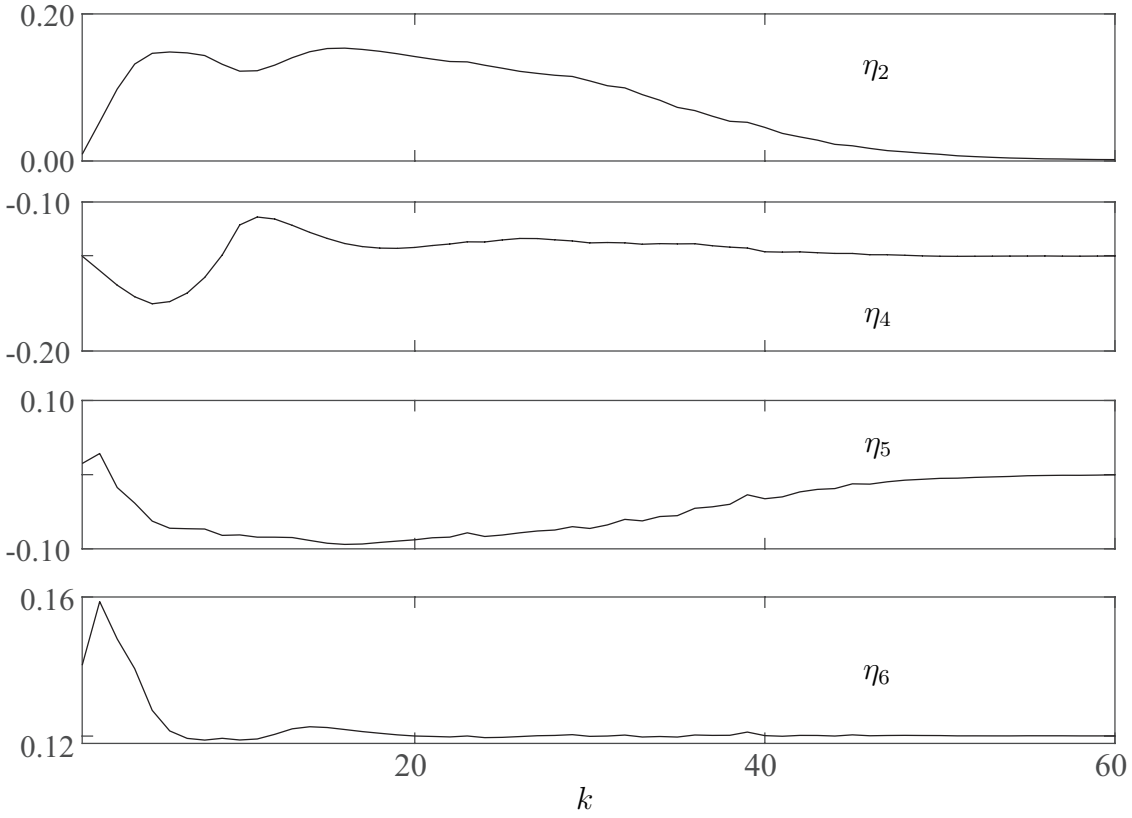

Figure 5.8: Plot of uncontrolled states at the end of each hop k during hopping locomotion.

to the vertical displacement of the COM during the flight phase. For apex height control and hopping locomotion, separate Poincaré maps are constructed at the point of touch-down. These maps are used to obtain a discrete-time model of the system and controllers are designed to meet the two control objectives. Simulation results are presented to validate the efficacy of the controllers. A video animation of hopping in place and hopping locomotion are includes to provide a glimpse of the dynamic behavior.

Chapter 6

Conclusion

In this dissertation we presented several control strategies for motion control of multi-link hoppers. Two and six degree-of-freedom hoppers were considered and the ground model was assumed to be rigid, elastic, and viscoelastic with inertia. For the two degree-of-freedom hoppers, the control objective was to converge the apex height for hopping on different ground models. For the six degree-of-freedom hopper, locomotion with a desired step size was the main control objective. We first presented a control strategy for controlling the apex height of a two-mass prismatic-joint robot hopping on a viscoelastic ground. This problem is challenging due to the losses in the total energy of the system due to impact and damping in the ground. A continuous-time backstepping controller was used in concert with a discrete-time integral controller to meet the control objective. The backstepping controller regulates the energy of the system using the internal degrees of freedom and is useful for apex height control on an elastic ground; for the viscoelastic ground with inertia, it results in steady state error. The discrete-time integral controller eliminates this error by commanding the backstepping controller to regulate the energy to a commensurately higher level. Since there is loss of energy in every hop, the backstepping controller has to remain active for all hops.

As the next step, we considered apex height control of the two degree-of-freedom ankle-knee-hip (AKH) robot. The AKH robot is more anthropomorphic but the control problem is more challenging due to the revolute nature of the joints. We considered apex height control of the AKH robot hopping on a rigid ground. The dynamics of the robot is modeled in flight, impact, and contact phases separately. A continuous-time controller is designed to make the robot behave like a mass-spring-damper system. In the contact phase, the continuous

controller employs positive damping to arrest the motion of the center-of-mass when it is moving downwards, and negative damping when the center-of-mass is moving upwards. The negative damping is introduced to compensate for the energy loss due to impact. A Poincaré map of the hopping behavior is constructed and asymptotic stability of the hybrid system to the desired apex height is guaranteed by designing a discrete controller with integral action. The constraint imposed by the robot structure and the effect of continuous controller parameters on hopping behavior is discussed. A simulation of the AKH robot, hopping to a desired apex height from rest, is presented.

Following the control strategy for the two-DOF AKH robot hopping on a rigid ground, we presented a control strategy to converge the apex height of an AKH robot hopping on an elastic ground and a viscoelastic ground with inertia. Similar to the two-DOF prismatic-joint robot, a continuous-time backstepping controller is used in conjunction with a discrete-time controller; the discrete-time controller is designed by linearizing a Poincaré map. For the elastic ground, the backstepping controller is used to control the energy level of the hopper and eliminate the relative displacement between the hopper masses. The discrete-time controller is used to guarantee the stability of the hybrid system and fast convergence of the apex height to the desired value. For the viscoelastic ground, the backstepping controller results in steady state error due to losses from impact between the hopper and the ground as well as viscous losses in the damper. To overcome these losses, the discrete-time controller is used with integral action. Simulation results prove the efficacy of the control strategy for both the elastic ground and the viscoelastic ground.

We extend the results of the two-DOF AKH robot hopping on a rigid ground to a four-link six-DOF robot with a body, thigh, leg and foot. We consider two separate problems, namely, controlling the apex height while hopping in one location and locomotion with a fixed step size on a rigid ground. The hybrid dynamics of the hopper is comprised of flight, impact, and contact phases and each phase is converted into normal form to identify the controllable and uncontrollable states. A partial feedback linearization controller constrains

the controllable states to behave like a mass-spring-damper system. To overcome the energy losses due to the impact with ground, we used two strategies. The first strategy introduces negative damping in the dynamics of the mass-spring-damper system corresponding to the vertical displacement of the COM during the contact phase. The second strategy alters the equilibrium height corresponding to the vertical displacement of the COM during the flight phase. For both control strategies, it is established that both controllable and uncontrollable states remain bounded. For apex height control and hopping locomotion, separate Poincaré maps are constructed at the point of touch-down. These maps are used to obtain a discrete-time model of the system and controllers are designed by linearizing the map to meet the control objectives. Simulation results are presented to validate the efficacy of the controllers.

Future research will focus on experimental verification of the control strategies developed for the four-link hopping robot. This is a challenging design problem. Hopping requires large torques to be applied by the actuators over relatively small intervals of time. Mechanical advantage such as a gearbox can amplify the torque generated but reduces the speed of response. On the other hand, direct-drive motors that can generate the desired torques are bulky and increase the weight of the robot. This compounds the design problem further as the motors in the lower links have to support the weight of the motors in the upper links. Another extension of this work is the development of control strategies for performing more complex maneuvers such as flipping in the flight phase. Flipping requires high angular momentum in the flight phase and the control torques should be able to generate this momentum at the time of takeoff. The speed of flipping during the flight phase depends on the moment of inertia about the COM, which can be controlled. The moment of inertia has to be controlled such that the robot completes the flip in the flight phase and has the correct orientation prior to touchdown. The design of a control strategy for flipping motion requires nontrivial extensions of the continuous controller discussed in Chapter 5.

APPENDIX

Appendix A

Computing the Dynamical Equations For Four-Link Hopper

To drive the dynamical of equations described in (5.1), and (5.9), we use the lagrangian equations, where

$$\frac{\partial}{\partial t}(\frac{\partial L}{\partial \dot{q}}) - \frac{\partial L}{\partial q} = Q, \qquad L \triangleq T - U \tag{A.1}$$

where T, and U are the total kinetic and potential energy of the system, respectively. This resulting the dynamical of equations described in (5.1), and (5.9), where $[M_{ij}]_{6\times 1}$, and $[N_i]_{6\times 6}$ and

$$\begin{aligned}
M_{11} =& M_{22} = \bar{m} \triangleq m_{\mathrm{f}} + m_{\mathrm{l}} + m_{\mathrm{t}} + m_{\mathrm{b}} \\
M_{12} =& M_{21} = 0 \\
M_{13} =& M_{31} = -l_{\mathrm{f}}\big[m_{\mathrm{f}} + 2(m_{\mathrm{l}} + m_{\mathrm{t}} + m_{\mathrm{b}})\big]\sin\theta_1 - l_{\mathrm{l}}\big[m_{\mathrm{l}} + 2(m_{\mathrm{t}} + m_{\mathrm{b}})\big]\sin(\theta_1 + \theta_2) \\
& - l_{\mathrm{t}}(m_{\mathrm{t}} + 2m_{\mathrm{b}})\sin(\theta_1 + \theta_2 + \theta_3) - l_{\mathrm{b}}m_{\mathrm{b}}\sin(\theta_1 + \theta_2 + \theta_3 + \theta_4) \\
M_{14} =& M_{41} = -l_{\mathrm{l}}\big[m_{\mathrm{l}} + 2(m_{\mathrm{t}} + m_{\mathrm{b}})\big]\sin(\theta_1 + \theta_2) - l_{\mathrm{t}}(m_{\mathrm{t}} + 2m_{\mathrm{b}})\sin(\theta_1 + \theta_2 + \theta_3) \\
& - l_{\mathrm{b}}m_{\mathrm{b}}\sin(\theta_1 + \theta_2 + \theta_3 + \theta_4) \\
M_{15} =& M_{51} = -l_{\mathrm{t}}(m_{\mathrm{t}} + 2m_{\mathrm{b}})\sin(\theta_1 + \theta_2 + \theta_3) - l_{\mathrm{b}}m_{\mathrm{b}}\sin(\theta_1 + \theta_2 + \theta_3 + \theta_4) \\
M_{16} =& M_{61} = -l_{\mathrm{b}}m_{\mathrm{b}}\sin(\theta_1 + \theta_2 + \theta_3 + \theta_4) \\
M_{23} =& M_{32} = l_{\mathrm{f}}\big[m_{\mathrm{f}} + 2(m_{\mathrm{l}} + m_{\mathrm{t}} + m_{\mathrm{b}})\big]\cos\theta_1 + l_{\mathrm{l}}\big[m_{\mathrm{l}} + 2(m_{\mathrm{t}} + m_{\mathrm{b}})\big]\cos(\theta_1 + \theta_2) \\
& + l_{\mathrm{t}}(m_{\mathrm{t}} + 2m_{\mathrm{b}})\cos(\theta_1 + \theta_2 + \theta_3) + l_{\mathrm{b}}m_{\mathrm{b}}\cos(\theta_1 + \theta_2 + \theta_3 + \theta_4)
\end{aligned}$$

$$
\begin{aligned}
M_{24} =& M_{42} = l_{\mathrm{l}}\big[m_{\mathrm{l}} + 2(m_{\mathrm{t}} + m_{\mathrm{b}})\big]\cos(\theta_1 + \theta_2) + l_{\mathrm{t}}(m_{\mathrm{t}} + 2m_{\mathrm{b}})\cos(\theta_1 + \theta_2 + \theta_3) \\
&+ l_{\mathrm{b}}m_{\mathrm{b}}\cos(\theta_1 + \theta_2 + \theta_3 + \theta_4) \\
M_{25} =& M_{52} = l_{\mathrm{t}}(m_{\mathrm{t}} + 2m_{\mathrm{b}})\cos(\theta_1 + \theta_2 + \theta_3) + l_{\mathrm{b}}m_{\mathrm{b}}\cos(\theta_1 + \theta_2 + \theta_3 + \theta_4) \\
M_{26} =& M_{62} = l_{\mathrm{b}}m_{\mathrm{b}}\cos(\theta_1 + \theta_2 + \theta_3 + \theta_4) \\
M_{33} =& I_{\mathrm{f}} + I_{\mathrm{l}} + I_{\mathrm{t}} + I_{\mathrm{b}} + l_{\mathrm{t}}^2 m_{\mathrm{t}} + 4l_{\mathrm{t}}^2 m_{\mathrm{b}} + l_{\mathrm{b}}^2 m_{\mathrm{b}} + l_{\mathrm{l}}^2\big[m_{\mathrm{l}} + 4(m_{\mathrm{t}} + m_{\mathrm{b}})\big] \\
&+ l_{\mathrm{f}}^2\big[m_{\mathrm{f}} + 4(m_{\mathrm{l}} + m_{\mathrm{t}} + m_{\mathrm{b}})\big] + 4l_{\mathrm{f}}l_{\mathrm{l}}\big[m_{\mathrm{l}} + 2(m_{\mathrm{t}} + m_{\mathrm{b}})\big]\cos\theta_2 \\
&+ 4l_{\mathrm{t}}(m_{\mathrm{t}} + 2m_{\mathrm{b}})\big[l_{\mathrm{l}}\cos\theta_3 + l_{\mathrm{f}}\cos(\theta_2 + \theta_3)\big] \\
&+ 4l_{\mathrm{b}}m_{\mathrm{b}}\big[l_{\mathrm{t}}\cos\theta_4 + l_{\mathrm{l}}\cos(\theta_3 + \theta_4) + l_{\mathrm{f}}\cos(\theta_2 + \theta_3 + \theta_4)\big] \\
M_{34} =& M_{43} = I_{\mathrm{l}} + I_{\mathrm{t}} + I_{\mathrm{b}} + l_{\mathrm{l}}^2 m_{\mathrm{l}} + 4l_{\mathrm{l}}^2 m_{\mathrm{t}} + l_{\mathrm{t}}^2 m_{\mathrm{t}} + m_{\mathrm{b}}\big[4(l_{\mathrm{l}}^2 + l_{\mathrm{t}}^2) + l_{\mathrm{b}}^2\big] \\
&+ 2l_{\mathrm{f}}l_{\mathrm{l}}\big[m_{\mathrm{l}} + 2(m_{\mathrm{t}} + m_{\mathrm{b}})\big]\cos\theta_2 + 4l_{\mathrm{l}}l_{\mathrm{t}}(m_{\mathrm{t}} + 2m_{\mathrm{b}})\cos\theta_3 \\
&+ 2l_{\mathrm{b}}m_{\mathrm{b}}\big[2l_{\mathrm{t}}\cos\theta_4 + 2l_{\mathrm{l}}\cos(\theta_3 + \theta_4) + l_{\mathrm{f}}\cos(\theta_2 + \theta_3 + \theta_4)\big] \\
&+ 2l_{\mathrm{f}}l_{\mathrm{t}}(m_{\mathrm{t}} + 2m_{\mathrm{b}})\cos(\theta_2 + \theta_3) \\
M_{35} =& M_{53} = I_{\mathrm{t}} + I_{\mathrm{b}} + l_{\mathrm{t}}^2(m_{\mathrm{t}} + 4m_{\mathrm{b}}) + l_{\mathrm{b}}^2 m_{\mathrm{b}} + 2l_{\mathrm{l}}l_{\mathrm{t}}(m_{\mathrm{t}} + 2m_{\mathrm{b}})\cos\theta_3 \\
&+ 2l_{\mathrm{b}}m_{\mathrm{b}}\big[2l_{\mathrm{t}}\cos\theta_4 + l_{\mathrm{l}}\cos(\theta_3 + \theta_4) + l_{\mathrm{f}}\cos(\theta_2 + \theta_3 + \theta_4)\big] \\
&+ 2l_{\mathrm{f}}l_{\mathrm{t}}(m_{\mathrm{t}} + 2m_{\mathrm{b}})\cos(\theta_2 + \theta_3) \\
M_{36} =& M_{63} = I_{\mathrm{b}} + l_{\mathrm{b}}^2 m_{\mathrm{b}} + 2l_{\mathrm{b}}m_{\mathrm{b}}\big[l_{\mathrm{t}}\cos\theta_4 + l_{\mathrm{l}}\cos(\theta_3 + \theta_4) + l_{\mathrm{f}}\cos(\theta_2 + \theta_3 + \theta_4)\big] \\
M_{44} =& I_{\mathrm{l}} + I_{\mathrm{t}} + I_{\mathrm{b}} + l_{\mathrm{b}}^2 m_{\mathrm{b}} + l_{\mathrm{t}}^2(m_{\mathrm{t}} + 4m_{\mathrm{b}}) + l_{\mathrm{l}}^2\big[m_{\mathrm{l}} + 4(m_{\mathrm{t}} + m_{\mathrm{b}})\big] \\
&+ 4\big[l_{\mathrm{l}}l_{\mathrm{t}}(m_{\mathrm{t}} + 2m_{\mathrm{b}})\cos\theta_3 + l_{\mathrm{b}}m_{\mathrm{b}}(l_{\mathrm{t}}\cos\theta_4 + l_{\mathrm{l}}\cos(\theta_3 + \theta_4))\big] \\
M_{45} =& M_{54} = I_{\mathrm{t}} + I_{\mathrm{b}} + l_{\mathrm{b}}^2 m_{\mathrm{b}} + l_{\mathrm{t}}^2(m_{\mathrm{t}} + 4m_{\mathrm{b}}) + 2l_{\mathrm{l}}l_{\mathrm{t}}(m_{\mathrm{t}} + 2m_{\mathrm{b}})\cos\theta_3 \\
&+ 2l_{\mathrm{b}}m_{\mathrm{b}}\big[2l_{\mathrm{t}}\cos\theta_4 + l_{\mathrm{l}}\cos(\theta_3 + \theta_4)\big] \\
M_{46} =& M_{64} = I_{\mathrm{b}} + l_{\mathrm{b}}^2 m_{\mathrm{b}} + 2l_{\mathrm{b}}m_{\mathrm{b}}\big[l_{\mathrm{t}}\cos\theta_4 + l_{\mathrm{l}}\cos(\theta_3 + \theta_4)\big] \\
M_{55} =& I_{\mathrm{t}} + I_{\mathrm{b}} + l_{\mathrm{t}}^2(m_{\mathrm{t}} + 4m_{\mathrm{b}}) + l_{\mathrm{b}}^2 m_{\mathrm{b}} + 4l_{\mathrm{b}}l_{\mathrm{t}}m_{\mathrm{b}}\cos\theta_4 \\
M_{56} =& M_{65} = I_{\mathrm{b}} + l_{\mathrm{b}}^2 m_{\mathrm{b}} + 2l_{\mathrm{b}}l_{\mathrm{t}}m_{\mathrm{b}}\cos\theta_4
\end{aligned}
$$

$$
\begin{aligned}
M_{66} =& I_{\mathrm{b}} + l_{\mathrm{b}}^2 m_{\mathrm{b}} \\
N_1 =& -\big[l_{\mathrm{f}}\big(m_{\mathrm{f}} + 2(m_{\mathrm{b}} + m_{\mathrm{l}} + m_{\mathrm{t}})\big)\cos\theta_1 + l_{\mathrm{l}}\big(m_{\mathrm{l}} + 2(m_{\mathrm{b}} + m_{\mathrm{t}})\big)\cos(\theta_1 + \theta_2) \\
&+ 2l_{\mathrm{t}} m_{\mathrm{b}}\cos(\theta_1 + \theta_2 + \theta_3) + l_{\mathrm{t}} m_{\mathrm{t}}\cos(\theta_1 + \theta_2 + \theta_3) \\
&+ l_{\mathrm{b}} m_{\mathrm{b}}\cos(\theta_1 + \theta_2 + \theta_3 + \theta_4)\big]\dot{\theta}_1^2 \\
&- \big[l_{\mathrm{l}}(m_{\mathrm{l}} + 2\big(m_{\mathrm{b}} + m_{\mathrm{t}}\big))\cos(\theta_1 + \theta_2) + l_{\mathrm{t}}(2m_{\mathrm{b}} + m_{\mathrm{t}})\cos(\theta_1 + \theta_2 + \theta_3) \\
&+ l_{\mathrm{b}} m_{\mathrm{b}}\cos(\theta_1 + \theta_2 + \theta_3 + \theta_4)\big]\dot{\theta}_2^2 \\
&- 2l_{\mathrm{t}} m_{\mathrm{b}}\cos(\theta_1 + \theta_2 + \theta_3)\dot{\theta}_3^2 - l_{\mathrm{t}} m_{\mathrm{t}}\cos(\theta_1 + \theta_2 + \theta_3)\dot{\theta}_3^2 \\
&- l_{\mathrm{b}} m_{\mathrm{b}}\cos(\theta_1 + \theta_2 + \theta_3 + \theta_4)\dot{\theta}_3^2 - 2l_{\mathrm{b}} m_{\mathrm{b}}\cos(\theta_1 + \theta_2 + \theta_3 + \theta_4)\dot{\theta}_3\dot{\theta}_4 \\
&- l_{\mathrm{b}} m_{\mathrm{b}}\cos(\theta_1 + \theta_2 + \theta_3 + \theta_4)\dot{\theta}_4^2 \\
&- 2\big[l_{\mathrm{t}}(2m_{\mathrm{b}} + m_{\mathrm{t}})\cos(\theta_1 + \theta_2 + \theta_3) + l_{\mathrm{b}} m_{\mathrm{b}}\cos(\theta_1 + \theta_2 + \theta_3 + \theta_4)\big]\dot{\theta}_2\dot{\theta}_3 \\
&- 2\big[l_{\mathrm{b}} m_{\mathrm{b}}\cos(\theta_1 + \theta_2 + \theta_3 + \theta_4)\big]\dot{\theta}_2\dot{\theta}_4 \\
&- 2\big[l_{\mathrm{l}}\big(m_{\mathrm{l}} + 2(m_{\mathrm{b}} + m_{\mathrm{t}})\big)\cos(\theta_1 + \theta_2) + l_{\mathrm{t}}(2m_{\mathrm{b}} + m_{\mathrm{t}})\cos(\theta_1 + \theta_2 + \theta_3) \\
&+ l_{\mathrm{b}} m_{\mathrm{b}}\cos(\theta_1 + \theta_2 + \theta_3 + \theta_4)\big]\dot{\theta}_1\dot{\theta}_2 \\
&- 2\big[l_{\mathrm{t}}(2m_{\mathrm{b}} + m_{\mathrm{t}})\cos(\theta_1 + \theta_2 + \theta_3) + l_{\mathrm{b}} m_{\mathrm{b}}\cos(\theta_1 + \theta_2 + \theta_3 + \theta_4)\big]\dot{\theta}_1\dot{\theta}_3 \\
&- 2\big[l_{\mathrm{b}} m_{\mathrm{b}}\cos(\theta_1 + \theta_2 + \theta_3 + \theta_4)\big]\dot{\theta}_1\dot{\theta}_4 \\
N_2 =& g m_{\mathrm{b}} + g m_{\mathrm{f}} + g m_{\mathrm{l}} + g m_{\mathrm{t}} \\
&- \big[l_{\mathrm{f}}\big(m_{\mathrm{f}} + 2(m_{\mathrm{b}} + m_{\mathrm{l}} + m_{\mathrm{t}})\big)\sin\theta_1 + l_{\mathrm{l}}\big(m_{\mathrm{l}} + 2(m_{\mathrm{b}} + m_{\mathrm{t}})\big)\sin(\theta_1 + \theta_2) \\
&+ 2l_{\mathrm{t}} m_{\mathrm{b}}\sin(\theta_1 + \theta_2 + \theta_3) + l_{\mathrm{t}} m_{\mathrm{t}}\sin(\theta_1 + \theta_2 + \theta_3) \\
&+ l_{\mathrm{b}} m_{\mathrm{b}}\sin(\theta_1 + \theta_2 + \theta_3 + \theta_4)\big]\dot{\theta}_1^2 \\
&- \big[l_{\mathrm{l}}(m_{\mathrm{l}} + 2\big(m_{\mathrm{b}} + m_{\mathrm{t}}\big))\sin(\theta_1 + \theta_2) + l_{\mathrm{t}}(2m_{\mathrm{b}} + m_{\mathrm{t}})\sin(\theta_1 + \theta_2 + \theta_3) \\
&+ l_{\mathrm{b}} m_{\mathrm{b}}\sin(\theta_1 + \theta_2 + \theta_3 + \theta_4)\big]\dot{\theta}_2^2 \\
&- 2l_{\mathrm{t}} m_{\mathrm{b}}\sin(\theta_1 + \theta_2 + \theta_3)\dot{\theta}_3^2 - l_{\mathrm{t}} m_{\mathrm{t}}\sin(\theta_1 + \theta_2 + \theta_3)\dot{\theta}_3^2 \\
&- l_{\mathrm{b}} m_{\mathrm{b}}\sin(\theta_1 + \theta_2 + \theta_3 + \theta_4)\dot{\theta}_3^2 - 2l_{\mathrm{b}} m_{\mathrm{b}}\sin(\theta_1 + \theta_2 + \theta_3 + \theta_4)\dot{\theta}_3\dot{\theta}_4 \\
&- l_{\mathrm{b}} m_{\mathrm{b}}\sin(\theta_1 + \theta_2 + \theta_3 + \theta_4)\dot{\theta}_4^2
\end{aligned}
$$

$$
\begin{aligned}
&- 2\big[l_{\mathrm{t}}(2m_{\mathrm{b}} + m_{\mathrm{t}})\sin(\theta_1 + \theta_2 + \theta_3) + l_{\mathrm{b}}m_{\mathrm{b}}\sin(\theta_1 + \theta_2 + \theta_3 + \theta_4)\big]\dot{\theta}_2\dot{\theta}_3 \\
&- 2\big[l_{\mathrm{b}}m_{\mathrm{b}}\sin(\theta_1 + \theta_2 + \theta_3 + \theta_4)\big]\dot{\theta}_2\dot{\theta}_4 \\
&- 2\big[l_{\mathrm{l}}\big(m_{\mathrm{l}} + 2(m_{\mathrm{b}} + m_{\mathrm{t}})\big)\sin(\theta_1 + \theta_2) + l_{\mathrm{t}}(2m_{\mathrm{b}} + m_{\mathrm{t}})\sin(\theta_1 + \theta_2 + \theta_3) \\
&+ l_{\mathrm{b}}m_{\mathrm{b}}\sin(\theta_1 + \theta_2 + \theta_3 + \theta_4)\big]\dot{\theta}_1\dot{\theta}_2 \\
&- 2\big[l_{\mathrm{t}}(2m_{\mathrm{b}} + m_{\mathrm{t}})\sin(\theta_1 + \theta_2 + \theta_3) + l_{\mathrm{b}}m_{\mathrm{b}}\sin(\theta_1 + \theta_2 + \theta_3 + \theta_4)\big]\dot{\theta}_1\dot{\theta}_3 \\
&- 2\big[l_{\mathrm{b}}m_{\mathrm{b}}\sin(\theta_1 + \theta_2 + \theta_3 + \theta_4)\big]\dot{\theta}_1\dot{\theta}_4 \\
N_3 =& g\big[l_{\mathrm{f}}\big(2m_{\mathrm{b}} + m_{\mathrm{f}} + 2(m_{\mathrm{l}} + m_{\mathrm{t}})\big)\cos\theta_1 + l_{\mathrm{l}}(2m_{\mathrm{b}} + m_{\mathrm{l}} + 2m_{\mathrm{t}})\cos(\theta_1 + \theta_2) \\
&+ l_{\mathrm{t}}(2m_{\mathrm{b}} + m_{\mathrm{t}})\cos(\theta_1 + \theta_2 + \theta_3) + l_{\mathrm{b}}m_{\mathrm{b}}\cos(\theta_1 + \theta_2 + \theta_3 + \theta_4)\big] \\
&- 2l_{\mathrm{f}}\big[l_{\mathrm{l}}\big(m_{\mathrm{l}} + 2(m_{\mathrm{b}} + m_{\mathrm{t}})\big)\sin\theta_2 + l_{\mathrm{t}}(2m_{\mathrm{b}} + m_{\mathrm{t}})\sin(\theta_2 + \theta_3) + l_{\mathrm{b}}m_{\mathrm{b}}\sin(\theta_2 + \theta_3 + \theta_4)\big]\dot{\theta}_2^2 \\
&- 2\big[l_{\mathrm{l}}l_{\mathrm{t}}(2m_{\mathrm{b}} + m_{\mathrm{t}})\sin\theta_3 + l_{\mathrm{f}}l_{\mathrm{t}}(2m_{\mathrm{b}} + m_{\mathrm{t}})\sin(\theta_2 + \theta_3) + l_{\mathrm{b}}m_{\mathrm{b}}(l_{\mathrm{l}}\sin(\theta_3 + \theta_4) \\
&+ l_{\mathrm{f}}\sin(\theta_2 + \theta_3 + \theta_4))\big]\dot{\theta}_3^2 \\
&- 2l_{\mathrm{b}}m_{\mathrm{b}}\big[l_{\mathrm{t}}\sin\theta_4 + l_{\mathrm{l}}\sin(\theta_3 + \theta_4) + l_{\mathrm{f}}\sin(\theta_2 + \theta_3 + \theta_4)\big]\dot{\theta}_4^2 \\
&- 4l_{\mathrm{f}}\big[l_{\mathrm{l}}\big(m_{\mathrm{l}} + 2(m_{\mathrm{b}} + m_{\mathrm{t}})\big)\sin\theta_2 + l_{\mathrm{t}}(2m_{\mathrm{b}} + m_{\mathrm{t}})\sin(\theta_2 + \theta_3) \\
&+ l_{\mathrm{b}}m_{\mathrm{b}}\sin(\theta_2 + \theta_3 + \theta_4)\big]\dot{\theta}_1\dot{\theta}_2 \\
&- 4\big[l_{\mathrm{l}}l_{\mathrm{t}}(2m_{\mathrm{b}} + m_{\mathrm{t}})\sin\theta_3 + l_{\mathrm{f}}l_{\mathrm{t}}(2m_{\mathrm{b}} + m_{\mathrm{t}})\sin(\theta_2 + \theta_3) \\
&+ l_{\mathrm{b}}m_{\mathrm{b}}\big(l_{\mathrm{l}}\sin(\theta_3 + \theta_4) + l_{\mathrm{f}}\sin(\theta_2 + \theta_3 + \theta_4)\big)\big]\dot{\theta}_1\dot{\theta}_3 \\
&- 4l_{\mathrm{b}}m_{\mathrm{b}}\big[l_{\mathrm{t}}\sin\theta_4 + l_{\mathrm{l}}\sin(\theta_3 + \theta_4) + l_{\mathrm{f}}\sin(\theta_2 + \theta_3 + \theta_4)\big]\dot{\theta}_1\dot{\theta}_4 \\
&- 4\big[l_{\mathrm{l}}l_{\mathrm{t}}(2m_{\mathrm{b}} + m_{\mathrm{t}})\sin\theta_3 + l_{\mathrm{f}}l_{\mathrm{t}}(2m_{\mathrm{b}} + m_{\mathrm{t}})\sin(\theta_2 + \theta_3) \\
&+ l_{\mathrm{b}}m_{\mathrm{b}}\big(l_{\mathrm{l}}\sin(\theta_3 + \theta_4) + l_{\mathrm{f}}\sin(\theta_2 + \theta_3 + \theta_4)\big)\big]\dot{\theta}_2\dot{\theta}_3 \\
&- 4l_{\mathrm{b}}m_{\mathrm{b}}\big[l_{\mathrm{t}}\sin\theta_4 + l_{\mathrm{l}}\sin(\theta_3 + \theta_4) + l_{\mathrm{f}}\sin(\theta_2 + \theta_3 + \theta_4)\big]\dot{\theta}_2\dot{\theta}_4 \\
&- 4l_{\mathrm{b}}m_{\mathrm{b}}\big[l_{\mathrm{t}}\sin\theta_4 + l_{\mathrm{l}}\sin(\theta_3 + \theta_4) + l_{\mathrm{f}}\sin(\theta_2 + \theta_3 + \theta_4)\big]\dot{\theta}_3\dot{\theta}_4
\end{aligned}
$$

$$
\begin{aligned}
N_4 =& g\big[l_{\mathrm{l}}(2m_{\mathrm{b}} + m_{\mathrm{l}} + 2m_{\mathrm{t}})\cos(\theta_1 + \theta_2) + l_{\mathrm{t}}(2m_{\mathrm{b}} + m_{\mathrm{t}})\cos(\theta_1 + \theta_2 + \theta_3) \\
&+ l_{\mathrm{b}}m_{\mathrm{b}}\cos(\theta_1 + \theta_2 + \theta_3 + \theta_4)\big] \\
&+ 2l_{\mathrm{f}}\big[l_{\mathrm{l}}\big(m_{\mathrm{l}} + 2(m_{\mathrm{b}} + m_{\mathrm{t}})\big)\sin\theta_2 + l_{\mathrm{t}}(2m_{\mathrm{b}} + m_{\mathrm{t}})\sin(\theta_2 + \theta_3) + l_{\mathrm{b}}m_{\mathrm{b}}\sin(\theta_2 + \theta_3 + \theta_4)\big]\dot{\theta}_1^2 \\
&- 2l_{\mathrm{l}}\big[l_{\mathrm{t}}(2m_{\mathrm{b}} + m_{\mathrm{t}})\sin\theta_3 + l_{\mathrm{b}}m_{\mathrm{b}}\sin(\theta_3 + \theta_4)\big]\dot{\theta}_3^2 \\
&- 2l_{\mathrm{b}}m_{\mathrm{b}}\big[l_{\mathrm{t}}\sin\theta_4 + l_{\mathrm{l}}\sin(\theta_3 + \theta_4)\big]\dot{\theta}_4^2 \\
&- 4l_{\mathrm{l}}\big[l_{\mathrm{t}}(2m_{\mathrm{b}} + m_{\mathrm{t}})\sin\theta_3 + l_{\mathrm{b}}m_{\mathrm{b}}\sin(\theta_3 + \theta_4)\big]\dot{\theta}_1\dot{\theta}_3 \\
&- 4l_{\mathrm{b}}m_{\mathrm{b}}\big[l_{\mathrm{t}}\sin(\theta_4) + l_{\mathrm{l}}\sin(\theta_3 + \theta_4)\big]\dot{\theta}_1\dot{\theta}_4 \\
&- 4l_{\mathrm{l}}\big[l_{\mathrm{t}}(2m_{\mathrm{b}} + m_{\mathrm{t}})\sin\theta_3 + l_{\mathrm{b}}m_{\mathrm{b}}\sin(\theta_3 + \theta_4)\big]\dot{\theta}_2\dot{\theta}_3 \\
&- 4l_{\mathrm{b}}m_{\mathrm{b}}\big[l_{\mathrm{t}}\sin\theta_4 + l_{\mathrm{l}}\sin(\theta_3 + \theta_4)\big]\dot{\theta}_2\dot{\theta}_4 \\
&- 4l_{\mathrm{b}}m_{\mathrm{b}}\big[l_{\mathrm{t}}\sin\theta_4 + l_{\mathrm{l}}\sin(\theta_3 + \theta_4)\big]\dot{\theta}_3\dot{\theta}_4 \\
N_5 =& g\big[l_{\mathrm{t}}(2m_{\mathrm{b}} + m_{\mathrm{t}})\cos(\theta_1 + \theta_2 + \theta_3) + l_{\mathrm{b}}m_{\mathrm{b}}\cos(\theta_1 + \theta_2 + \theta_3 + \theta_4)\big] \\
&+ 2\big[l_{\mathrm{t}}l_{\mathrm{l}}\big(m_{\mathrm{t}} + 2m_{\mathrm{b}}\big)\sin\theta_3 + l_{\mathrm{t}}l_{\mathrm{f}}(2m_{\mathrm{b}} + m_{\mathrm{t}})\sin(\theta_2 + \theta_3) \\
&+ l_{\mathrm{b}}m_{\mathrm{b}}\big(l_{\mathrm{l}}\sin(\theta_3 + \theta_4) + l_{\mathrm{f}}\sin(\theta_2 + \theta_3 + \theta_4)\big)\big]\dot{\theta}_1^2 \\
&+ 2l_{\mathrm{l}}\big[l_{\mathrm{t}}(2m_{\mathrm{b}} + m_{\mathrm{t}})\sin\theta_3 + l_{\mathrm{b}}m_{\mathrm{b}}\sin(\theta_3 + \theta_4)\big]\dot{\theta}_2^2 \\
&- 2l_{\mathrm{b}}m_{\mathrm{b}}l_{\mathrm{t}}\sin\theta_4\dot{\theta}_4^2 \\
&+ 4l_{\mathrm{l}}\big[l_{\mathrm{t}}(2m_{\mathrm{b}} + m_{\mathrm{t}})\sin\theta_3 + l_{\mathrm{b}}m_{\mathrm{b}}\sin(\theta_3 + \theta_4)\big]\dot{\theta}_1\dot{\theta}_2 \\
&- 4l_{\mathrm{b}}m_{\mathrm{b}}l_{\mathrm{t}}\sin\theta_4\dot{\theta}_4(\dot{\theta}_1 + \dot{\theta}_2 + \dot{\theta}_3) \\
N_6 =& g\big[l_{\mathrm{b}}m_{\mathrm{b}}\cos(\theta_1 + \theta_2 + \theta_3 + \theta_4)\big] + 2l_{\mathrm{b}}m_{\mathrm{b}}\big[l_{\mathrm{l}}\sin(\theta_3 + \theta_4) + l_{\mathrm{t}}\sin\theta_4 + l_{\mathrm{f}}\sin(\theta_2 + \theta_3 + \theta_4)\big]\dot{\theta}_1^2 \\
&+ 2l_{\mathrm{b}}m_{\mathrm{b}}\big[l_{\mathrm{t}}\sin\theta_4 + l_{\mathrm{l}}\sin(\theta_3 + \theta_4)\big]\dot{\theta}_2^2 + 2l_{\mathrm{b}}m_{\mathrm{b}}l_{\mathrm{t}}\sin\theta_4\dot{\theta}_3^2 \\
&+ 4l_{\mathrm{b}}m_{\mathrm{b}}\big[l_{\mathrm{t}}\sin\theta_4 + l_{\mathrm{l}}\sin(\theta_3 + \theta_4)\big]\dot{\theta}_1\dot{\theta}_2 + 4l_{\mathrm{b}}m_{\mathrm{b}}l_{\mathrm{t}}\sin\theta_4\dot{\theta}_1\dot{\theta}_3 \\
&+ 4l_{\mathrm{b}}m_{\mathrm{b}}l_{\mathrm{t}}\sin\theta_4\dot{\theta}_2\dot{\theta}_3
\end{aligned}
\tag{A.2}
$$

BIBLIOGRAPHY

BIBLIOGRAPHY

[1] H. S. Seifert, "The lunar pogo stick.," *Journal of spacecraft and Rockets*, vol. 4, no. 7, pp. 941–943, 1967.

[2] K. Matsuoka, "A model of repetitive hopping movements in man," *Fifth World Congress on Theory of Machines and Mechanisms*, 1979.

[3] M. Raibert, *Legged Robots that Balance*. The MIT Press, Cambridge, MA, 1985.

[4] R. Alexander, "Three uses for springs in legged locomotion," *International Journal of Robotics Research*, vol. 9, no. 2, pp. 53–61, 1990.

[5] W. Schwind and D. Koditschek, "Control of forward velocity for a simplified planar hopping robot," in *Proc. IEEE International Conference on Robotics and Automation*, vol. 1, pp. 691–696, IEEE, 1995.

[6] N. Cherouvim and E. Papadopoulos, "Control of hopping speed and height over unknown rough terrain using a single actuator," in *2009 IEEE International Conference on Robotics and Automation*, pp. 2743–2748, IEEE, 2009.

[7] M. Ahmadi and M. Buehler, "Stable control of a simulated one-legged running robot with hip and leg compliance," *IEEE Transactions on Robotics and Automation*, vol. 13, no. 1, pp. 96–104, 1997.

[8] I. Poulakakis and J. Grizzle, "Formal embedding of the spring loaded inverted pendulum in an asymmetric hopper," in *Proc. of the European Control Conference*, 2007.

[9] I. Poulakakis and J. Grizzle, "The spring loaded inverted pendulum as the hybrid zero dynamics of an asymmetric hopper," *IEEE Transactions on Automatic Control*, vol. 54, no. 8, pp. 1779–1793, 2009.

[10] I. Poulakakis and J. W. Grizzle, "Modeling and control of the monopedal robot thumper," in *2009 IEEE International Conference on Robotics and Automation*, pp. 3327–3334, IEEE, 2009.

[11] U. Saranli, W. Schwind, and D. Koditschek, "Toward the control of a multi-jointed, monoped runner," in *Proc. IEEE International Conference on Robotics and Automation*, vol. 3, pp. 2676–2682, IEEE, 1998.

[12] Q. Zhu, W. Wu, Y. Zhao, J. Wu, and R. Xiong, "Design and control of stiffness coordination between knee and ankle joints for a hopping legged robot," in *2017 IEEE International Conference on Unmanned Systems (ICUS)*, pp. 624–630, IEEE, 2017.

[13] B. Vanderborght, N. G. Tsagarakis, C. Semini, R. Van Ham, and D. G. Caldwell, "Maccepa 2.0: Adjustable compliant actuator with stiffening characteristic for energy efficient hopping," in *2009 IEEE International Conference on Robotics and Automation*, pp. 544–549, IEEE, 2009.

[14] H. Q. Vu, X. Yu, F. Iida, and R. Pfeifer, "Improving energy efficiency of hopping locomotion by using a variable stiffness actuator," *IEEE/ASME transactions on mechatronics*, vol. 21, no. 1, pp. 472–486, 2015.

[15] B. Morris and J. W. Grizzle, "A restricted poincaré map for determining exponentially stable periodic orbits in systems with impulse effects: Application to bipedal robots," in *IEEE Conference on Decision and Control*, vol. 44, p. 4199, IEEE; 1998, 2005.

[16] J. E. Seipel and P. Holmes, "Running in three dimensions: Analysis of a point-mass sprung-leg model," *The International Journal of Robotics Research*, vol. 24, no. 8, pp. 657–674, 2005.

[17] R. Altendorfer, D. E. Koditschek, and P. Holmes, "Stability analysis of legged locomotion models by symmetry-factored return maps," *The International Journal of Robotics Research*, vol. 23, no. 10-11, pp. 979–999, 2004.

[18] I. Mikhailova, "Energy-based state-feedback control of systems with mechanical or virtual springs," in *Proc. IEEE International Conference on Robotics and Automation (ICRA)*, pp. 2509–2514, May 2013.

[19] X. Yu and F. Iida, "Minimalistic models of an energy-efficient vertical-hopping robot," *IEEE Transactions on Industrial Electronics*, vol. 61, pp. 1053–1062, Feb 2014.

[20] F. B. Mathis and R. Mukherjee, "Apex height control of a two-mass hopping robot," in *Proc. IEEE International Conference on Robotics and Automation (ICRA)*, (Karlsruhe, Germany), pp. 4785–4790, 2013.

[21] F. B. Mathis and R. Mukherjee, "Apex height control of a two-mass robot hopping on a rigid foundation," *Mechanism and Machine Theory*, vol. 105, pp. 44–57, 2016.

[22] Y. Saitou, T. Nagano, T. Seki, M. Ishikawa, and S. Hara, "Optimal high-jump control of linear 1-dof trampoline robot," in *Proc. of the 41st SICE Annual Conference*, vol. 4, pp. 2527–2530, IEEE, 2002.

[23] M. Ishikawa, A. Neki, J. Imura, and S. Hara, "Energy preserving control of a hopping robot based on hybrid port-controlled Hamiltonian modeling," in *Proc. IEEE Conference on Control Applications*, vol. 2, pp. 1136–1141, IEEE, 2003.

[24] M. Hutter, C. D. Remy, M. A. Höpflinger, and R. Siegwart, "Slip running with an articulated robotic leg," in *2010 IEEE/RSJ International Conference on Intelligent Robots and Systems*, pp. 4934–4939, IEEE, 2010.

[25] F. B. Mathis and R. Mukherjee, "Two-mass robot hopping on an elastic foundation: Apex height control," in *2016 IEEE First International Conference on Control, Measurement and Instrumentation (CMI)*, pp. 167–171, IEEE, 2016.

[26] H. K. Khalil, *Nonlinear Systems*. Prentice Hall, 3rd ed., 2002.

[27] N. Boccara, *Modeling complex systems*. Springer Verlag, 2004.

[28] E. Scholl and H. Schuster, *Handbook of chaos control*. Wiley-VCH, Weinheim, 2008.

[29] F. B. Mathis and R. Mukherjee, "Apex height control of a four-link hopping robot," in *IEEE/RSJ International Conference on Intelligent Robots and Systems (IROS)*, (Tokyo, Japan), pp. 5121–5126, 2013.

[30] N. Boccara, *Modeling complex systems*. Springer Science & Business Media, 2010.

[31] E. Schöll and H. G. Schuster, *Handbook of chaos control*, vol. 2. Wiley Online Library, 2008.

[32] A. Allafi, F. B. Mathis, and R. Mukherjee, "Apex height control of a two-mass robot hopping on a viscoelastic foundation with inertia," in *ASME 2018 Dynamic Systems and Control Conference*, American Society of Mechanical Engineers Digital Collection, 2018.

[33] F. B. Mathis and R. Mukherjee, "Two-mass robot hopping on an elastic foundation: Apex height control," in *Proc. IEEE First International Conference on Control, Measurement and Instrumentation (CMI)*, (Kolkata, India), pp. 167–171, Jan 2016.

[34] A. Allafi and R. Mukherjee, "Apex height control of a two-dof ankle-knee-hip robot hopping on a rigid foundation," in *ASME 2019 Dynamic Systems and Control Conference*, American Society of Mechanical Engineers Digital Collection, 2019.

[35] A. Isidori, "Nonlinear control systems: An introduction((book))," *Berlin and New York, Springer-Verlag(Lecture Notes in Control and Information Sciences.*, vol. 72, 1985.